

# **ACQUISITION AND ANALYSIS OF CUSTOMISED POSTURAL SUPPORT SYSTEMS**

---

**REHABILITATION ENGINEERING UNIT (MEDICAL PHYSICS & CLINICAL ENGINEERING),  
ABERTAWA BRO MORGANNWG UNIVERSITY NHS TRUST, MORRISTON HOSPITAL,  
SWANSEA SA6 6NL**

**Lorna Helen Tasker**

**SUPERVISOR: NIGEL SHAPCOTT**

---

## SUMMARY

---

For 30 years or so specialists in wheelchair seating services in the developed world have captured many thousands of shapes (contours) in various forms for custom seating systems. The predominant methodology employs a plaster casting technique and as a result, shape information is often retained in the plaster cast, therefore has not been measured and may well not be recoverable over time due to storage issues. Consequently, no comparable measurement or outcome data is available which ultimately hinders any scientific evaluation from taking place.

This project has developed shape acquisition and analysis processes to scientifically advance the knowledge of individuals' shapes with complex disabilities. The processes have employed 3D laser scanning technologies where results validated the use of the lower cost laser scanner for both research purposes and clinical work utilising CAD/CAM techniques (Digital Seating Service). These results inform manufacturers of special seating systems that more affordable scanning technologies (such as the Microscan) should be considered as a viable option to advance the routine clinical services and research within the field.

Shape analysis processes were devised by representing the shape volume as standardised geometric shapes (column rods) which allowed comparisons to be made. A potential low-cost manufacturing technique was explored using these geometric shape representations. These valuable results suggest that small-scale manufacturers of customised seating systems, such as small NHS Special Seating Units, may be able to fabricate their customised seating systems using the proposed geometric representations for a certain proportion of the shapes. For the remaining proportion of shapes, external CAD/CAM technologies could be sourced. To increase the accuracy of the geometric representations, statistical measures were investigated, where standard deviation values for each grid cell highlighted areas where the geometric representations exceeded the  $\pm 10\text{mm}$  tolerance.

---

## ACKNOWLEDGMENTS

---

I would like to express my acknowledgements to:

- The Posture & mobility Group (PMG) who provided funding for this project as a result of a successful proposal for the Small Research Study Funding Scheme which has provided access to a high-cost laser scanner (the FARO scanner) and other resources which would otherwise not have been available. The PMG is an organization that was created to advance and disseminate knowledge about the posture and mobility needs of people with disabilities. As part of the group's aims, the group supports research and development which will help promote best practice, provide training, collate information and advise stakeholders in relation to posture and wheeled mobility services. (PMG 2008)
- The National Leadership and Innovation Agency For Healthcare (NLIAH) and Welsh Assembly Government for funding my Clinical Scientist training and postgraduate degree. Abertawe Bro Morgannwg University NHS Trust at Rehabilitation Engineering Unit (Medical Physics and Clinical Engineering at Morriston Hospital) where my training and research has been based.

I would like to thank the following people for their support and help throughout the project:

- Nigel Shapcott for providing his continued support and being a source of expertise within the area specialist seating.
- Anthony Beddow and the workshop for help manufacturing the 3D shape models and for help moving the plaster casts to and from storage
- Dave Randell and Kevin Schmeyz from Digital Design Partnership for 3D scanning/comparison services
- Paul Marl (North Wales Rehabilitation Engineering Unit) and Dr Donna Cowan (Chailey Clinical Services, East Sussex) for supplying plaster casts for the project.
- Alan Sykes who has helped with the statistical content of the project
- Chris Williams for help developing the java program
- Bill Davies for proof reading
- Dr Diane Crawford for proof reading
- Peter Watson, (Musgrave Hospital, Belfast) for support regarding equipment and software queries.
- Patrick Thorn for training and support regarding equipment and software queries.
- David Brienza for equipment recommendations and supply of other information very rapidly

---

# CONTENTS

---

1	INTRODUCTION .....	1
1.1	Wheelchairs and Specialist Seating.....	1
1.2	Pressure Ulcers.....	2
1.3	Seating Service at Swansea .....	3
2	OBJECTIVES .....	6
2.1	The Problem .....	6
2.2	Aims and Objectives .....	6
2.3	Research question.....	6
2.4	Purpose.....	7
3	SHAPE ACQUISITION METHODS & LITERATURE REVIEW .... <b>Error! Bookmark not defined.</b>	
3.1	Shape acquisition methods .....	8
3.1.1	Vacuum consolidation and plaster casts .....	8
3.1.2	Otto Bock Shape System .....	9
3.1.3	Invacare Pin Dot Machine .....	10
3.1.4	Stereo Photogrammetry .....	11
3.1.5	Moire Fringe.....	12
3.1.6	Prosthetics Tracer CAD .....	13
3.1.7	Handy Scan 3D .....	14
3.1.8	Summary .....	14
3.2	Literature review of shape acquisition methods .....	15
3.2.1	Ultrasonic contouring system .....	16
3.2.2	Force sensing probe system .....	16
3.2.3	Strain gauge system .....	17
3.2.4	Shape sensing array system using optical fibre technology .....	17

3.2.5	Summary .....	19
4	SHAPE ANALYSIS .....	21
4.1	Reason for shape analysis .....	21
4.2	General shape representation and classification.....	22
4.2.1	Summary .....	25
4.3	Classification of human shape .....	25
4.3.1	Medical imaging 3D shape analysis .....	25
4.3.2	Archaeometry and anthropometric shape analysis .....	25
4.3.3	Body-seat interface shape analysis.....	27
4.3.4	Summary .....	32
5	METHODOLOGY.....	33
5.1	Equipment.....	33
5.1.1	Faro Scanner .....	33
5.1.2	Microscan system .....	37
5.2	Shapes .....	42
5.3	Scanner comparison/validation .....	44
5.4	Data Analysis .....	46
5.4.1	Column rod representation concept .....	46
5.4.2	3D coordinate raw data .....	47
5.4.3	Manual calculations .....	50
5.4.4	Java program.....	53
6	RESULTS .....	57
6.1	Validation of Microscan .....	57
6.1.1	Nominal tolerance $\pm 0.5\text{mm}$ , critical tolerance $\pm 1.0\text{mm}$ .....	57
6.1.2	Nominal tolerance $\pm 1.0\text{mm}$ , critical tolerance $\pm 2.0\text{mm}$ .....	62

6.2	Shape analysis .....	63
6.2.1	Bounding box sizes.....	63
6.2.2	Column representation and Histograms.....	65
6.2.3	Proposed manufacturing concept .....	70
6.2.4	Standard Deviation and Coefficient of Variation.....	76
6.2.5	Tolerance between represented shape and scan data .....	81
6.3	Generic shapes investigation .....	81
6.3.1	Smoothed histograms.....	82
6.3.2	Cluster analysis and Chi-squared test.....	85
7	DISCUSSION .....	88
7.1	Shape acquisition comparisons and Microscan validation .....	88
7.2	Shape analysis processes .....	91
7.2.1	Bounding box sizes.....	92
7.2.2	Geometric shape representations .....	92
7.2.3	Use of statistical measures as grid cell size dictator.....	93
7.3	Manufacturing approach .....	97
8	CONCLUSION .....	100
9	FUTURE WORK.....	101
10	REFERENCES.....	104
11	APPENDICES .....	a
11.1	Photographs of samples (Plaster casts) .....	a
11.2	Scanner comparison reports .....	e
11.3	Java program code .....	f
11.4	Results: Grid Layout and Histograms .....	q
11.5	Chi-squared test calculations .....	v

---

# 1 INTRODUCTION

---

## 1.1 Wheelchairs and Specialist Seating

The development of special seating has transformed wheelchairs from simple mobility devices into postural aids, allowing people with learning disabilities and/or severe physical impairments to leave the confines of institutional life and access the wider community (Watson & Woods 2005). Contoured seating systems may exist in two general forms, one being a pre-contoured cushion which is manufactured using standard shapes whereas custom-contoured systems take the shape directly from the client offering an intimate fit to accommodate or correct, for example, skeletal deformities or range of motion problems in the hip and/or lower extremities. The chosen approach depends on the degree of the client's postural involvement.

More recent research and service delivery improvements has led to the realization that specialized or custom seat cushions and supports are often necessary to enhance functional ability, provide protection from tissue breakdown (pressure ulcers), prevent skeletal deformities and provide postural control and body stability (Brienza D. et al. 1996). The clinical objective is that optimum seating is achieved when the soft tissues are subjected to the least distortion.

Custom moulded seating systems (as shown in Figure 1) offer a solution when the support provided by a standard off-the-shelf seating system is inadequate or inappropriate, which may include the following criteria (Pope 2007):

- **Established contracture and deformity-** for example: scoliosis, severe kyphosis or a combination of these, gross deviation of the lower limb relative to the pelvis (windsweeping)
- **Severe lack of hip flexion**
- **Severe hypotonus** (low muscle tone)
- **Severe chronic, athetoid/dystonic movement-** Custom moulded systems can provide greater trunk stability which in some cases can facilitate greater control and possibly functional use of limb movement.



**Figure 1. An example of a customised seating system**

With the exception of the small number of services and commercial companies who use CAD/CAM techniques to produce their products (e.g. Ottobock's Shape System), the predominant methodology employs a hand-sculpted technique. These hand-sculpted techniques are heavily reliant on highly skilled professionals, where the shape of the client is often retained within a plaster cast. Current practice is often based on trial and error where customised systems are iteratively altered until satisfactory results are obtained. Despite advances in seating techniques, materials and technology, the annual cost of pressure ulcers in the UK is £1.4 - 2.1 billion (Bennett et al. 2004) which equates to £100M spent every year treating pressure ulcers in NHS Wales. This high incidence of pressure ulcers (Section 1.2) provides evidence of the need for development in the design and manufacturing of customised support systems.

The current situation is that there is insufficient knowledge or scientific evaluation of these shapes. The ability to classify or identify generic shapes from the captured contours will allow advancements in the field and in particular influence the future fabrication of these seating systems.

## **1.2 Pressure Ulcers**

Pressure ulcers are a frequent and distressing aspect of the management of persons with complex physical disability. Pressure ulcers are areas of skin that have broken down as a result of excess pressure which can develop in any area of the body; however this usually

occurs over bony prominences. In simple terms, excess pressure causes restricted blood supply to the area which prevents essential nutrients to be supplied and waste to be removed, and consequently the tissue dies.

The causes of pressure ulcers are as a result of a complex set of interactions of intrinsic (e.g. nutritional status, incontinence, vascular insufficiency) and extrinsic factors (e.g. positioning, lifting techniques and surface shear properties). Pressure sores are one of the most detrimental results of improper seating, and have adverse implications on both the person and the healthcare system (in extreme cases surgical intervention is required and untreated pressure ulcers can lead to septicaemia) (Wall & Colley 2003). It for this reason that pressure ulcers should be prevented and specialist seating services should develop their clinical and technical techniques to facilitate this.

### **1.3 Seating Service at Swansea**

At Swansea's Rehabilitation Engineering Unit (REU) (AMBU Trust), a special seating service is provided to clients with complex postural needs. The REU staff assess individual clients to prescribe the most suitable type of wheelchair, seating system and accessories. On-site workshop facilities allow staff to assemble and manufacture the bespoke systems and also provide continual technical modifications.

The most commonly employed technique at Swansea REU was a technique called Foam in Place which used liquid viscoelastic foam to form the desired shape from the plaster cast. This technique was labour intensive and outcomes were unpredictable. In addition, the materials are costly (at approximately £500 for a large adult mould).

The Digital Seating Service (DSS) is a new service based at Swansea. Swansea REU have purchased a Microscan 3D laser scanner (with Microscribe), and a G-code Technology FLATCOM 3 axis CNC machine to form part of a Digital Seating Service to manufacture customised seating systems. This work is based on the processes developed and used by Peter Watson, Musgrove Park Hospital, Belfast.

A plaster cast or more usually a vacuum consolidated bead bag (Section 3.1.1) is scanned to capture the client's shape data. The scanner provides an accuracy that is significantly

greater than currently used tolerances for the manufacturing of moulded seating systems (where a typical tolerance is estimated to be approximately 10-12mm at present) (Shapcott 2008).

During the scan, a great deal of data is collected and file sizes can be large (in the region of 40-70MB). However, the post-processing software allows for the removal of a defined proportion of this data which reduces the file sizes to a more manageable size (2-5MB). Figure 2 shows an example of smoothed post-processed shape data from a plaster cast. This shape information is exported as a STL (Stereolithography) file to CAD/CAM software to generate milling tool paths which are then exported to the CNC (Computer Numerical Controlled) foam carver. The total cost of the equipment is about £35 000, which is initially a high set-up cost; however material costs are significantly reduced and therefore is economically justified in the long-term. The ability to digitally record shape data is another advantage which eliminates the problems associated with storing plaster casts and allows the re-manufacture of a mould if required. From experience the other benefits of CAD/CAM production of customised seating systems have found to be:

- A reduction in the risk of pressure sores due to the enhanced distribution of pressure over the body.
- The use of digital manipulation to enhance or reduce features of the seat or the shape can be tilted or rotated within the foam blocks to enhance the postural effects for the client.
- Different foams can be specified to be used in different sections of the seat, depending on the desired effect- e.g. softer foam for pressure relief for the buttocks and stiffer foam for upper-body support.
- Surfaces can be modified or patterned to allow for clothing, covers and heat reduction
- Reduction in fabrication and clinical time, therefore providing a more efficient turn-around time for the client

Finally, the use of these technologies provides several research opportunities where it is possible to analyse the 3D coordinate data of these shapes at a high accuracy.

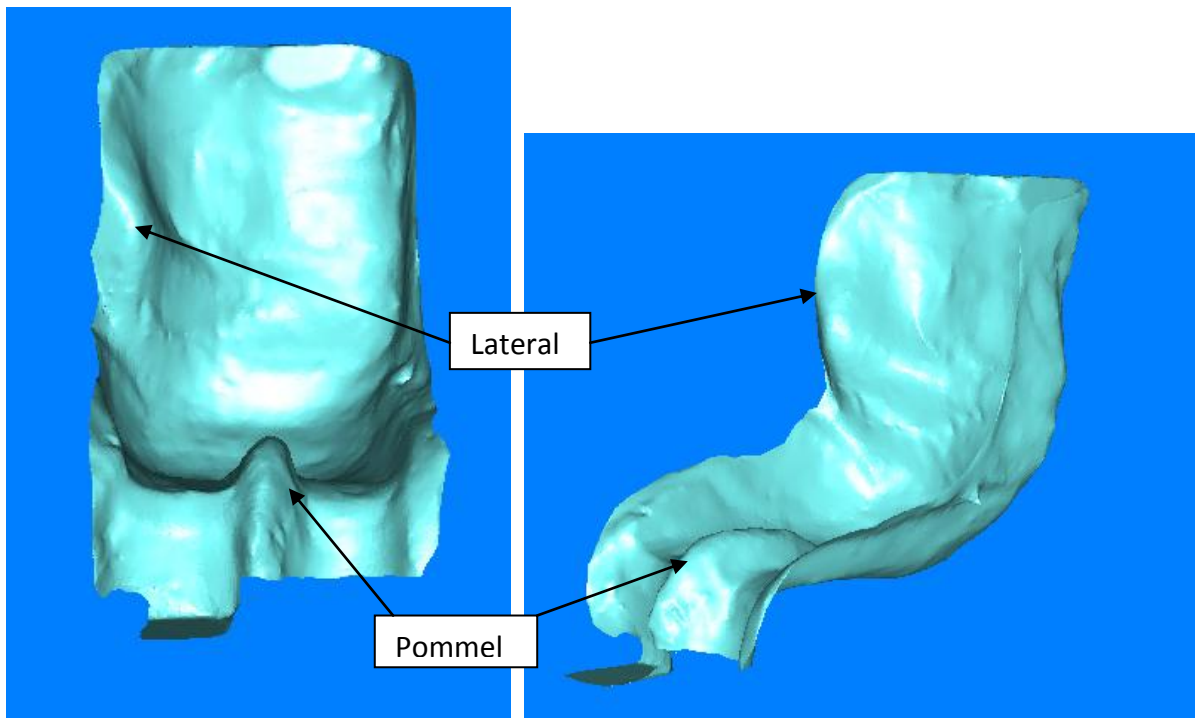


**Figure 2. Microscan Tools images of plaster cast (post processed and smoothed), indicating common features in seating system (Pommel and lateral)**

---

## **2 OBJECTIVES**

---

### **2.1 The Problem**

For 30 years or so specialists in seating services in the developed world have captured many thousands of shapes (contours) in various forms for custom seating systems. Despite this there is insufficient knowledge or scientific evaluation of these postural support shapes. At present, most customised seating systems are expensive; are labour-intensive; can require highly skilled professionals and are not reproducible. The predominant methodology employs a plaster casting technique and as a result, shape information is often retained in the plaster cast, therefore has not been measured and may well not be recoverable over time due to storage issues. Consequently, no comparable measurement or outcome data is available which ultimately hinders any scientific evaluation from taking place.

### **2.2 Aims and Objectives**

The primary aim of this study is to develop a technique for 3D shape data collection and analysis of custom seating systems, in order to develop a better understanding of human shape to influence fabrication techniques. To achieve this, shape acquisition and analysis techniques will be reviewed to provide an overview of the current state of technology and research. An appreciation of shape analysis techniques shall be obtained to establish potential techniques transferable to this study.

A secondary aim of the project is to investigate two shape acquisition technologies by scanning a selection of shapes by both methods. These scanning technologies include: the Faro scanner (a high-cost industrial laser scanner) and the Microscan desktop laser scanner. This investigation will enable recommendations to be made regarding the most appropriate scanning methodology and accuracy required for research purposes and CAD/CAM manufacturing of seating systems.

### **2.3 Research question**

Can 50% of the customised support systems be represented (and manufactured) using standardised geometric shapes that are within  $\pm 10\text{mm}$  from the actual shape? This tolerance was selected on the basis of clinical judgement.

## 2.4 Purpose

The purpose of this project is to utilise scanning technologies to capture 3D information of customised support systems. A collection of 25 shapes from around the UK will allow quantitative shape analysis and comparisons to be made. It is anticipated that the development of data capturing, processing and analysis techniques will provide the following benefits:

- Advance the understanding of these shapes
- Allow quantitative shape comparisons to be made
- Influence fabrication techniques by the definition and utilisation of generic shapes, hence reducing the need for expensive one-off CAD/CAM customised fabrication

---

## **3 SHAPE ACQUISITION METHODS & LITERATURE REVIEW**

---

### **3.1 Shape acquisition methods**

Several shape acquisition methods have been explored to ascertain the current state of the technology available. Attendance at the IPEM (Institute of Physics and Engineering in Medicine) Human Shape meeting in January 2007 brought many disciplines together to share shape-capturing technologies. Several different human measurement and shape capture technologies were discussed including: X-rays, Moire Fringe, Stereo Photogrammetry, Mechanical Shape Sensing, Electromagnetic shape sensing, Laser scanning, and finally the ubiquitous vacuum consolidation, described in the following section.

#### **3.1.1 Vacuum consolidation and plaster casts**

The capturing of shape information is essential for the manufacturing of custom moulded seating systems. The simplest way of doing this is measurement which may be complemented by rapid and gross fabrication using foam or other materials. Some of these custom made shapes are taken directly from the client, using vacuum consolidation, to accommodate or correct, for example, skeletal deformities or range of motion problems in the lower extremities.

The vacuum consolidation technique typically involves the use of a polystyrene bead bag in a wheelchair frame or a dedicated casting chair. A vacuum is applied by evacuating air using a suction pump through a valve. A rough shape of the bead bag is made corresponding to the client's shape and size by manipulating the bead bag before the client is placed on the bag, which reduces the amount of handling of the client during the casting process, Figure 3. When the shape is considered correct, the vacuum is increased in steps resulting in a hard impression. Care must be taken to avoid using too much vacuum which may result in significant shrinkage of the captured shape due to the compressibility of the polystyrene beads.



**Figure 3. Vacuum consolidation process using a bead bag and pump**

A plaster cast of the bead bag is commonly used to record the desired shape, and is used in a variety of ways to manufacture the seating system. This shape acquisition method using Plaster of Paris is time-consuming and it may lead to unpredictable inaccuracies in recording the shape due to materials used.

### **3.1.2 Otto Bock Shape System**

Otto Bock is one of the few commercial companies involved in shape acquisition and CAD/CAM manufacturing for special seating systems. The process is called the Otto Bock Shape System (OBSS). An evacuated latex bead bag is used in a similar way as described in Section 3.1.1. The bag surface is digitized using a probe (Figure 4), and Otto Bock proprietary software, developed in cooperation with Polhemus (Colchester, VT) (Manufacturing Engineering 2008). The stylus used to digitize the surface requires no mechanical arm or optical markers because it utilizes magnetic tracking technology. The quoted accuracy of Polhemus's Patriot Digitizer is 1.3mm (absolute) and 0.48mm (relative). One disadvantage of this technology, is that large metallic objects (such as desks or cabinets) located near the shape capturing area may adversely affect the performance of the system (Polhemus 2007).



Figure 4. Otto Bock Shape System (OBSS) utilising a bead bag and digitising probe

### 3.1.3 Invacare Pin Dot Machine

This shape capturing tool is used locally at Cardiff's Rehabilitation Engineering Unit to create the Cardiff Body Match (CBM) contoured cushions. The casting frame consists of back and seat surfaces which contain a matrix of pins, as shown in Figure 5. These are displaced when a client is positioned on the assessment machine, which quantifies a client's shape by recording the depth of these pins on a sheet of paper. These markings are manually digitized to control an automated foam carver machine which fabricates the custom-contoured cushion. The shape measuring resolution of this system is poor (approximately 45mm distance between each pin). The system is also limited by the measuring depth (approximately 75mm) which would be unsuitable for deep, complex shapes required for some individuals. In addition, some may consider that this shape acquisition technique is unsuitable because a considerable force is required to push the client into the matrix of pin to achieve the desired shape for the back support.



Figure 5. Invacare Pin Dot Machine

### 3.1.4 Stereo Photogrammetry

Passive stereo photogrammetry is used to derive accurate, high resolution 3D surface data from a series of images acquired using standard digital stills cameras (Figure 6) shows two different photogrammetry systems). The technology employs an array of digital cameras, the images of which are processed into complete 3D models. One example of these systems is the Di3D™ system (Di3D 2008) which is used in the field of facial surgery, offering the clinician the ability to simulate the results of surgery. The technology also has widespread application in orthodontics and the entertainment (games and film) industry. Figure 7 shows the result of experimentation with the system used by Morriston Hospital's Maxillofacial department. The system is not very portable and requires calibration at each set-up.



**Figure 6. Two examples of photogrammetry systems**



**Figure 7. Experimental image from photogrammetry system used at Morriston Hospital's Maxillofacial department**

### 3.1.5 Moire Fringe

Moire Fringe topography is used to assess for postural asymmetry in adults which may be causing lower back pain, shoulder and neck pain, or sciatica. Moire Fringe is also used to monitor spinal asymmetry in growing children. The technique involves shining a bright light positioned at an angle to the frame that is strung with approximately 100 fine wires, Figure 8. When the shadows fall on an undulating surface such as a person's spine, two series of contour lines are created relating to the surface's spatial orientation. For example around the buttocks a series of concentric lines are formed, as illustrated in Figure 9. If asymmetry is detected then a heel raise is provided under the suspect leg and this image is captured for comparison. This shape acquisition method is not quantitative and therefore relies heavily on the clinician's skill and therefore would not be a suitable shape acquisition technique for customised postural supports.

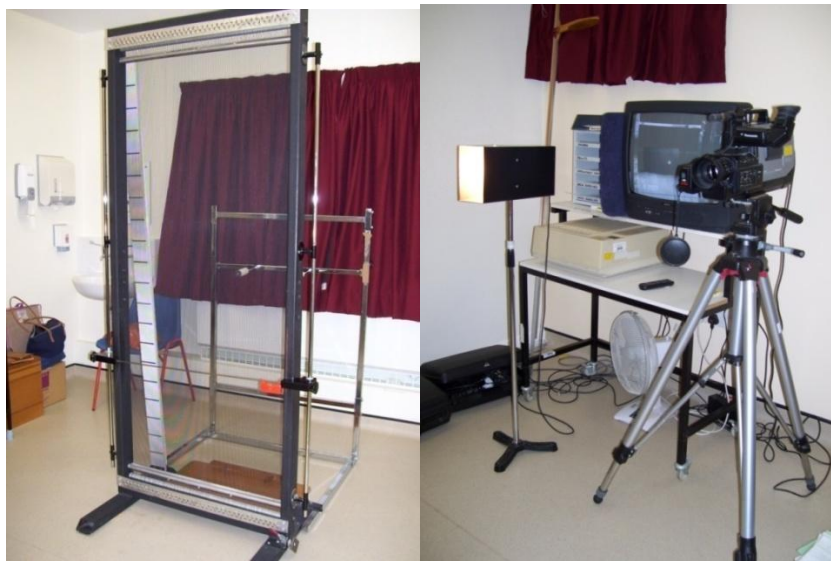


Figure 8. Moire Fringe equipment

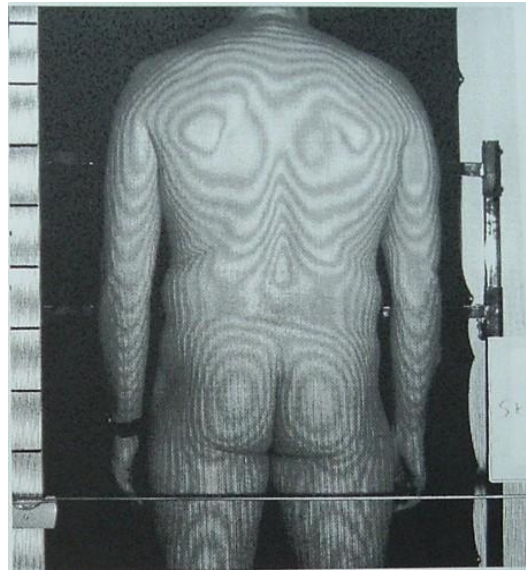


Figure 9. Moire Fringe image

### 3.1.6 Prosthetics Tracer CAD

The use of electronic shape capture in the prosthetics field reduces the fabrication time of a positive model of the patient's residual limb; it can also eliminate the use of the labour-intensive plaster process. The system used at Morrision Hospital, Swansea, is Omega's TracerCAD Pen, Figure 10. This technology uses a similar principle to the Otto Bock Shape System where an electromagnetic signal is emitted to determine the location of the Tracer Pen in space and conveys this information to the software. Alternatively, the software is used by entering circumferential dimensions of the limb and the prosthetist selects templates from a library of shapes that have been gathered and installed into the software. This use of a library of shapes bears similarities to certain concepts of this project.



Figure 10. The use of the Tracer Pen to record the 3D shape of the patient's limb (Ohio Willow Wood 2007)

### 3.1.7 Handy Scan 3D

The ERGOscan (Creaform 2008) is the scanner from the Handyscan 3D line-up that was developed especially for medical applications. This hand-held, portable and self-positioning laser scanner has many applications in the fields of orthotics, prosthetics, plastic surgery, podiatry and wound care. The system uses self-adhesive reflective markers to provide positioning targets which are used to create a reference coordinate system so eliminating the need for external tracking or digitizing arms, as shown in Figure 11. The advantage of this is that the object being scanned can move without corrupting the scan data. This feature can be particularly important if direct human scanning is being performed. The specified resolution is 0.1mm and up to 0.5mm for the accuracy.

The successful use of this scanner in the automotive industry has been reported where car seats are scanned in relation to the car interior for analysis purposes (Creaform 2007).



Figure 11. The Handy Scan 3D (Creaform 2007)

### 3.1.8 Summary

This review has investigated a variety of shape acquisition technologies, some of which are currently used (and commercially available) in the special seating field (such as the Otto Bock Shape System and Invacare's Pin Dot Machine). The use of electronic shape capture is well established in the prosthetics and orthotics fields (Ohio Willow Wood 2007), where several commercial shape measurement and design products exist. In contrast, much less has been accomplished within the specialised seating field. For the purposes of this project,

the shape acquisition method should be quantitative to a degree of accuracy and resolution which matches or exceeds the reviewed methods. The literature review in Section 3.2 discusses these attributes further. The system should also be suitable to capture the shape and sizes of seating system casts which have recorded the individuals' loaded shape.

Laser scanners are widely used in the automotive and aerospace industries, and also in the entertainment industry to digitise 3D models for movies and video games, for example. In addition, laser scanners are becoming more common in the medical field, such as in orthotics, prosthetics and facial surgery to capture 3D shape of patients. 3D laser scanners are used to acquire the x, y and z coordinates of millions of points of an object to generate a polygonal mesh of the part to recreate it in 3D. 3D scanners also aid the understanding and analysis of complex forms.

Shape analysis in the field of special seating has not been reported at the proposed level of accuracy and resolution potentially available with the use of laser scanners. The shape acquisition technologies employed in this study are 2 different laser scanners (the Microscan and Faro Scanner). The Microscan is the in-house scanner used as part of the Digital Seating Service at Swansea REU (Section 1.3). Access to the Faro scanner at a local college was gained as a result of a successful grant application. Section 5.1 details these shape capturing technologies. As part of this investigation, technical comparisons will be made between the scanners.

### **3.2 Literature review of shape acquisition methods**

There are many methods and techniques that measure 3D shapes (some of which were investigated above in Section 3.1), but few of them allow measurements to be taken in the seated position and most of them cannot be adapted to a wheelchair. The following literature review summarises four main systems which have been developed to measure body-seat interface shape; however each have their individual limitations which are described below in Sections 3.2.1 to 3.2.4.

### **3.2.1 Ultrasonic contouring system**

A method was devised which measured the contour of the buttock-cushion interface by using ultrasonic dimension gauging techniques (Kadaba et al. 1984). The ultrasonic transducers were placed (at 50mm intervals) in a Perspex frame beneath a gel cushion. This technique is limited to the material used for the buttock interface, for example ultrasound propagates poorly in foam type cushions (Kadaba et al. 1984). The use of this technique to predict internal stresses during sitting has more potential than for shape acquisition.

### **3.2.2 Force sensing probe system**

Brienza et. al developed a system with closed-loop functionality to provide the dynamic formulation of support surface on the basis of programmable criteria. The CASS (computer-aided seating system) aims to provide optimum seating conditions when the soft tissues are subjected to the least distortion, as shown in Figure 12. Pressures are measured over an 11x12 rectangular array (which equates to an area of 43x47cm) and a measuring resolution of 4.27cm. The pressure sensors are contained within swivelling heads on top of each support element; this is to ensure that the pressure transducer is orientated in a direction normal to the direction of the net force. The optimised shape surface can then be recorded according to the height of each actuator. The vertical position of each support element can be controlled through a range of 15cm by its stepper-motor-driven lead screw assembly (Brienza D. et al. 1996). This depth would be limited for the shape acquisition of complex shapes.

The outcome of this study revealed successful pilot experiments on ten able-bodied subjects, where the authors conclude that the system is unlikely to be developed into a clinical assessment tool, however may influence research into the design of custom-contoured support surfaces (Brienza D. et al. 1996) . Some of these systems could not be adapted to a wheelchair cushion because the probes passed through holes in foam cushions and therefore changed the supporting properties of the foam.

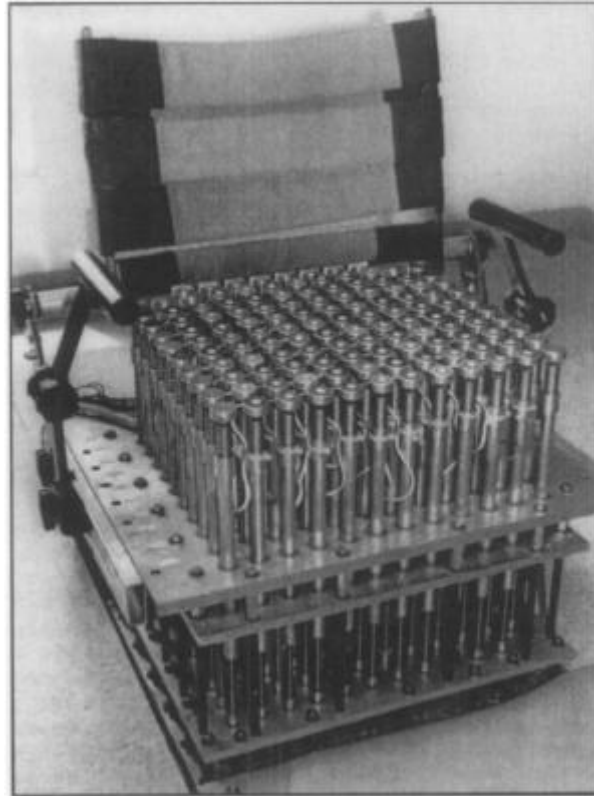


Figure 12. Computer-aided seating system (CASS) (Brienza et al. 1993)

### 3.2.3 Strain gauge system

A system has been designed to measure contact shapes and postures of thirty-two male drivers with two types of seat cushions and sitting postures (described as ‘free’ and ‘recommended’) (Yamazaki 1992). The measurement system consisted of flexible, thin sensor tapes each containing twenty strain gauges, measuring at a resolution of 30mm. The selected posture and resultant pressure determined the contact shape of the seat surface (Yamazaki 1992). This system could be adapted to wheelchair seating but was sensitive to electronic noise and calibration difficulty.

### 3.2.4 Shape sensing array system using optical fibre technology

Li et. al have developed an efficient, low-cost and easy-to-use device called the shape sensing array (SSA) system to rapidly capture the body-cushion interface shape in a clinical setting. The SSA mat is flexible, non-invasive and can be placed between the subject and seat without disturbing the subject’s natural feeling (Li et al. 2004).

The main component of the system is ten ShapeTape™s, which is a thin array of fibre optic curvature sensors laminated on a ribbon substrate. Each tape has a cross section of 1.2x12.5mm and has 12 sensors along a 480mm long sensing zone. The signals from the photodiodes and amplifiers are inputted into a C++ program that performs calibration, interpolation, integration, transformation, and imaging functions. The resultant shape of the ShapeTape™ is reconstructed by summing the bends and twists of the sensors.

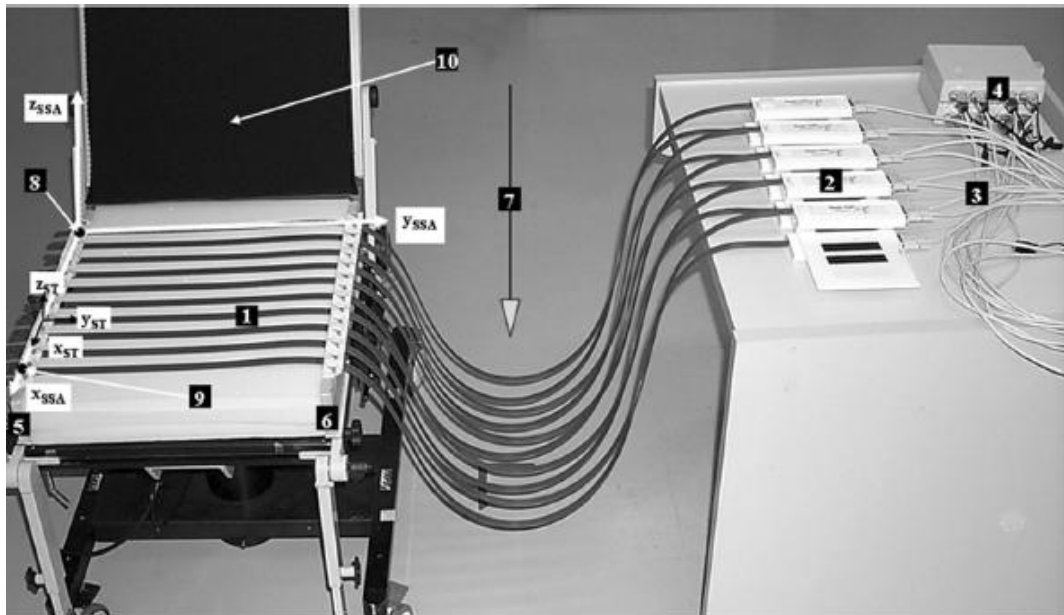


**Figure 13. SSA system (1) ShapeTape; (2) Interface boxes of ShapeTapes; (3) Serial cable with a power inlet connector; (4) 4\_1 serial-USB converter; (5) Fixture-A; (6) Fixture-B; (7) Plumb line; (8) "base" of ST1; (9) "base" of ST10; (10) Seating simulator. (Li et al. 2004)**

The resolution for the SSA system was 40mm which was chosen based on previous experiments (Brienza D. et al. 1993), where the optimal resolution was reported to be between 25 to 50mm, where low resolutions could cause attenuation of contour features. It is unclear of the justification for this, but it may be assumed that the optimal resolution choice was based on knowledge of the current or available technology. More recently, technology has allowed much greater resolution at a lower cost, see Section 0. The authors (Li et al. 2004) do accept that the SSA system may not be appropriate for measuring and evaluating a child's cushion, which have finer contour features than an adult one.

The accuracy of the SSA measurements were evaluated by comparing the results obtained by the SSA to measurement obtained by the Microscribe G2 digitiser (see Section 5.1.2),

where the accuracy of the Microscribe is 0.38mm. The rms (root mean square) error of the system in the Z direction was 2.19mm in absence of pressure and 4.72mm with pressure (Li et al. 2004). This error may be significant to certain individual's seating needs. The literature within the special seating field does not provide any guidelines regarding the optimum tolerances for different patient population. However from clinical experience, it is known that some clients (e.g. those more prone to pressure ulcers) have higher demands for more accurate shapes for seating, such as Motor Neurone Disease and Duchenne Muscular Dystrophy.

The SSA system's measurements were also influenced by pressure patterns and different interface materials, which is as expected. Despite the limitations of the SSA system, it has the potential for quick and effective cushion evaluation and clinical guidelines for cushion prescription. In addition, the system was also designed for research purposes which has the potential to prove fundamental to the successful design of generic-shape contoured support surfaces.

### **3.2.5 Summary**

These shape acquisition methods provide an overview of the technologies used for the collection of shape data in this area of research. The measuring resolutions ranged from 3.9 to 50mm in the reviewed methods. However, it is assumed that these resolutions were chosen due to the mechanisms and technology employed. Shape acquisition techniques using laser scanners offer a much greater resolution at a low cost, but it is unknown what the required accuracy is for special seating manufacturing. This project utilises high-cost (resolution of 61 $\mu$ m) and low-cost scanning (resolution of 100 $\mu$ m) technology which can capture very detailed shape information to enable optimum shape analysis to be performed.

The shape acquisition studies reviewed used consistent measuring apparatus which is clearly essential for research purposes where comparisons are required. The shapes used in this project have been sourced from three special seating centres and therefore each centre employs slightly different shape capturing methods, this may introduce some variations

which cannot be controlled. Inconsistencies may also occur due to different clinicians' shape capturing technique. These limitations are explored further in Section 7.1.

The shape acquisition methods reviewed in the literature have only been designed to capture base cushion shapes, and not backrests (with the exception of (Yamazaki 1992)). It therefore appears that there is a lack of research into backrest shapes. It may be that the range of backrest shapes is comparatively more diverse and this therefore poses more challenges for measurement tools and comparative analysis. This agrees with clinical experience, where the range of upper body support shapes can be greater than lower body/pelvic shapes.

---

## **4 SHAPE ANALYSIS**

---

The primary aim of the project is to perform quantitative shape analysis on 3D shape data. To achieve this, shape analysis approaches and techniques were explored. The following review aims to obtain an appreciation of these techniques to identify possible techniques that may be transferable to this project. The literature reveals that very few studies have explored the area of shape classification for special seating surfaces. In contrast, there has been widespread research into characterising human shape variation using anthropometric data and research within the automotive industry for car interior design. However, these classification techniques have not had to handle the variability in human posture that is experienced in customised seating as a consequence of disability.

### **4.1 Reason for shape analysis**

Many shape analysis techniques have been formulated to aid the retrieval process within database systems. An increasing number of digital images are being generated and therefore there is a demand to facilitate the searching of images. Good retrieval accuracy requires a shape descriptor to effectively find similar shapes from a database. The demand for and the supply of 3D models has increased because of faster graphics hardware and cheaper 3D scanning hardware. Large digital repositories of 3D models help create demand for search engines that are able to retrieve the data of interest and for data mining algorithms to discover relationships among them (Funkhouser et al. 2005).

Shape analysis is required in many scenarios, for example to enable a doctor to use an automatic classification system to aid diagnosis of a disease from the shapes of diseased organs. Similarly, a palaeontologist might use shape analysis to link similar 3D models scanned from animal skeletons of different species. The main challenge with 3D surfaces is that they rarely have similar parameterisations, making searches for pose registration, feature correspondences, and model parameters more difficult. Therefore, a specialised set of shape analysis methods are required for 3D data (Funkhouser et al. 2005). Methods for computer-aided shape analysis and retrieval are being pursued in several fields, including computer vision, computational geometry, and computer graphics (Funkhouser et al. 2005).

## 4.2 General shape representation and classification

The primary challenge in building a shape analysis and retrieval system is to develop a computational representation of shape (or shape descriptor or signature) for which an index can be built to allow similarity queries to be performed. These are important in object recognition to enable geometric attributes of an object to be described which are required for classifying, matching and recognising objects.

Dengsheng et al describe shape representation and description as a difficult task because when a 3D real world object is projected onto a 2D image plane, one dimension of object information is lost (Dengsheng & Guojun 2004). Shape representation and description techniques can be generally classified into two classes of methods: contour-based and region-based methods. The classification is based on whether shape features are extracted from the contour only or are extracted from the whole shape region (Dengsheng & Guojun 2004). For example, shape contexts are used by representing a discrete set of points sampled from the internal or external contours on the shape. These are obtained as locations of edge pixels as found by an edge detector (Mori et al. 2001). In region-based techniques, all the pixels within a shape region are taken into account to obtain the shape representation, rather than only use boundary information as in contour-based methods (Dengsheng & Guojun 2004).

Shape representation generally looks for effective and important shape features based on shape boundary information or boundary plus interior content. Perceptually similar shapes usually mean rotated, translated, scaled shapes and transformed shapes from a database (Dengsheng & Guojun 2004). Common global descriptors are area, circularity, eccentricity (length of major axis divided by length of minor axis), major axis orientation, and bending energy (obtained by integrating the squared curvature along the entire contour). These simple descriptors can only discriminate shapes with large differences and therefore are usually used as filters to eliminate false hits in database searches (Dengsheng & Guojun 2004).

Alternatively, many shapes can be represented by statistical properties. Some methods use histograms of geometric statistics (such as distances between points and the angles

between lines and planes). One research group uses the bins of the histogram as a uniform log-polar space (Mori et al. 2001). The histogram is made more sensitive to positions of nearby points than those of points farther away; these vectors are put into a log-polar plot. The matching of two shapes is done by matching two context maps of the shapes, which is known as matrix-based matching (Mori et al. 2001).

For 3D shapes, shape histograms can be obtained by decomposing concentric shells and sectors around a model's centroid (Ankerst et al. 1999). Figure 14 illustrates this concept where shape histograms for the protein, 1SER-B, are created for different shell and sector bins configurations. The histograms represent the number of surface points taken from the image (Ankerst et al. 1999). These histograms provide a shape descriptor to enable analysis or to act as a database retrieval mechanism.

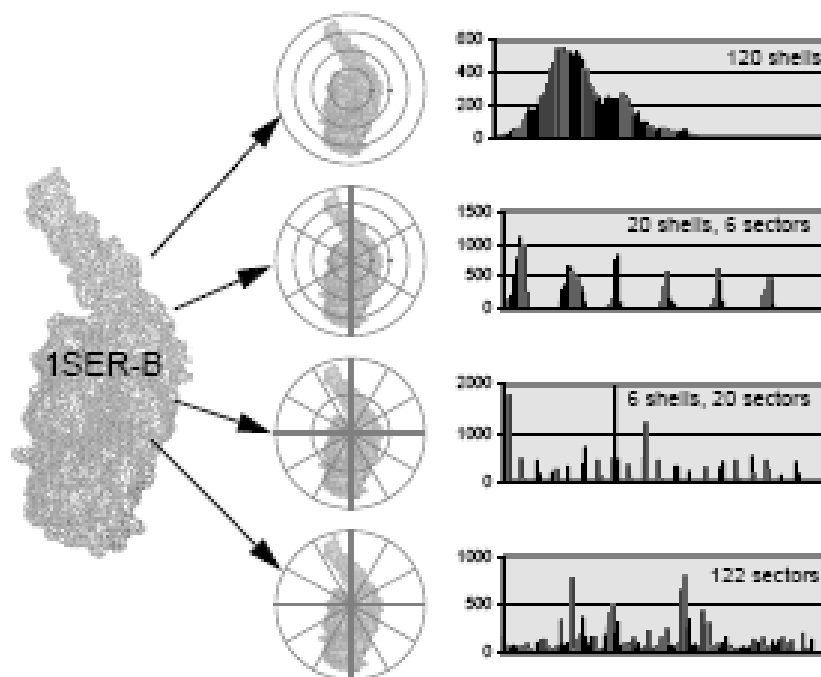


**Figure 14. Use of shape histograms by decomposing concentric shells and sectors around a model's (protein 1SER-B) centroid (Ankerst et al. 1999)**

These statistical methods are recommended for characterising large-scale shape features (Funkhouser et al. 2005). The mid-range of these methods includes view-based representations where the shape of a 3D object is described by a set of 2D projections from different views (Chen et al. 2003).

At the high-end of the range of methods, a shape can be decomposed into its parts automatically through algorithms that decompose its surface along concave seams, compute an approximation to its medial axis, or approximate its volume with a set of simple primitives (such as covering it with ellipsoids). However, these methods are generally time-consuming to compute, overly sensitive to small features and hence difficult to match and/or index for retrieval applications (Funkhouser et al. 2005).

Grid based (GB) methods was proposed where a grid of fixed cell size is overlaid on a shape, the grid is then scanned from left to right and top to bottom (Lu & Sajjanhar 1999). The cells which are covered by the shape are assigned 1 and those not covered are assigned 0 which results in a unique binary number. With this method, an object is first normalised for rotation and scale and is then mapped onto the grid (Lu & Sajjanhar 1999). The similarity measure of the GB method is that two objects are similar in shape, if and only if the difference between their binary representations is less than a specified threshold. Eccentricity of the shape was also measured to improve the efficiency of this method (Lu & Sajjanhar 1999). Eccentricity of shape is the ratio of the number of cells used in the x-direction to the number of cells used in the y-direction to represent the shape. Therefore for two objects to be similar, their shape signatures and their eccentricities values should be similar (Lu & Sajjanhar 1999).

Shape descriptors range from those that are simple to compare and are not very discriminating to sophisticated shape analysis which require expensive computations. Shape-based descriptors should generally be concise; efficient to compute; insensitive to noise and small extra features; and representative of key shape features (Funkhouser et al. 2005). It is “unlikely that any single shape descriptor will satisfy all these properties, as there are usually trade-offs between computational expense and discrimination power” (Funkhouser et al. 2005).

The comparison of shape representation and analysis techniques is difficult because results can be subjective. However, lower-level statistical shape descriptors are generally more successful in the application involving recognition, matching, and retrieval while higher-level methods are more appropriate to segmentation, classification and synthesis applications (Funkhouser et al. 2005).

### **4.2.1 Summary**

This review has provided an overview of the various techniques used for shape classification and representation which are essential to perform any form of shape analysis. This review has aided the identification of shape analysis methods that may apply to this project. For example, the use of global features such as area or volume may aid the classification of the customised seating systems. However, these descriptors will not provide the detail of analysis that is required to meet the objectives of the project. Instead, the volume of the shapes may be approximated to reduce the variables involved. With this approach, statistical techniques such as the use of histograms to act as shape descriptors may also be investigated.

## **4.3 Classification of human shape**

### **4.3.1 Medical imaging 3D shape analysis**

The move towards digital medical imaging has resulted in digital medical storage systems (e.g. PACS-Picture Archiving and Communication System), which enables a medical image database to be built. To enable clinicians to access this database, the image has to be classified or represented in some way to enable the retrieval within the database. In general, there are two kinds of features commonly used to represent image contents. One is obtained in the spatial domain, e.g. image pixel distribution, colour distribution and texture characteristic (Lee & Lou 2003). The other is obtained in the frequency domain, because some images have more distinct features in the frequency domain than in the spatial domain. For example, the use of Fast Fourier Transforms can be recorded as features of the image (Lee & Lou 2003).

### **4.3.2 Archaeometry and anthropometric shape analysis**

The increase in computer power and the development of multivariate statistics has made it possible to search for patterns in human variation. Cluster analysis is the most widely used multivariate technique in archaeometry, with the majority of applications being exploratory (Papageorgiou et al. 2001). Cluster analysis has a wide range of applications, which includes: pattern recognition, image segmentation, market research, and information retrieval and

DNA analysis. A cluster is a collection of objects that are similar to one another and are dissimilar to the objects in other clusters (Paquet 2004).

Pontikos shows that cranial variation and cluster analysis can be used to infer ethno-racial affiliation. Model-based clustering was applied to 2504 crania of 28 populations of homo sapiens, where fourteen separate clusters were identified, each of which corresponds strongly to either one of the original populations or a racial group (Pontikos 2004).

Other classification studies use cluster analysis to explore anthropometric data (Paquet 2004). Anthropometric data refers to a collection of physical dimensions of the human body. Understanding and characterising human shape variation is essential for better ergonomic design, e.g. clothing and automobiles (Azouz et al. 2006). Traditional anthropometry is based on a set of measurements corresponding to linear dimensions between anatomical landmarks and circumference values at predefined locations. Clearly, this provides limited information of the human body shape. CAESAR (Civilian American and European Surface Anthropometry Resource) was the first 3D surface anthropometry survey performed in the USA and Europe, where body measurements were taken from about 6000 civilians between the ages of 18 and 65 (Robinette et al. 1999). The Cyberware WB4 was employed which uses four laser scanning instruments mounted on two vertical towers where each tower moves the scanning instrument vertically (Cyberware 1999). Each generated 3D model containing around 300 000 triangles. A set of 74 white markers were placed at anatomical landmarks prior to scanning which were used to extract 3D locations of these landmarks.

Shape analysis of human shape is problematic due to the large number of measured points and the lack of consistent representations between different shapes. To aid the classification of the data, the initial task is to reduce the dimension of the data set and then find the clusters in the new dimensional space (Paquet 2004). There are different techniques available for dimensionality reduction, which include Principal Component Analysis (PCA). It is evident that PCA is widely used for shape analysis, particularly human shape analysis where the number of variables in a data set is large and is difficult to represent. PCA is used to represent data in few dimensions (e.g. three or less) by retaining the characteristics that contribute most to its variance. The principal components are uncorrelated between themselves, so that each component describes a different dimension

of the data. PCA was applied to the CAESAR data set to extract a reduced number of components representing the main modes of variation of the human body (Azouz et al. 2006). Azouz et. al show that some of these components correspond to commonly used body measurements such as height and weight (Azouz et al. 2006).

Jackowski et al. describes a surface recovery method which approximates digital 3D (of spherical topology) shape by a rational Gaussian (RaG) surface. The method uses a subdivision algorithm that positions large triangles in flat areas and small triangles in detailed areas in a shape to achieve a high compression rate (Jackowski et al. 2003). The triangulation uses an octahedron as the base mesh and subdivides it until the error between the mesh and the shape reaches a required tolerance, as illustrated in Figure 15.

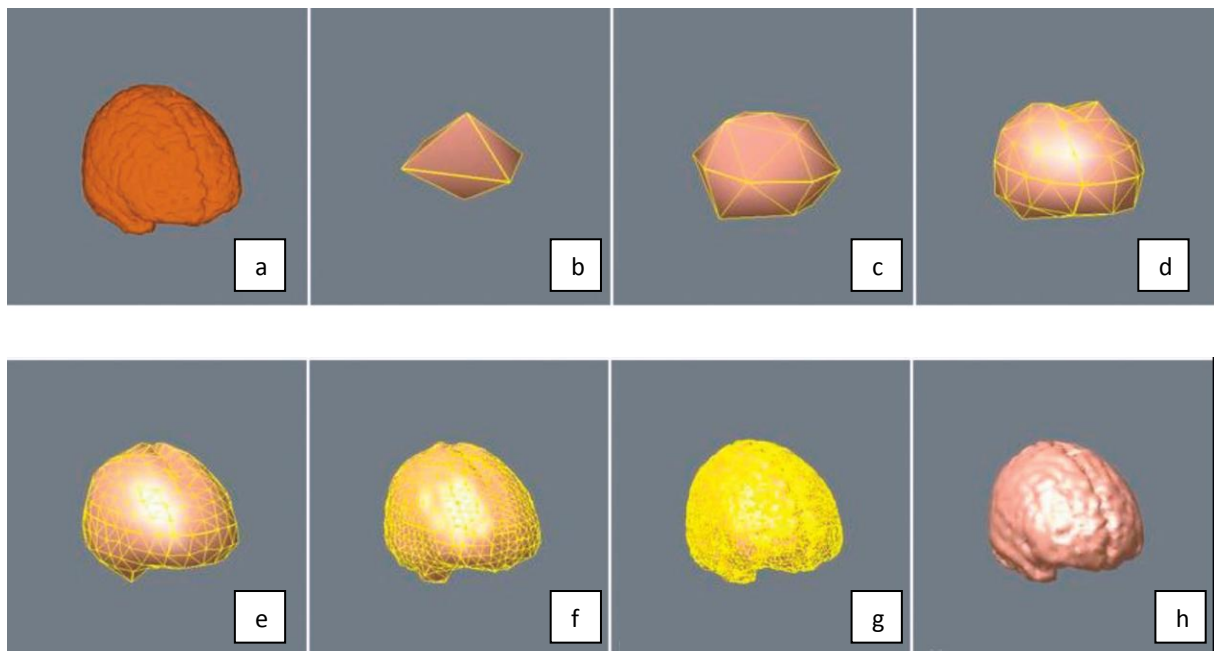


**Figure 15. (a) A digital volumetric brain. (b) Initial approximation of the brain by an octahedron. (c)-(g) Intermediate subdivision steps. (h) Brain shown by the final mesh in shaded form (Jackowski et al. 2003)**

### 4.3.3 Body-seat interface shape analysis

More specifically, few methods have been developed for the characterisation and classification of body-seat interface methods. The analysis and modelling of automotive seating has been extensively reported in the literature (Wahab et al. 2008); (Na et al. 2005); (Nakaya & Okiyama 1993); (Verver et al. 2005); (Yamazaki 1992). Yamazaki measured contact shapes and postures in thirty two male drivers with two types of seat cushion and

sitting posture: free and recommended (Yamazaki 1992), as described in Section 3.2.3. The author concluded that contact shape patterns provided data for seat design, however it was reported that there were large variations in contact shape when different subjects were sitting on the same driver's seat. The only classification that was provided was that the measured shapes were either concave or flat (Yamazaki 1992). Human back-backrest interface contours in automotive seating were also measured using a direct contact probe measurement system to reconstruct the statistical back contour of the American 50 and 95-percentile male. The model was used to suggest a revised SAE (Society of Automotive Engineers) manikin used to represent the driver populations (Nakaya & Okiyama 1993).

Perkash et. al developed a universal wheelchair seat cushion by taking plaster impressions of the seating area of spinal cord injured individuals (Perkash et al. 1984). The contours of the cushion were refined through eight iterations using feedback from a patient group. The study concluded that one seat design was effective for 52 out of 66 subjects that were investigated. Threshold pressures were defined to dictate the effectiveness of the cushion (Perkash et al. 1984).

(Li et al. 2000) et. al analysed the shapes of the body-seat interface using an electronic shape sensor to determine typical or generic shape patterns of thirty elderly people who were wheelchair users over the age of 65 years old (Li et al. 2000). The study used instrumentation as described in Section 3.2.2, where deflections of the 11x12 spring-loaded support elements were recorded. This data was interpolated to a 101x101 array. Five horizontal contours and five cross-sectional curves (three anterior-posterior A-P, and two medial-lateral M-L) were identified by a fixed percentage of length, width and height for the shape, as illustrated in Figure 16.

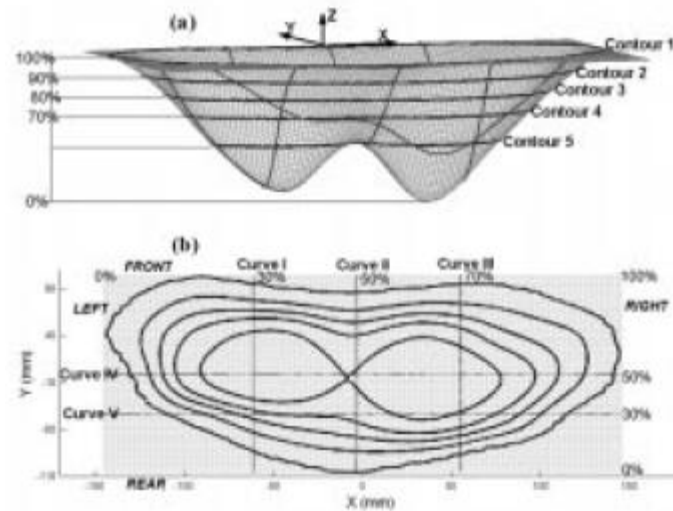


**Figure 16. Location of five contours on 3D shape data, e.g. Curve I is 30% of the width of the shape (Li, Y et al. 2000)**

A global description for each of the 30 shapes based on parameters developed by Li et al. (Li et al. 1998) provided 114 measurements, where 14 geometric parameters were measured on each A-P curve and 23 on each M-L cross-sectional curve. The number of measurements was reduced to 56 measurements by performing PCA to reveal the dominant geometrical characteristics of the interface shape which were related to anthropometric measurements, such as the distance between the ischial tuberosities. The authors considered that seventeen out of the 56 measurements played an important part in distinguishing the shapes, using ANOVA (analysis of variance) tests (where statistical difference was defined at the level of  $p < 0.05$ ). Some of these defining measurements include:

- Measurements indicating symmetry of the shape by defining a ratio between the volumes of the left and right part of the shape.
- Measurements describing the difference between the two lobes of the shape defined by a particular curve divided by the maximum depth of the shape
- Measurements describing the flatness of the shape, defined by the maximum depth of curve III divided by the maximum length of curve III.

Cluster analysis was used to detect natural groupings amongst the shape data. The Ward's hierarchical method was used to develop a dendrogram (as shown in Figure 17) where a derived distance measure was used (Pearson Product Moment) to quantify the

dissimilarities between shapes. This distance measure was used as it was not influenced by differences in scale between observations (which the Euclidean distance can do).

The dendrogram illustrates the presence of larger clusters characterising loose associations of shape patterns and smaller clusters that represent more closely related patterns. The first dichotomy (as indicated by A in Figure 17) divided the original 30 shapes into two clusters of 25 and 5 shapes. The larger cluster is hierarchically subdivided into two clusters of 6 and 19 shapes at the second dichotomy (B). At linkage distance 0.2, a four-cluster solution presents. Clusters C1 and C4 were subdivided into two more clusters at a linkage distance of 0.1, to form 6 clusters.

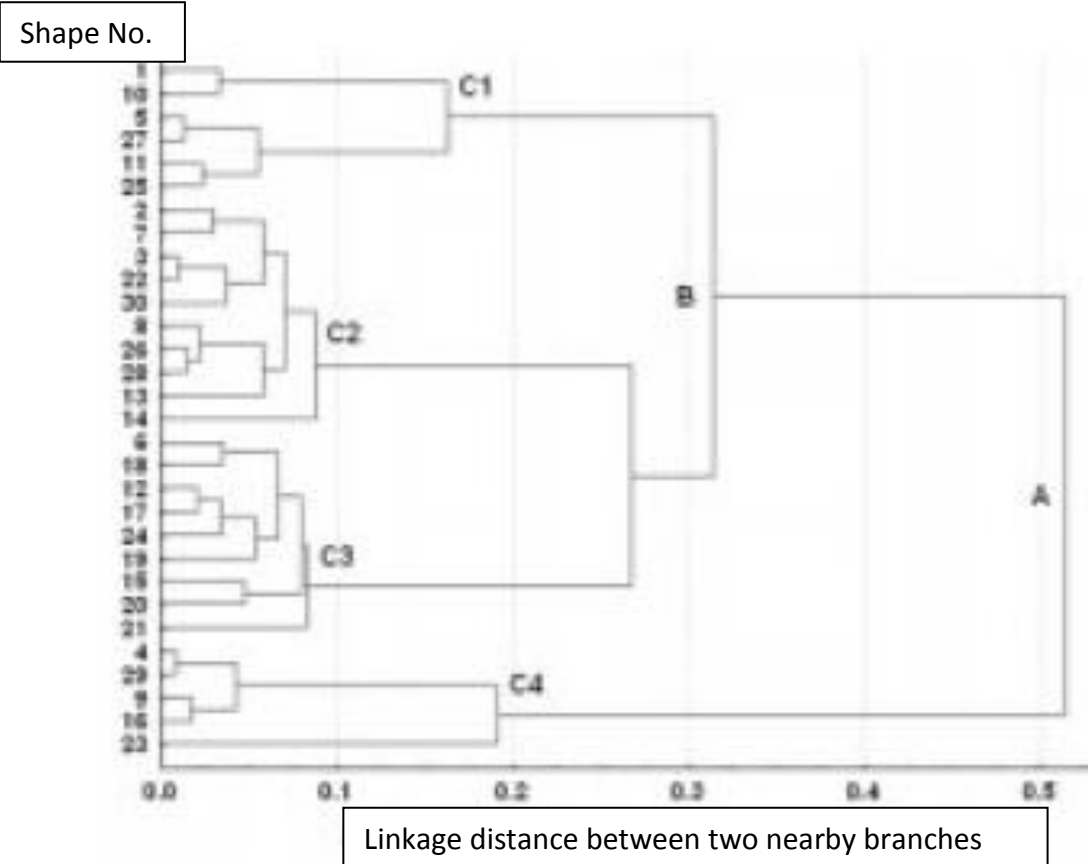
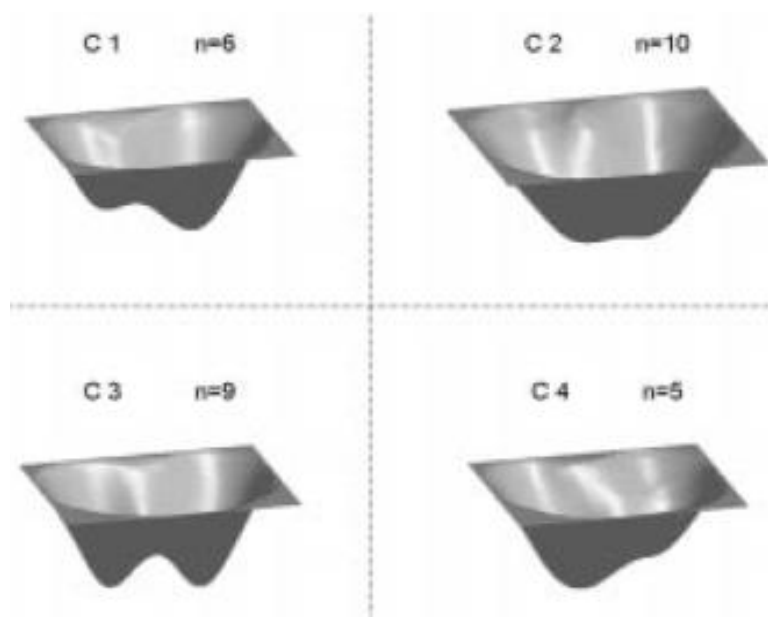


Figure 17. Dendrogram constructed using cluster analysis displaying 4 main clusters (C1, C2, C3, C4) (Li, Y et al. 2000)

The mean shapes for clusters C1, C2, C3 and C4 are displayed in Figure 18, which was calculated by finding the mean value of the 17 measurements for each cluster. These mean shapes are considered to be generic shapes.

Between-analysis showed that there were significant differences amongst the four clusters; however it was unclear whether differences between shapes were associated with intrinsic characteristics of the subjects (e.g. BMI-Body Mass Index, tissue tone, and skeletal structures) or extrinsic factors such as an adopted posture during the measurement procedure. The only notable relationship was that the difference between C2 and C3 likely occurred as a result of different BMI or weight. The study also concluded that subjects tend to have deeper contours and obese subjects tend to have flatter contours. This general finding was consistent to (Yamazaki 1992)'s study which qualitatively related deformation of the interface shape with body weight, and stated that the contact shapes of obese subjects were flatter and smoother than thin subjects (Yamazaki 1992).



**Figure 18. Mean shapes for clusters C1, C2, C3 and C4, considered to be generic shapes (Li et al. 2000)**

Li et al. do not consider the relationship between the subject's posture at the time of measurement and the resultant shape pattern. The study was designed to reduce these affects by ensuring a neutral position was adopted during each data collection process. In addition, photographs were taken to ensure that no obvious posture differences were

detected amongst the subjects. The authors suggest that future work may try to quantify the subject's seating position where more emphasis should be placed on bone structure deformity on shape pattern (Li et al. 2000). The authors do not describe any diagnosis or condition (if any) of the 30 geriatric subjects, however it is reported that the geriatric population will usually adopt a slumped, kyphotic posture and or asymmetrical posture (Zacharkow 1988); (Buck 1996) that might lead to pelvic obliquity (which is evident in Li et al.'s work).

This identification of generic shapes has the potential to develop generic-contoured seat cushions, which could be an alternative to the custom-contoured seat cushions and pre-contoured seat cushions where the results could influence the design of off-the-shelf devices to achieve a more accurate fit to individuals.

#### **4.3.4 Summary**

This review reveals that cluster analysis is a common statistical technique used to investigate the grouping of variables in human shape classification. The work of Li et al. (Li et al. 2000) exhibits similar goals to this project; however the investigation did not have to address the variations in shapes which were found with customised shapes in this project. In addition, the amount of data captured is considerably more due to the laser scanner employed in this project. This presents challenges due to the abundance of data collected. To perform cluster analysis, a method was devised to reduce the data to explore the use of cluster analysis, as described in Section 5.4. Another interesting classification approach which may be transferable to this project is the concept of representing surfaces as a rational Gaussian (RaG) surface, where a subdivision algorithm positions large triangles in flat areas and small triangles in detailed areas in a shape.

---

## **5 METHODOLOGY**

---

The main objective of this study is to develop a technique for 3D shape data collection and analysis of custom seating systems to advance the understanding and influence the fabrication process. To achieve this, laser acquisition technology was employed to scan 3D shape information from a sample of customised mould shapes. Two scanning technologies were compared which provided recommendations regarding the required accuracy. Shape analysis techniques were investigated for their ability to identify the global features of the shapes. Statistical properties of the shapes were also obtained to provide Shape Frequency Tables (or shape descriptors) by representing the customised shapes using standardised geometric shapes (column rods).

### **5.1 Equipment**

#### **5.1.1 Faro Scanner**

The Posture & Mobility Group Small Research Funding Scheme provided grant money to allow access to the Faro ScanArm (FARO Technologies Inc., Florida, USA). The FARO Scanner and services was provided by Digital Design Partnership (DDP), Coleg Sir Gar, Engineering Faculty, Graig Campus, Sandy Road, Pwll, Llanelli. The team provide high precision engineering services to Welsh companies related to digital design work, in particular reverse engineering is used by scanning a product to produce a CAD version. Quality assurance work is also carried out by the company where comparison software is used to compare the original CAD file to the scanned product, providing deviation results according to permitted tolerances.

The Faro scanner (specification detailed in Table 2, Section 5.1.2) is a seven-axis articulated positional measurement device, where a laser scanner head can be attached to a probe arm (a FARO platinum arm) to produce a non-contact system. Geomagic Studio software, version 9 (Geomagic Inc., CA) was used as the scanning and processing software.

Initially exploratory sessions were carried out with the DDP team to investigate the use of the scanner with different materials (Figure 19). A subsequent trial scanning session provided familiarisation with the equipment and a scanning protocol was agreed with the team to ensure consistent parameters are used for each scan. These requirements included:

- The external surface of the plaster casts was scanned. This represents the true shape of the client as captured from the vacuum consolidation technique. (Section 5.2 describes the different types of the casts).
- Automatic register colour function was used for each scan. This function on the laser scanner automatically adjusts the camera's parameters according to the material scanned

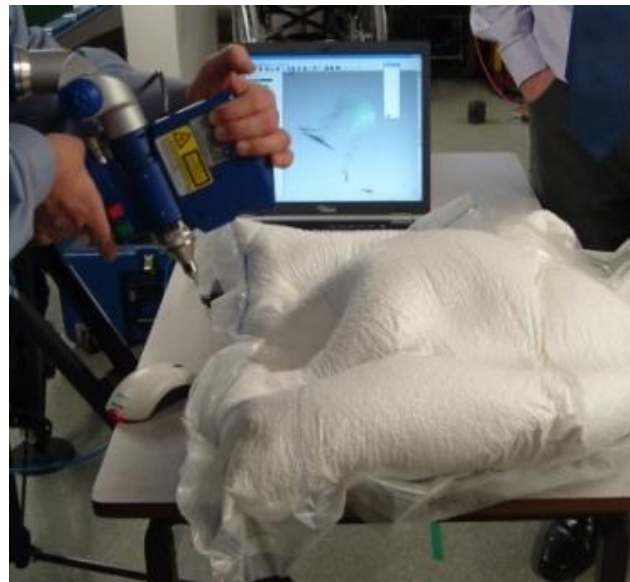


**Figure 19. Experimentation with Faro Scanner**

The processing of the scanned data was completed using the stages described in Table 1.

**Table 1. Description of processing of raw scanned data (Faro scanner)**

<b>Step</b>	<b>Process</b>	<b>Detail</b>	<b>Parameters</b>
<b>1</b>	Trim collected point cloud data to remove excess/ erroneous data	Use selection tools, including lasso, rectangle and brush tools	Lasso, line cutting and/or brush tools
<b>2</b>	Clean point cloud data	Use Select Disconnected  Select Outliers and Reduce Noise  in the Point Operation toolbar	Separation-Medium, Size 1  Sensitivity – 66.667%  Smoothness - Middle
<b>3</b>	Reduce points	Reduce points and create a Uniform Sample. Point spacing can be absolute spacing distance between points or target number of points.	Input – Absolute – Spacing = 1mm
<b>4</b>	Generate Wrap File	Creates a polygon mesh from the point cloud data (wrap). The wrap type can be Surface of Volume depending on what has been scanned.	Wrap Type – Surface Sampling: Point spacing – 1mm Noise Reduction - Auto
<b>5</b>	Clean polygon Data	Use, Clean  Repair Intersection  Remove Spikes  In the Polygon Operation toolbar.	Free Form  Select and Clean  Smoothness Level-Middle
<b>6</b>	Fill Holes	Fill any gaps in the data (holes) to create a mesh with only one boundary curve.	Use Bridge tools. Fill holes tools and/or fill partial.
<b>7</b>	Make Manifold	Create polygon mesh after filling missing data (fill holes) to make sure you have a mesh with one boundary curve.	Make Manifold-Open
<b>8</b>	Export as STL	Save file as an STL file. Options are ASCII or Binary STL.	Export as STL (ASCII) file

Calibration is performed once a year by the manufacturers. The calibration is in two parts: the touch probe is calibrated by touching a spherical ball, this ensures the Faro Arm knows where the scanner head is in relation to where the base of the arm (the 0, 0, 0 position) is. Secondly, the laser scanner is calibrated by using a calibration plate where the touch probe is used to register the plane and then the scanner head is moved in arc motions over the plate.

Each scan was performed on a specially constructed table which the scanner was mounted to. The table is a granite bed (1800 x 1800x150mm) mounted on a steel frame with isolated rubber feet, as illustrated in Figure 20. The cost of the table is approximately £1000 plus installation.



**Figure 20. Faro Scanner and scanning table**

The FARO scanner collects tens of millions of points, where the raw pointcloud file sizes are between 5-30MB. The converted STL files range from 50MB to 160MB depending on the size of the cast. Figure 21 illustrates an example of the Faro scanned images. The time of each scan varied from half an hour to an hour depending on the complexity of the cast. Deep recesses resulted in longer scanning times. This is therefore relatively time-consuming when compared to the Microscan (Section 5.1.2), and is reflected in the slightly slower scanning speed from the scanner's specification (Table 2).

Once the scan was complete, the raw point cloud data was converted to a wrap file and then exported as a STL (Stereolithography file) using ASCII format. This file format is consistent with the file format which is exported from the Microscan, which was important for the scanner comparison work (Section 5.3).

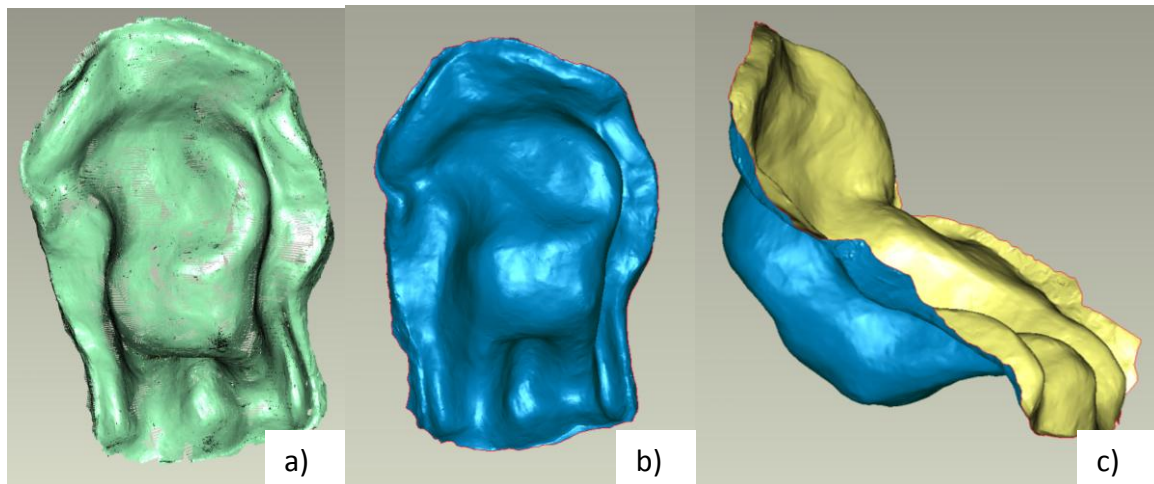


Figure 21. Faro scanner images a) Raw sweep data b) and c) Meshed STL files

### 5.1.2 Microscan system

The Microscribe G2LX/Microscan (Immersion Corp., San Jose, CA, USA) is the in-house scanner at Swansea REU which is used routinely for clinical work as part of the Digital Seating Service (described in Section 1.3). The Microscan is constructed similarly to the Faro scanner, where the scanner head is attached to the digitising arm, as shown in Figure 22. The system may be used as a point-and-click touch probe or the scanner head may be used to image the surface as the laser head is swept a short distance above the surface by moving the arm. The digital encoders in the joints of the arms provide the 3D positional data relative to the laser captured information. The scanner is the preferable data capturing method for clinical work at Swansea REU, because it provides a quick and easy technique, which is likened to spray painting. An excess of points are often collected, but these can be reduced accordingly during the post processing steps. Microscan Tools (v 1.1.19, Patrick Gutbell) is the software which is used for shape capturing and for post processing.

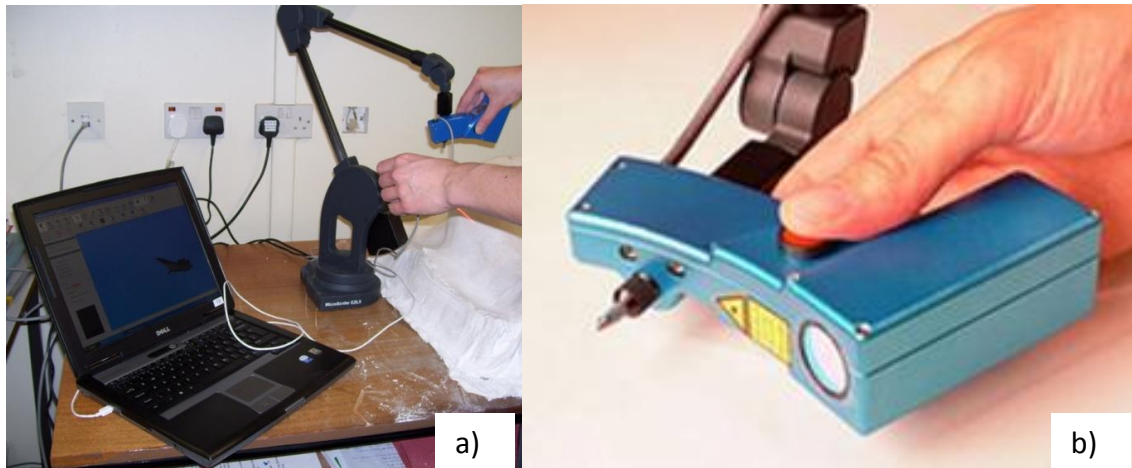


Figure 22. Microscan a) Scanning in progress b) Scanner component

The Microscribe's (touch probe) measuring resolution is dependent on a combination of the user technique and settings, this may create inconsistencies and therefore may not be ideal for research purposes, for example certain contours of the shapes may be omitted due to the chosen digitised points on the shape.

Table 2 lists the specification for the Microscan (Immersion Corp., San Jose, CA, USA) compared to specification of the Faro ScanArm (FARO Technologies Inc., Florida, USA).

Table 2. Microscan and Faro scanner specification compared

Specification	Microscan	Faro
Degrees of Freedom	6	7
Resolution	$\pm 100\mu\text{m}$	$\pm 61\mu\text{m}$
Accuracy	$\pm 100\mu\text{m}$	$\pm 61\mu\text{m}$
Weight	7kg	9.5kg
Speed	Up to 28,000 points per second	19,200 points per second
Size	150mm square	200mm square
Workspace	1.675m spherical volume	2.8m spherical volume
Laser type	Laser type 660nm, 1mW	Laser type 660nm, CDRH Class II/IEC Class 2M
Cost	£15,000	£100,000 (including £20,000 for software)

The Microscan must be calibrated whenever the scanner head (as shown as the blue component in Figure 22) is detached and reattached to the Microscribe (the digitising arm), which may be required if the scanner is transported. The calibration is necessary for the software to establish its alignment between the Microscribe's 6<sup>th</sup> axis (i.e. where the

Microscan is attached) and the Microscan. A calibration sphere is used which sits on a mini tripod, and a scanning sequence of 40 sweeps of the sphere is performed. The resultant calibration result is the average deviation of the scanned data from an ideal sphere which has been fitted into the scanned data (specified acceptable calibration values are 0.11-0.13mm).

Before each scan the digitising arm is placed in the 'Home' position and the system is reset, this calibrates the encoders in the joints and established an origin at the base of the digitising arm.

Laser scanners rely on a signal reflected back from the object surface to the receiving unit. White surfaces provide strong reflections whereas reflections are weak from black surfaces. Environmental conditions can affect the function of the scanner, such as temperature and interfering radiation (e.g. sunlight or lamps). This agrees with clinical experience where the best material to scan is matt white, such as a plaster cast. However, it has been established as part of our clinical work that by changing the camera's parameter other materials can be scanned equally well. Table 3 describes the camera's parameters and the values used for this study. The exposure (in milliseconds) of the camera can be adjusted (range 1-10ms) according to the colour and type of material being scanned: the higher the value the more sensitive the camera is (to reflections and noise). Therefore, for black materials an exposure of 10ms is required. Other parameters of the camera may be adjusted to tolerate shiny surfaces. However, reflections can also be reduced by turning some of the lights off in the room where scanning is being performed.

All scans using the Microscan were performed in the same room where the scanner was positioned on an office desk. The Microscribe/Microscan manufacturers state that mounting the digitising arm to a table is optional using a single bolt through the base of the system. This was not considered necessary because the scanner is often moved for each scan to accommodate the cast on the desk. However, any environmental vibrations that may have been present during scanning may have influenced the measurements. This less secure mounting was chosen as it represented the clinical situation (e.g. in a patient's home) and these tests are designed to inform whether or not the results are acceptable. The scanner camera's parameters were kept consistent for each scan, Table 3 details these parameters

**Table 3. Microscan camera parameters used**

<b>Parameter</b>	<b>Detail</b>	<b>Value</b>
Scan rate	Adjusts the rate of profiles the scanner is capturing per second (Maximum value= 50Hz)	20 Hz
Exposure	Adjusts the camera exposure time in milliseconds. The higher the value the more sensitive the sensor is. (Maximum value = 10ms)	5ms
Tolerance	This changes the width of the laser beam, the higher the value the more tolerant the sensor is to reflections and irritations in the reflected laser light (Maximum 50 pixels).	50 pixels

Experimentation with the Microscan has been ongoing as part as the Digital Seating Service at Swansea REU. This is provided the knowledge of the optimum parameters and technique. A scanning protocol was created to ensure consistency between scanning of shapes; the parameters chosen are detailed in Table 4.

**Table 4. Description of processing of raw scanned data (Microscan)**

Step	Process	Detail	Parameters
1	Trim sweeps to remove excess/ erroneous data	Use cutting tools	Lasso and/or line cutting tools
2	Reduce points	Reduce points	Detect 1 in every 2 points
3	Register sweeps	Registers each sweep to all other sweeps in an object by distance, which minimizes the deviation between sweeps and improves the quality of the final mesh.	2.00mm 10 iterations
4	Generate Pointcloud	Converts the scanned sweeps into a pointcloud and adds a defined reduction value. A point cloud is a set of vertices in a three-dimensional coordinate system, defined by X, Y and Z coordinates.	Keep every 3 <sup>rd</sup> point
5	Detect noise	This counts for the neighbouring points in the specified radius	Radius=2.5mm Count= 3
6	Smooth Pointcloud	The smoothing is done by locally computing a polynomial surface at each point and then projecting the point on this surface (also known as the moving least squares method MLS).	Radius=2mm Degree=3 Density=5mm
7	Mesh formation	Triangulation function	Open object selected
8	Smooth Mesh	Smooths the mesh by averaging between neighbouring points. The algorithm computes for all points the average of all its neighbours and then assigns the point the weighted sum of its average and original position	Average Complete Iteration=5 Weight=0.4
9	Split back and base (only applicable to full moulds)	Use cutting tool to split full moulds into two components. Rotate mould and use side on view and split where sides of base are horizontal.	Use rectangular cutting tool
10	Export as ASCII	This file format contains the x, y, z coordinates of the processed points . The file is also comma-delimiting, therefore can be read as a text file.	Export as ASCII file

Figure 23 illustrates examples of processed Microscan images. For each shape, scan information was recorded during the defined post-processing method (Table 4), e.g. volume of scan data.

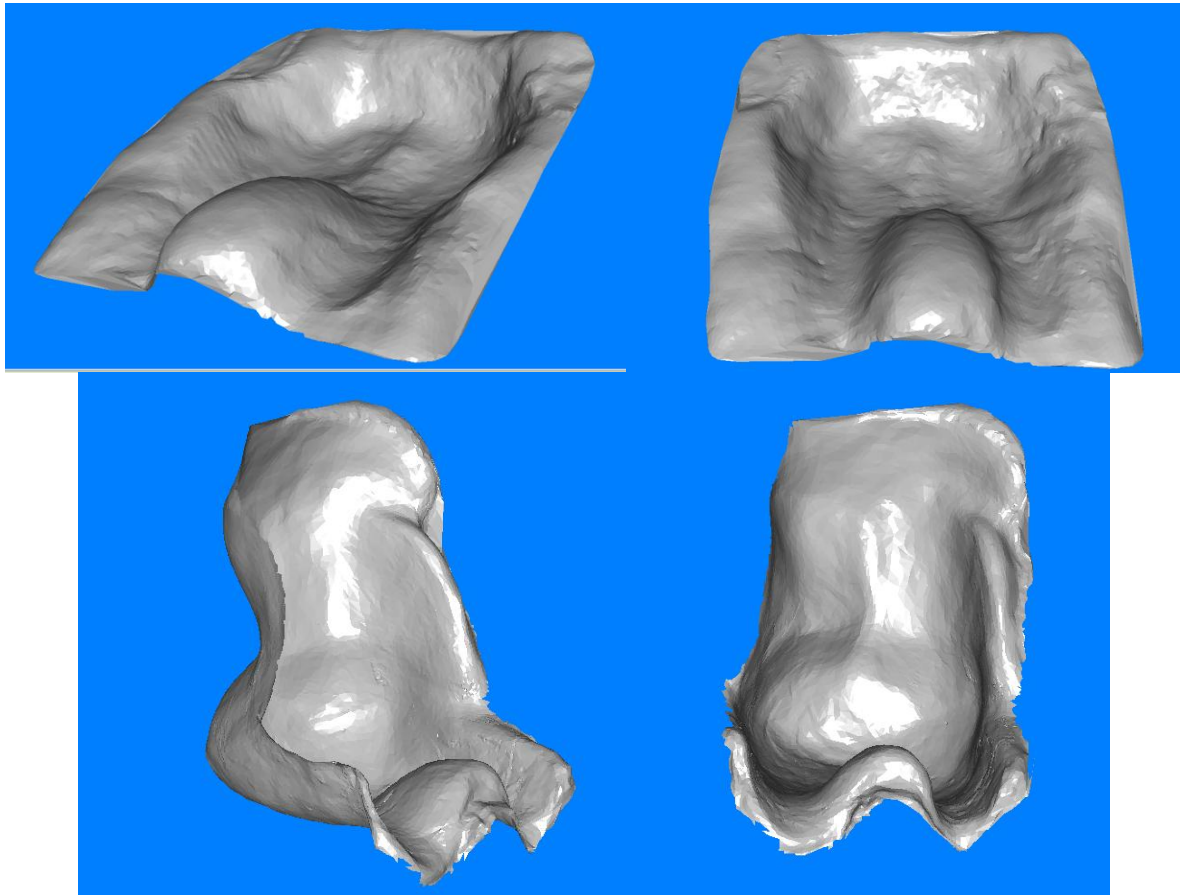


Figure 23. Processed Microscan images (Shape ID SWJM and CH1)

## 5.2 Shapes

The study population was 25 original casts used in the manufacture of customised seating systems and/or final moulded seats for patients with complex postural needs. The Appendices, Section 11.1 contains photographs of the casts used. No ethical approval was required as no direct patient contact was part of the study and all patient information associated with the custom seating system remained anonymous.

The inclusion criterion for the casts was: any available seating systems for scanning from 3 special seating centres: Swansea (SW), North Wales (NW) and Chailey Heritage Services (CH) in East Sussex. The exclusion criterion was that damaged or severely worn systems were

excluded. Table 5 provides details of the 25 casts. It was considered important to obtain a representative sample of postural shapes from the UK with a range of postural deformities.

The sample size was 25 casts; which were scanned by both the Faro Scanner and Microscan. The time associated with the data collection and post-processing for each cast influenced the chosen sample size of 25. The project is a pilot, the purpose of which is to develop protocols for acquisition and analysis of 3D information of seating systems. It is envisaged that this work will form the foundation of a larger study in the future with larger sample sizes.

**Table 5. Details of Samples (Casts)**

Cast ID	Origin	Details	Photo of example cast
SW	Swansea Rehabilitation Engineering Unit, Morrison Hospital, Swansea SA6 6NL	11 plaster casts: <ul style="list-style-type: none"> <li>• 7x full moulds</li> <li>• 2 x Bases</li> <li>• 2 x Backs</li> </ul> Manufactured using Plaster of Paris	
NW	North Wales Rehabilitation Engineering Unit, Bryn Y Neuadd Hospital, Llanfairfechan, Conwy, LL33 0HH	10 plaster casts: <ul style="list-style-type: none"> <li>• 4 x full moulds</li> <li>• 3x Bases</li> <li>• 3x Backs</li> </ul> Plaster of Paris filled with expanding foam	
CH	Chailey Heritage Clinical Services, Rehabilitation Engineering Service, Beggars Wood Road North Chailey Nr Lewes BN8 4JN	4 x full moulds  Liquid plaster poured into plaster shell which is very heavy causing transportation problems.	

### 5.3 Scanner comparison/validation

One of the aims of the project is to compare the three shape acquisition techniques, which may provide recommendations regarding the most appropriate scanning methodology required for research purposes and CAD/CAM manufacturing of these systems.

The scans from the Faro and Microscan were compared for 10 shapes. A range of casts were chosen to achieve a representation from the different locations. The chosen shapes are listed below.

- CH1
- CH2
- CH8
- NW2
- NW3
- NW4
- NW9
- NW10
- SWJD
- SWLM

Using Geomagic Qualify, version 9 (Geomagic Inc., CA), the 3D shape information was overlaid and compared to produce 3D comparison results, providing deviation results. Geomagic Qualify, version 9 (Geomagic Inc., CA) is inspection software which enables accurate, graphical comparisons between CAD models and as-built parts to provide 3D deviation results used for quality assurance, trend analysis and in-depth assessment.

The file formats for from both scanners were exported as STLs (ASCII type). Both files were imported in Geomagic Qualify, and were assigned as follows:

- Faro= "Reference", Microscan= "Test"

The "Reference" model acts as the gold standard and would typically be an original CAD model, the "Test" model is the shape to be investigated and would typically be a built part in a conventional quality inspection scenario. For the purposes of this investigation, the Faro scans are considered the reference because of the FARO's higher specification (Table 2).

The 'Best Fit Alignment' function was used to overlay the two images, this is performed in two stages where a rough alignment is performed by using 300 points and this is followed by a finer adjustment which uses 10,000 points to align the two scans.

The '3D compare' function was then used to create the deviation results, the following tolerances were entered:

- Max deviation allowed (default)= 36.5mm, this means that any deviation larger than this will appear grey
- Colour segments=7
- Max critical=1.0
- Max nominal=0.5
- Min nominal=-0.5
- Min critical=-1.0

The 'Create Report' function allows the graphical 3D deviations to be created as a pdf and word document. This provides statistical results which summaries the deviations between the two scans.

The reports using these narrow tolerances did not adequately describe the 3D deviations for some of the shapes, because some of the deviations exceeded the tolerances. Therefore, a proportion of the shapes were re-evaluated with the following tolerances being used to generate duplicate reports:

- Colour segments=7
- Max critical=2.0
- Max nominal=1.0
- Min nominal=-1.0
- Min critical=-2.0

Section 6.1 summaries these results and the Appendices, Section 11.2, contains the complete 3D comparison reports.

## 5.4 Data Analysis

### 5.4.1 Column rod representation concept

The review of shape analysis techniques in Section 4 provided an overview of the various techniques used for shape classification and representation which are essential to perform any form of shape analysis. This review indicated ways to classify the shapes using global features such as area or volume. The bounding box sizes were obtained from the samples and are detailed in Section 6.2.1. These descriptors will not provide the detail of analysis that is required to meet the objectives of the project. However, the vast amount of 3D coordinate data that has been collected by the scanner has to be represented in some way to provide an efficient analysis process. Funkhouser et al described the following: a shape can be decomposed into its parts automatically through algorithms that decompose its surface or approximate its volume with a set of simple primitives (Funkhouser et al. 2005). Representing the shape volume into its primitives reduces the variables for analysis to take place. This concept was considered applicable to the project as it provides a method of analysing the shapes, however it is not analysing the surface directly but instead a 'shape function' is derived. This shape function is referred to as a 'Shape Frequency Table' in the results. In addition, this shape representation approach provides a representation of the volume that would equate to the final manufactured seating system.

The concept of representing these shapes using 50x50mm column rods (with variable heights) was explored by virtually building the representation in CAM software called Maya Expert (version 7, Picasoft). These images are shown in Figure 24, where the resolution appears too large and smaller sized columns should be used. The 3D coordinate data from the scans can be analysed to calculate the heights of these rods. The following sections describe the methodology adopted to obtain these column heights.

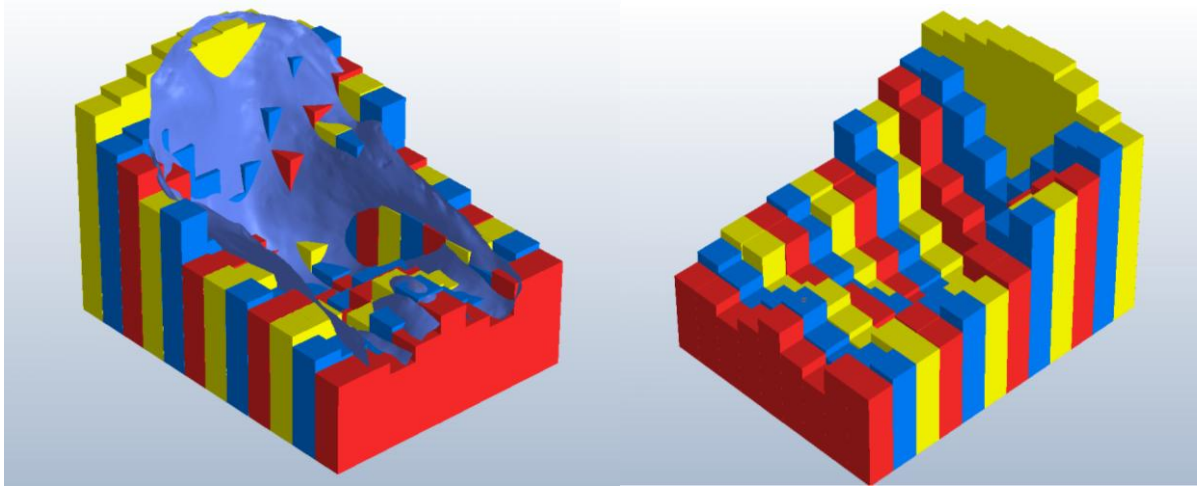


**Figure 24. Column Rod representation of 3D scan of customised mould illustrated using Maya Expert (version 7, Picasoft)**

#### **5.4.2 3D coordinate raw data**

The results as described in Section 6.1 validated the use of the Microscans for research purposes and was therefore considered suitable for the 3D shape analysis work in this project.

The ASCII files containing the processed raw data (which were exported from the Microscan) were imported into Rhinoceros 3D, version 4.0 (Robert McNeel & Associates, Seattle, WA). Figure 25 and Figure 26 illustrates the raw points imported into Rhino.

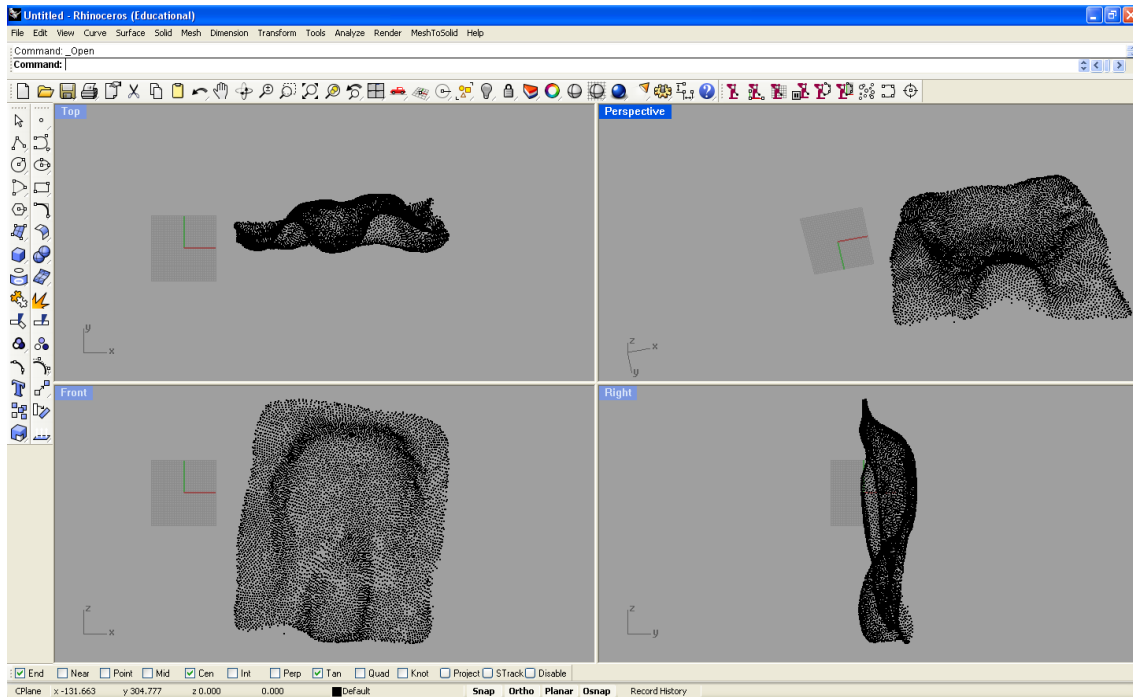


**Figure 25. Raw points imported into Rhinoceros 3D version 4.0 (Robert McNeel & Associates, Seattle, WA) from an ASCII file**

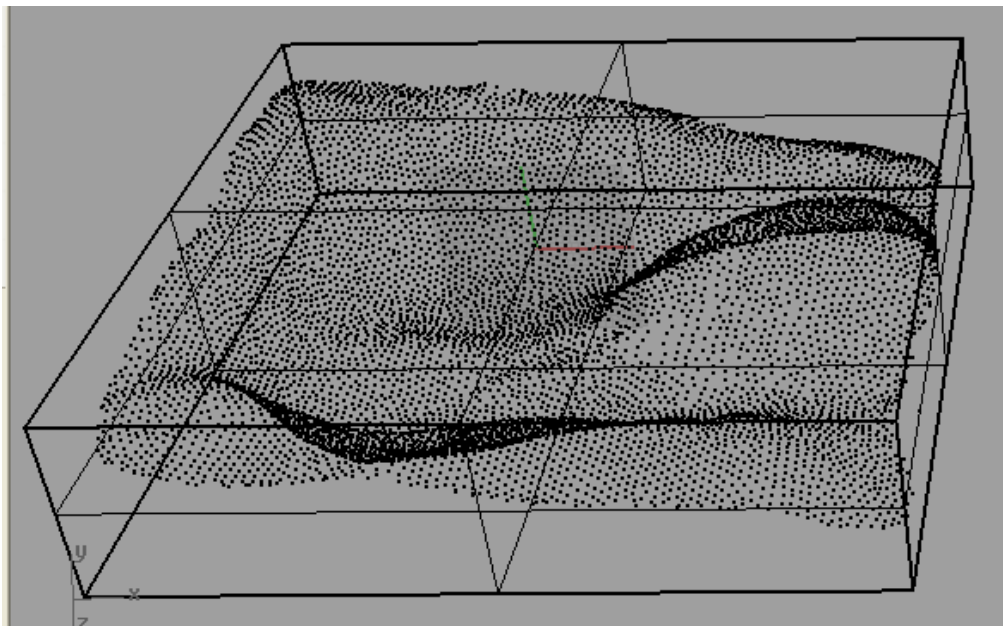


**Figure 26. Raw points imported into Rhinoceros 3D 4.0 (Robert McNeel & Associates, Seattle, WA) from an ASCII file, with bounding box**

The software allowed the orientation of the shape to be changed by rotating the object to a horizontal/level position (as shown in Figure 27 and Figure 28). For a 'Base' a consistent approach was used where a neutral position was set where the thighs were considered in a

horizontal position. For a 'Back' shape the orientation was set where the sides of the backrest were positioned vertically. This ensured that each shape was positioned in the same axes system. This consistent axes system is illustrated in Figure 29, where the y axis represents the height of the shape. A bounding box was also added to each shape, which is calculated by the minimum and maximum point in each axes plane (as shown by the boxes displayed in Figure 27 to Figure 29). The dimensions of the bounding box were recorded and the results are described in Section 6.2.1.

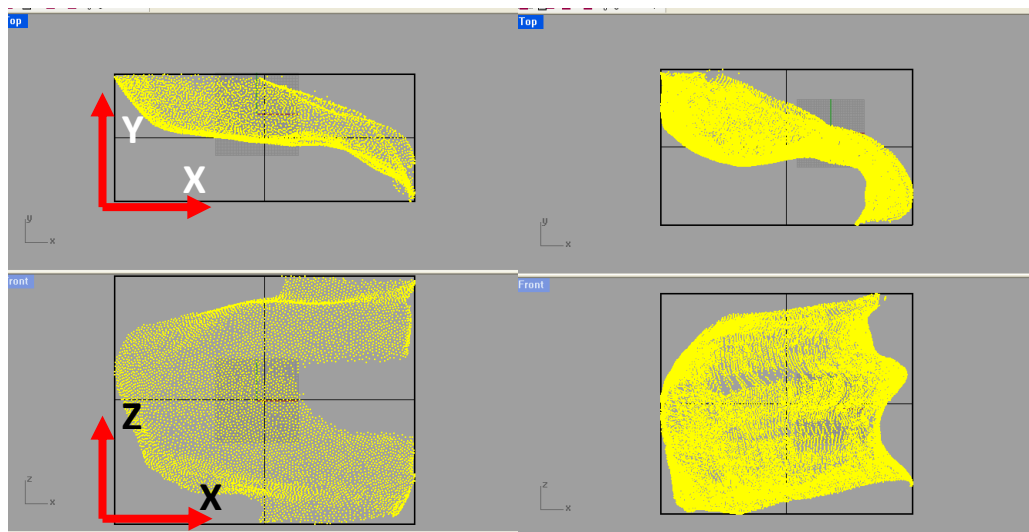


Figure 27. Consistent orientation of Base shapes (SWGJ and SWLM) where thigh position is approximately horizontal

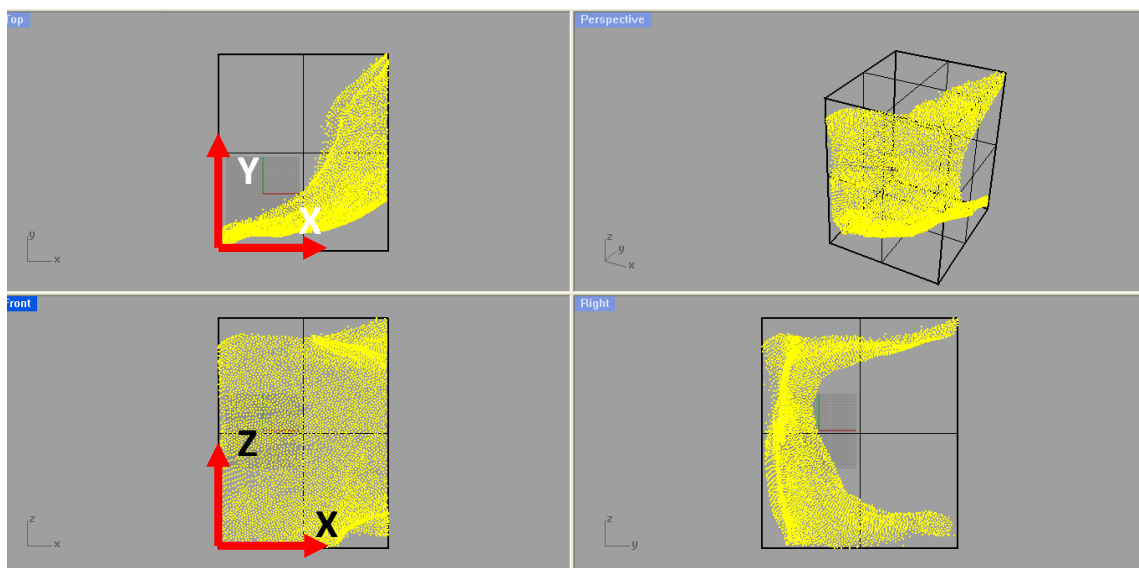


Figure 28. Consistent orientation of Back shapes (SWGJ) where sides of back are positioned vertically.

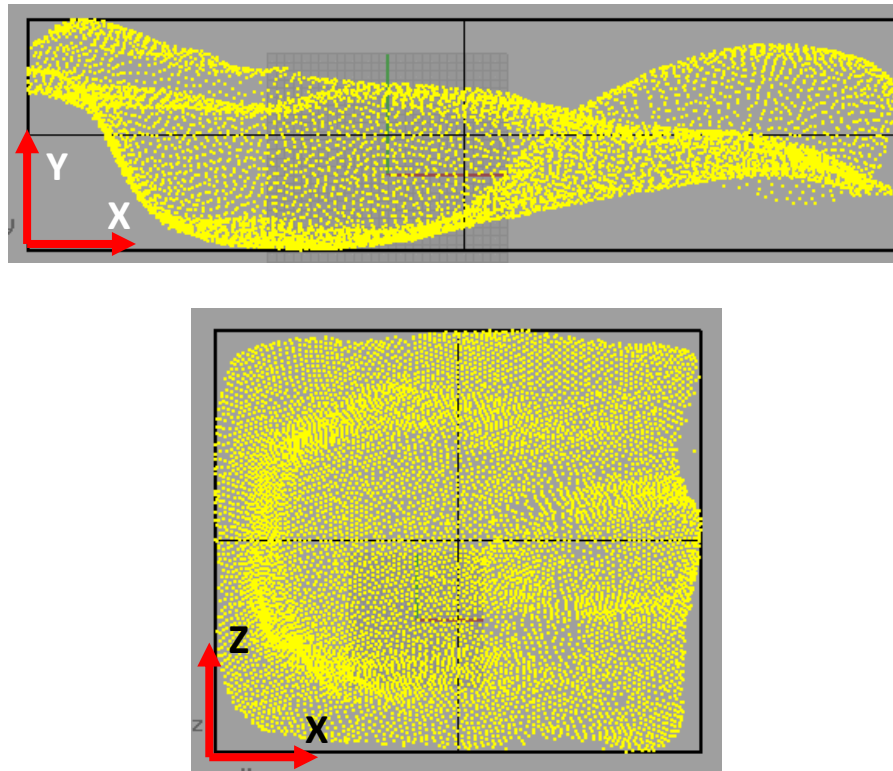
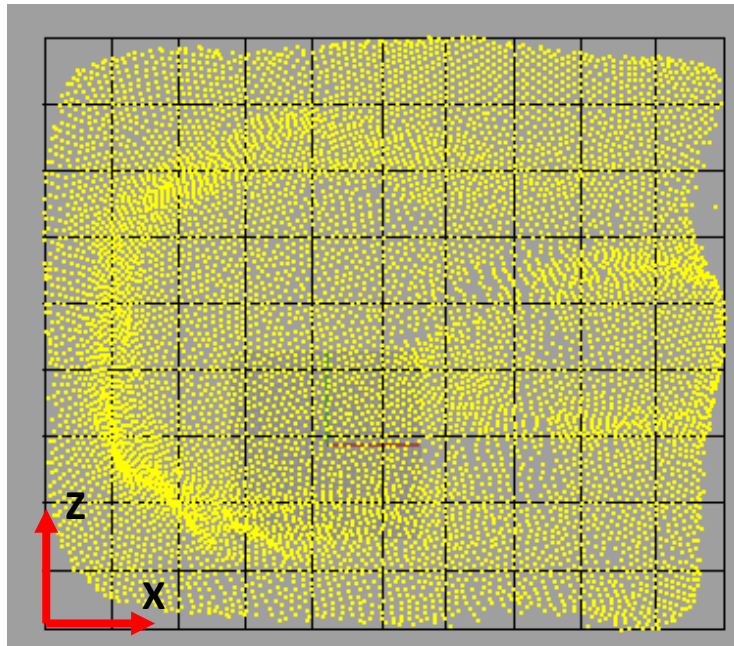


Figure 29. Axes system adopted for all shape analysis, where  $x$ = length,  $y$ =height, and  $z$ = width

The re-orientated raw data was then exported as comma separated values (.csv) file which resembles a text file with  $x,y,z$  coordinates of all the points listed.

### 5.4.3 Manual calculations

A method was required which provided an output of the height of these columns representations for a given shape using the 3D coordinate data (the input). The average  $y$  coordinate value from 3D raw data was required for each grid cell. Figure 30 shows the cast SWJM with a grid overlaid onto the shape to illustrate the analysis technique required. The image highlights that more points exist in some grid cells than others, in particular in highly contoured areas.



**Figure 30. Cast SWJM with a grid overlaid to illustrate proposed analysis technique**

The calculations required to find the average  $y$  coordinate value for each grid cell is described in Figure 31 and Table 6.

x_raw	y_raw	z_raw	x (sorted)	y (sorted)	z (sorted)	x_norm	y_norm	z_norm	x_location	y_norm	z_location	x_location	y_norm	z_location	x_location	y_norm	z_location	Mean	Deviation from mean	mean of AD	S.D for Grid ref 0,7
-18.718	-52.115	-86.621	-245.269139	-115.2832	-184.4959	226.5513	63.16844	97.87454	11	63.1684	4	0	61.1105	10	0	54.1044	7	52.9941276	1.232683325	0.962346423	0.98099257
-16.778	-59.619	-79.005	-244.849184	-115.2139	-184.4555	228.4915	55.66398	105.4912	11	55.664	5	0	64.3311	11	0	51.5368	7		2.123713328		
-33.162	-57.899	-82.776	-244.539524	-115.2017	-183.3874	212.1072	57.38371	101.72	10	57.3837	5	0	64.7434	11	0	52.1867	7		0.651900011		
46.5936	-27.051	161.014	-244.276963	-115.1743	-183.1138	291.8627	88.23211	345.5095	14	88.2321	17	0	66.7118	11	0	53.3096	7		0.099492204		
40.391	-27.451	160.766	-243.997742	-115.1601	-183.1024	285.6601	87.83234	345.2616	14	87.8323	17	0	52.5999	8	0	53.8331	7		0.703943247		
-55.867	-44.45	-98.007	-242.898215	-115.1308	-182.9042	189.4026	70.83351	86.48892	9	70.8335	4	0	72.2855	12	0	52.5999	8	52.9958336	0.156759455		
-56.586	-54.026	-89.348	-242.787538	-115.0934	-182.7513	188.6833	61.2574	95.1478	9	61.2574	4	0	69.1355	11	0	54.8699	8		3.511984963		
-55.162	-57.162	-86.085	-242.551941	-115.0541	-182.3383	190.1071	58.12129	98.41105	9	58.1213	4	0	62.9	10	0	51.6199	8		1.893254468		
-58.815	-68.753	-74.879	-242.435481	-115.0477	-181.3745	186.4538	46.52989	109.6174	9	46.5299	5	0	62.9932	11	0	52.5928	8		0.162425385		
-75.738	-35.965	-111.47	-242.407077	-114.9585	-180.963	169.5311	79.31817	73.02373	8	79.3182	3	0	57.8773	10	0	53.2967	8		0.090526182		
-83.369	-47.996	-96.466	-241.768869	-114.9577	-180.7857	161.8997	67.28684	88.02967	8	67.2868	4	0	58.3544	10	0	56.3705	9				
29.882	-22.495	162.05	-241.245521	-114.9326	-180.7813	275.1512	92.78835	346.5464	13	92.7884	17	0	59.3571	10	0	54.4491	9				

Figure 31. Extract from Microsoft Excel spreadsheet describing calculation steps required to obtain column heights for 20x20 grid, see Table 6 and Figure 32

Table 6. Key describing manual calculations in Figure 31

KEY	
	Raw 3D coordinates
	Raw 3D coordinates sorted by lowest to highest value. This is obtain the minimum value on each axes (this is the same as the minimum dimensions of the bounding box)
	3D coordinates normalised by subtracting each value by minimum value (as described above)
	Grid reference number calculated for a grid size of 20mm. Each x and z value is subtracted from it's modulus and divided by 20 e.g.  Modulus of 226.55 = 0.3275 (because 226.5/20= 11.3275)  → 0.3275 x 20= 6.55  → 226.55-6.55= 220  → 220/20= 11
	X grid reference sorted by lowest to highest value
	Z grid reference sorted by lowest to highest value
	Points in Grid reference x=0 and z=7. The mean of these y values is calculated to give 52.9941
	Points in Grid reference x=0 and z=8. The mean of these y values is calculated to give 52.9855



**Table 7. Outputs required from program**

<b>Outputs required from program</b>	<b>Description</b>
Frequency distribution of column heights according to a defined class width (Shape frequency table)	This allows statistical analysis of the frequency of the column heights to be carried out (Shape Frequency Tables)
Standard deviation (S.D) value for each grid cell	Figure 30 illustrates that certain grid cells contain more points and usually more highly contoured areas will have a greater range of heights. To highlight these areas, the standard deviation provides an indication into the range of heights- where a grid cell with a steep contour will have a higher S.D- and therefore the average y height may not be an adequate representation of that grid cell.
Coefficient of variation (CoV) for each grid cell. CoV is the ratio of the S.D to the mean.	In addition to S.D, the coefficient of variation for each cell was calculated which provides a dimensionless ratio which may be more useful to allow comparisons to be made between shapes. It may be that criteria can be specified where if the CoV is above a certain threshold then the grid size (or resolution) in this area would need to be reduced to capture a closer representation to the shape's contour.
Total Grid size, i.e. 'X' x 'Z'	The total grid size is useful to investigate the feasibility of manufacturing these shape representation as a series of column rods.
Each average column height rounded to nearest 10 and new frequency distribution for these new values	Similarly, the use of column heights rounded to the nearest 10 would be useful to investigate the feasibility of manufacturing these shape representation as a series of column rods.

The program is organised into three classes. The main processes that occur at each of these classes (or levels) are summarised in Table 8. The code is listed in the Appendices, Section 11.3.

**Table 8. Description of main program processes**

Class/Object	Description
<b>CSVExport</b>	<ul style="list-style-type: none"> <li>• Starting point of the program which finds the files (.txt) in the defined directory</li> <li>• Creates a new 'Analysis' Class and calls processData method (See Analysis Class below)</li> <li>• Displays the size of the grid by calling the getMaxGridX and getMaxGridZ method in Analysis class.</li> <li>• Displays average y value by looping through all cells and retrieves the mean from getMeanY method in the analysis class</li> <li>• Displays standard deviation by looping through all cells and retrieves the SD from the getSDY in the analysis class</li> <li>• Displays coefficient of variation by looping through all cells and retrieves SD and mean from analysis class. Formula SD/mean used for CoV calculation.</li> <li>• Loop through all the mean values returned from getMeanY method in analysis class and count number of y within defined range to produce frequency distribution.</li> <li>• Loop through all the mean values returned from getMeanY method in analysis class, rounds this value to the nearest 10 and counts number of y within defined range to produce frequency distribution.</li> <li>• End result of above produces the .csv file</li> </ul>
<b>Analysis</b>	<p>processData Creates a new point object (i.e. x, y, z ) (see 'Point' class below) for each new line from the input file (.txt file)</p> <ul style="list-style-type: none"> <li>• All points are stored in an array by creating new Point object (point class)</li> <li>• Array iterates through points to find: <ul style="list-style-type: none"> <li>○ Min x</li> <li>○ Min y</li> <li>○ Min z</li> </ul> </li> <li>• These values are subtracted from each point in the array to normalise the data set</li> <li>• Array is iterated to set grid positions for each point and find the maximum value on X and Z (which defines the total grid size) - using modulus calculation described in Table 6 (Excel spreadsheet example).</li> </ul> <p>getMeanY • Iterates through points to find points for each grid reference and obtain mean</p> <p>getSDY • Iterates through points to find standard deviation of values in each grid reference</p> <p>getMaxGridX • Returns the maximum value of X (calculated on processData method)</p> <p>getMaxGridZ • Returns the maximum value of Z (calculated on processData method)</p>
<b>Point</b>	<ul style="list-style-type: none"> <li>• This is the class which defines each point i.e. x, y, z (as dictated from analysis class)</li> </ul>

To run the program, a command window is opened in the appropriate directory and the following script is entered “java -jar analysis.jar grid range”, where grid has to be defined (e.g. 20 for a 20x20 grid) and range has to be defined as the class interval (e.g. 10 for  $0 \leq y < 10$ )

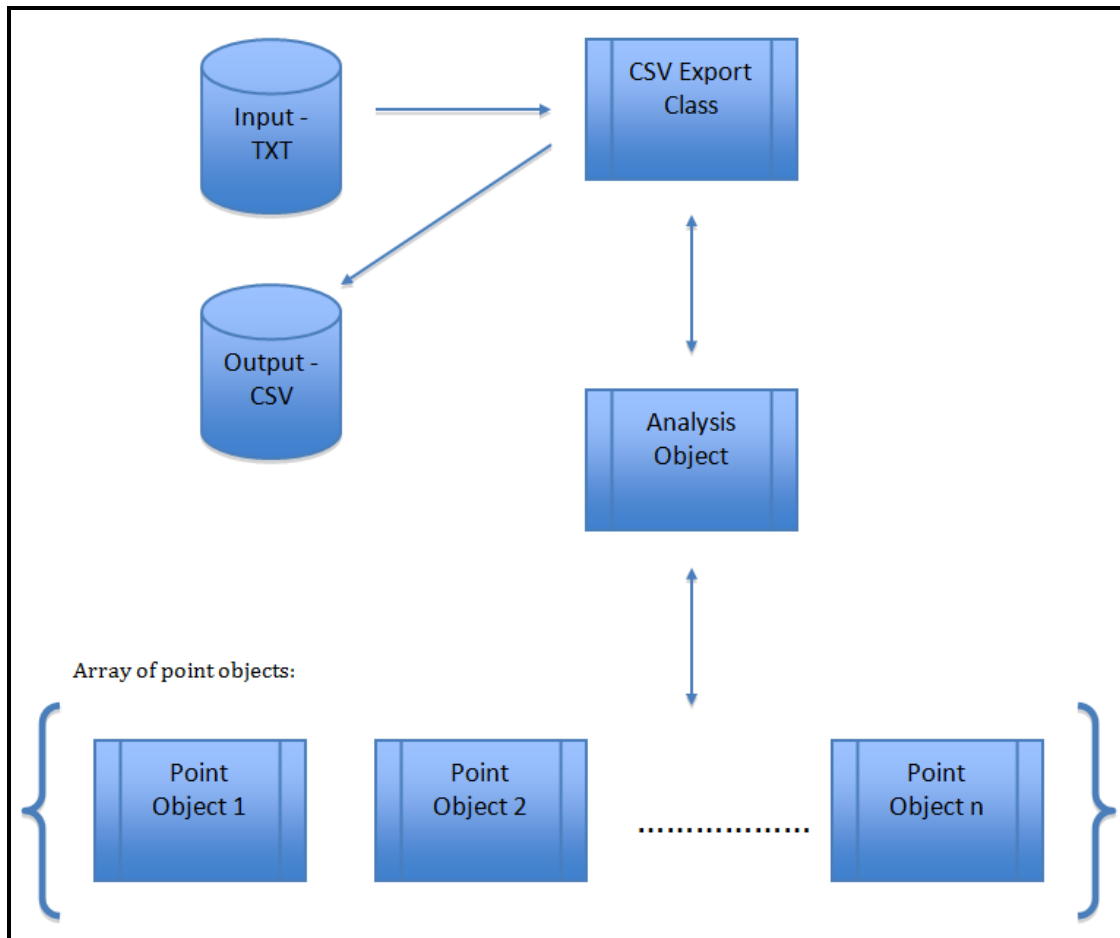


Figure 33. Process diagram describing java program

---

## 6 RESULTS

---

The main results of this project can be divided into two subsections:

1. Scanner comparison and validation of Microscan
2. Shape analysis using 3D coordinates from scan data

3D inspection software was used to provide deviation results between the Microscan and Faro scan (the gold standard) for a sample of 10 casts. Two different tolerances ( $\pm 0.5\text{mm}$  and  $\pm 1.0\text{mm}$ ) were tested which revealed that the Microscan was validated for both research and clinical purposes.

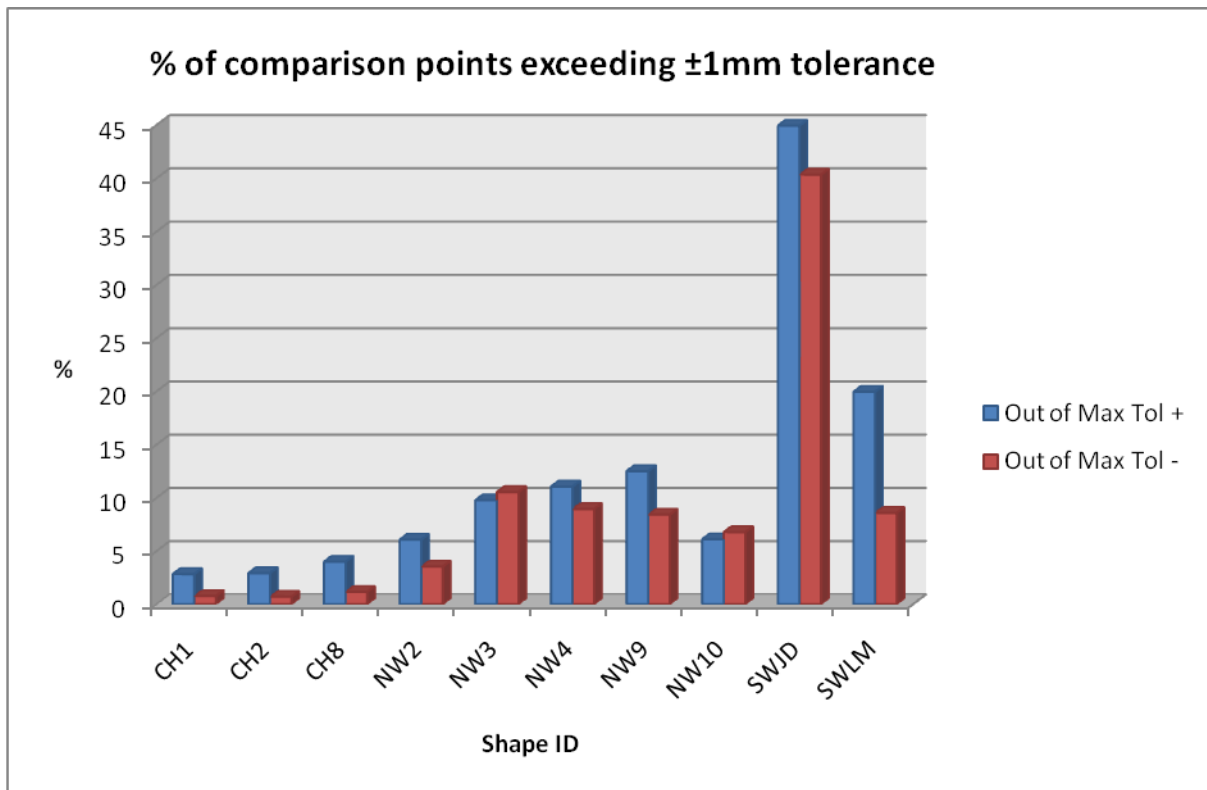
Shape analysis was performed by obtaining global dimensions (such as volume from the bounding box sizes). Further detailed analysis was performed by deriving shape functions (or Shape Frequency Tables) for each shape which provides information about the representation of these shapes as column rods for different grid cell sizes.

### 6.1 Validation of Microscan

#### 6.1.1 Nominal tolerance $\pm 0.5\text{mm}$ , critical tolerance $\pm 1.0\text{mm}$

Figure 34 summarises the 3D comparison of Microscans compared to Faro Scans (gold standard) of 10 shapes by examining the percentage of comparison points which exceeded the critical tolerance of  $\pm 1.0\text{mm}$ . This tolerance was chosen partly due to convenience but also acted as a starting point where the magnitude of the deviations was unknown. This level of accuracy is far superior to the current tolerances which are used within manufacturing of special seating systems. These results are generated by using the Geomagic Qualify, version 9 (Geomagic Inc., CA) inspection software.

Figure 34 clearly shows there is an error with the comparison of shape SWJD, where about 40-45% of Microscan comparison points exceed the critical tolerance of  $\pm 1.0\text{mm}$ . This is confirmed by examining the coloured-graphical image of SWJD in Table 11, possible reasons for this are discussed in Section 7.1.



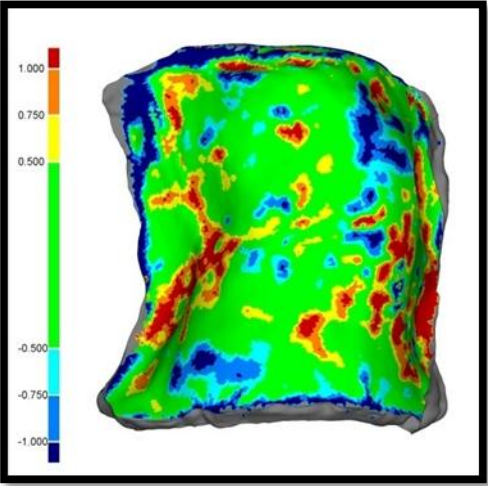
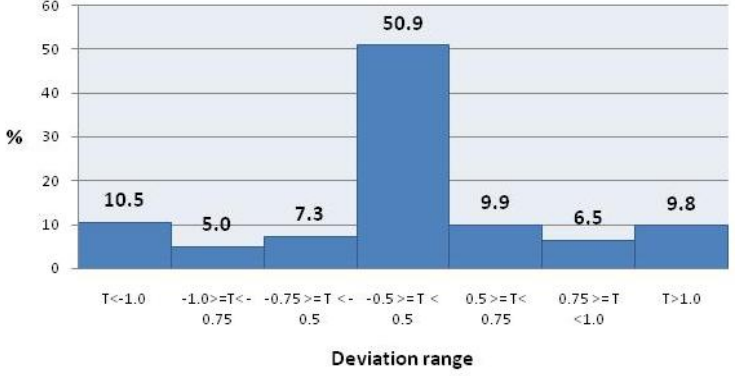
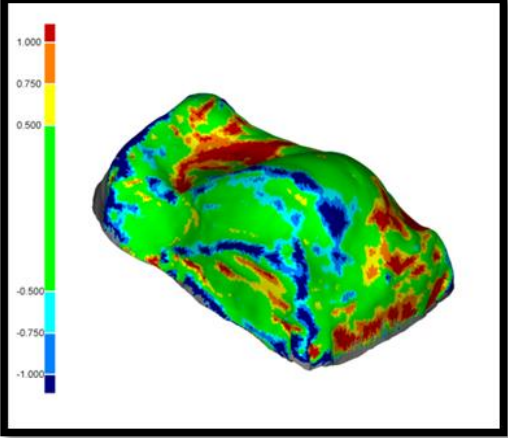
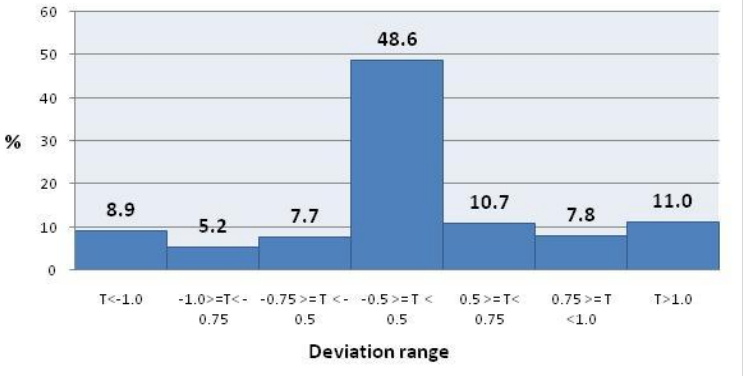
**Figure 34.** Graph showing the percentage of Microscan comparison points which exceeded the critical tolerance of  $\pm 1.0\text{mm}$  when compared to the Faro scans. The graph clearly shows an error with shapes SWJM and SWLM.

Table 9 to Table 11 describes a selection of the comparisons and the full set of comparison reports is located in the Appendices, Section 11.2. The results from the reports generated by Geomagic Qualify provide 3D coloured-graphical comparison and deviation distribution results.

**Table 9. CH1 and CH8 scan comparison results (nominal tolerance  $T \pm 0.5\text{mm}$ )**

	<table border="1"> <caption>CH1 deviation distribution</caption> <thead> <tr> <th>Deviation range</th> <th>%</th> </tr> </thead> <tbody> <tr> <td><math>T &lt; -1.0</math></td> <td>0.8</td> </tr> <tr> <td><math>-1.0 \geq T &lt; -0.75</math></td> <td>0.9</td> </tr> <tr> <td><math>-0.75 \geq T &lt; -0.5</math></td> <td>4.3</td> </tr> <tr> <td><math>-0.5 \geq T &lt; 0.5</math></td> <td>76.9</td> </tr> <tr> <td><math>0.5 \geq T &lt; 0.75</math></td> <td>11.1</td> </tr> <tr> <td><math>0.75 \geq T &lt; 1.0</math></td> <td>3.3</td> </tr> <tr> <td><math>T &gt; 1.0</math></td> <td>2.8</td> </tr> </tbody> </table>	Deviation range	%	$T < -1.0$	0.8	$-1.0 \geq T < -0.75$	0.9	$-0.75 \geq T < -0.5$	4.3	$-0.5 \geq T < 0.5$	76.9	$0.5 \geq T < 0.75$	11.1	$0.75 \geq T < 1.0$	3.3	$T > 1.0$	2.8
Deviation range	%																
$T < -1.0$	0.8																
$-1.0 \geq T < -0.75$	0.9																
$-0.75 \geq T < -0.5$	4.3																
$-0.5 \geq T < 0.5$	76.9																
$0.5 \geq T < 0.75$	11.1																
$0.75 \geq T < 1.0$	3.3																
$T > 1.0$	2.8																
<p><b>CH1</b></p> <p>Average deviation=0.401 /-0.310 (S.D. for all deviations =0.514)</p>																	
	<table border="1"> <caption>CH8 Deviation distribution</caption> <thead> <tr> <th>Deviation range</th> <th>%</th> </tr> </thead> <tbody> <tr> <td><math>T &lt; -1.0</math></td> <td>0.7</td> </tr> <tr> <td><math>-1.0 \geq T &lt; -0.75</math></td> <td>0.7</td> </tr> <tr> <td><math>-0.75 \geq T &lt; -0.5</math></td> <td>3.1</td> </tr> <tr> <td><math>-0.5 \geq T &lt; 0.5</math></td> <td>78.6</td> </tr> <tr> <td><math>0.5 \geq T &lt; 0.75</math></td> <td>10.0</td> </tr> <tr> <td><math>0.75 \geq T &lt; 1.0</math></td> <td>3.9</td> </tr> <tr> <td><math>T &gt; 1.0</math></td> <td>2.9</td> </tr> </tbody> </table>	Deviation range	%	$T < -1.0$	0.7	$-1.0 \geq T < -0.75$	0.7	$-0.75 \geq T < -0.5$	3.1	$-0.5 \geq T < 0.5$	78.6	$0.5 \geq T < 0.75$	10.0	$0.75 \geq T < 1.0$	3.9	$T > 1.0$	2.9
Deviation range	%																
$T < -1.0$	0.7																
$-1.0 \geq T < -0.75$	0.7																
$-0.75 \geq T < -0.5$	3.1																
$-0.5 \geq T < 0.5$	78.6																
$0.5 \geq T < 0.75$	10.0																
$0.75 \geq T < 1.0$	3.9																
$T > 1.0$	2.9																
<p><b>CH8</b></p> <p>Average deviation=0.409 /-0.303 (S.D. for all deviations =0.527)</p>																	
<p><b>Main findings</b></p>	<ul style="list-style-type: none"> <li>• Microscan scans for CH shapes provided very good agreement results with the FARO scanner</li> <li>• Deviation results show that 76.9% and 78.6% of comparison points were within a <math>\pm 0.5\text{mm}</math> tolerance.</li> <li>• Coloured 3D images show that these areas appear to be at the edges and within deep recesses of the shapes.</li> </ul>																

**Table 10. NW3 and NW4 scan comparison results (nominal tolerance  $T \pm 0.5\text{mm}$ )**

	<p style="text-align: center;"><b>NW3 deviation distribution</b></p>  <table border="1"> <thead> <tr> <th>Deviation range</th> <th>Percentage (%)</th> </tr> </thead> <tbody> <tr> <td><math>T &lt; -1.0</math></td> <td>10.5</td> </tr> <tr> <td><math>-1.0 &gt;= T &lt; -0.75</math></td> <td>5.0</td> </tr> <tr> <td><math>-0.75 &gt;= T &lt; -0.5</math></td> <td>7.3</td> </tr> <tr> <td><math>-0.5 &gt;= T &lt; -0.5</math></td> <td>50.9</td> </tr> <tr> <td><math>0.5 &gt;= T &lt; 0.75</math></td> <td>9.9</td> </tr> <tr> <td><math>0.75 &gt;= T &lt; 1.0</math></td> <td>6.5</td> </tr> <tr> <td><math>T &gt; 1.0</math></td> <td>9.8</td> </tr> </tbody> </table>	Deviation range	Percentage (%)	$T < -1.0$	10.5	$-1.0 >= T < -0.75$	5.0	$-0.75 >= T < -0.5$	7.3	$-0.5 >= T < -0.5$	50.9	$0.5 >= T < 0.75$	9.9	$0.75 >= T < 1.0$	6.5	$T > 1.0$	9.8
Deviation range	Percentage (%)																
$T < -1.0$	10.5																
$-1.0 >= T < -0.75$	5.0																
$-0.75 >= T < -0.5$	7.3																
$-0.5 >= T < -0.5$	50.9																
$0.5 >= T < 0.75$	9.9																
$0.75 >= T < 1.0$	6.5																
$T > 1.0$	9.8																
<p><b>NW3</b></p> <p>Average deviation=<math>0.649 / -1.081</math> (S.D. for all deviations =<math>2.095</math>)</p>																	
	<p style="text-align: center;"><b>NW4 deviation distribution</b></p>  <table border="1"> <thead> <tr> <th>Deviation range</th> <th>Percentage (%)</th> </tr> </thead> <tbody> <tr> <td><math>T &lt; -1.0</math></td> <td>8.9</td> </tr> <tr> <td><math>-1.0 &gt;= T &lt; -0.75</math></td> <td>5.2</td> </tr> <tr> <td><math>-0.75 &gt;= T &lt; -0.5</math></td> <td>7.7</td> </tr> <tr> <td><math>-0.5 &gt;= T &lt; -0.5</math></td> <td>48.6</td> </tr> <tr> <td><math>0.5 &gt;= T &lt; 0.75</math></td> <td>10.7</td> </tr> <tr> <td><math>0.75 &gt;= T &lt; 1.0</math></td> <td>7.8</td> </tr> <tr> <td><math>T &gt; 1.0</math></td> <td>11.0</td> </tr> </tbody> </table>	Deviation range	Percentage (%)	$T < -1.0$	8.9	$-1.0 >= T < -0.75$	5.2	$-0.75 >= T < -0.5$	7.7	$-0.5 >= T < -0.5$	48.6	$0.5 >= T < 0.75$	10.7	$0.75 >= T < 1.0$	7.8	$T > 1.0$	11.0
Deviation range	Percentage (%)																
$T < -1.0$	8.9																
$-1.0 >= T < -0.75$	5.2																
$-0.75 >= T < -0.5$	7.7																
$-0.5 >= T < -0.5$	48.6																
$0.5 >= T < 0.75$	10.7																
$0.75 >= T < 1.0$	7.8																
$T > 1.0$	11.0																
<p><b>NW4</b></p> <p>Average deviation=<math>0.651 / -0.666</math> (S.D. for all deviations =<math>0.940</math>)</p>																	
<p><b>Main findings</b></p>	<ul style="list-style-type: none"> <li>NW shapes do not show as good an agreement between Microscans and Faro scan as the CH shapes (Table 9).</li> <li>Deviation results show that 50.9% and 48.6% are still within a <math>\pm 0.5\text{mm}</math> tolerance.</li> <li>Coloured 3D images do not reveal any consistent areas where large deviations are prevalent.</li> </ul>																

**Table 11. SWJD and SWLM scan comparisons (nominal tolerance  $T \pm 0.5\text{mm}$ )**

	<p style="text-align: center;"><b>SWJD deviation distribution</b></p> <table border="1"> <thead> <tr> <th>Deviation range</th> <th>%</th> </tr> </thead> <tbody> <tr> <td><math>T &lt; -1.0</math></td> <td>40.3</td> </tr> <tr> <td><math>-1.0 \geq T &lt; -0.75</math></td> <td>1.7</td> </tr> <tr> <td><math>-0.75 \geq T &lt; -0.5</math></td> <td>1.9</td> </tr> <tr> <td><math>-0.5 \geq T &lt; 0.5</math></td> <td>7.5</td> </tr> <tr> <td><math>0.5 \geq T &lt; 0.75</math></td> <td>1.7</td> </tr> <tr> <td><math>0.75 \geq T &lt; 1.0</math></td> <td>1.9</td> </tr> <tr> <td><math>T &gt; 1.0</math></td> <td>44.9</td> </tr> </tbody> </table>	Deviation range	%	$T < -1.0$	40.3	$-1.0 \geq T < -0.75$	1.7	$-0.75 \geq T < -0.5$	1.9	$-0.5 \geq T < 0.5$	7.5	$0.5 \geq T < 0.75$	1.7	$0.75 \geq T < 1.0$	1.9	$T > 1.0$	44.9
Deviation range	%																
$T < -1.0$	40.3																
$-1.0 \geq T < -0.75$	1.7																
$-0.75 \geq T < -0.5$	1.9																
$-0.5 \geq T < 0.5$	7.5																
$0.5 \geq T < 0.75$	1.7																
$0.75 \geq T < 1.0$	1.9																
$T > 1.0$	44.9																
<p><b>SWJD</b></p> <p><b>Average deviation=4.582 /-7.091 (S.D. for all deviations =8.813)</b></p>																	
	<p style="text-align: center;"><b>SWLM deviation distribution</b></p> <table border="1"> <thead> <tr> <th>Deviation range</th> <th>%</th> </tr> </thead> <tbody> <tr> <td><math>T &lt; -1.0</math></td> <td>8.6</td> </tr> <tr> <td><math>-1.0 \geq T &lt; -0.75</math></td> <td>6.8</td> </tr> <tr> <td><math>-0.75 \geq T &lt; -0.5</math></td> <td>10.0</td> </tr> <tr> <td><math>-0.5 \geq T &lt; 0.5</math></td> <td>45.2</td> </tr> <tr> <td><math>0.5 \geq T &lt; 0.75</math></td> <td>5.1</td> </tr> <tr> <td><math>0.75 \geq T &lt; 1.0</math></td> <td>4.3</td> </tr> <tr> <td><math>T &gt; 1.0</math></td> <td>19.9</td> </tr> </tbody> </table>	Deviation range	%	$T < -1.0$	8.6	$-1.0 \geq T < -0.75$	6.8	$-0.75 \geq T < -0.5$	10.0	$-0.5 \geq T < 0.5$	45.2	$0.5 \geq T < 0.75$	5.1	$0.75 \geq T < 1.0$	4.3	$T > 1.0$	19.9
Deviation range	%																
$T < -1.0$	8.6																
$-1.0 \geq T < -0.75$	6.8																
$-0.75 \geq T < -0.5$	10.0																
$-0.5 \geq T < 0.5$	45.2																
$0.5 \geq T < 0.75$	5.1																
$0.75 \geq T < 1.0$	4.3																
$T > 1.0$	19.9																
<p><b>SWLM</b></p> <p><b>Average deviation=1.273 /-0.584 (S.D. for all deviations =1.482)</b></p>																	
<p><b>Main findings</b></p>	<ul style="list-style-type: none"> <li>• SW shapes do not show as good an agreement between Microscans and Faro scans as the CH shapes (Table 9).</li> <li>• The deviation distribution for SWJD clearly shows that a significant error exists, where only 7.5% of comparison points fall within the nominal tolerance of <math>\pm 0.5\text{mm}</math>.</li> <li>• SWJD's coloured-comparison image shows an interesting pattern where an overall distortion of the shape appears to have occurred rather than localised areas as in NW3 and NW4. Similarly, SWLM appears to have experienced some distortion particularly at the edges.</li> </ul>																

### 6.1.2 Nominal tolerance $\pm 1.0\text{mm}$ , critical tolerance $\pm 2.0\text{mm}$

To investigate these tolerances further, the nominal and critical tolerances were adjusted (widened) in the Geomagic Qualify software to generate duplicate reports. These results are summarised in Table 12, Table 13 and Table 14 for shapes CH8, NW4 and SWLM respectively.

**Table 12. CH8 scan comparison (nominal tolerance  $T \pm 1.0\text{mm}$ )**

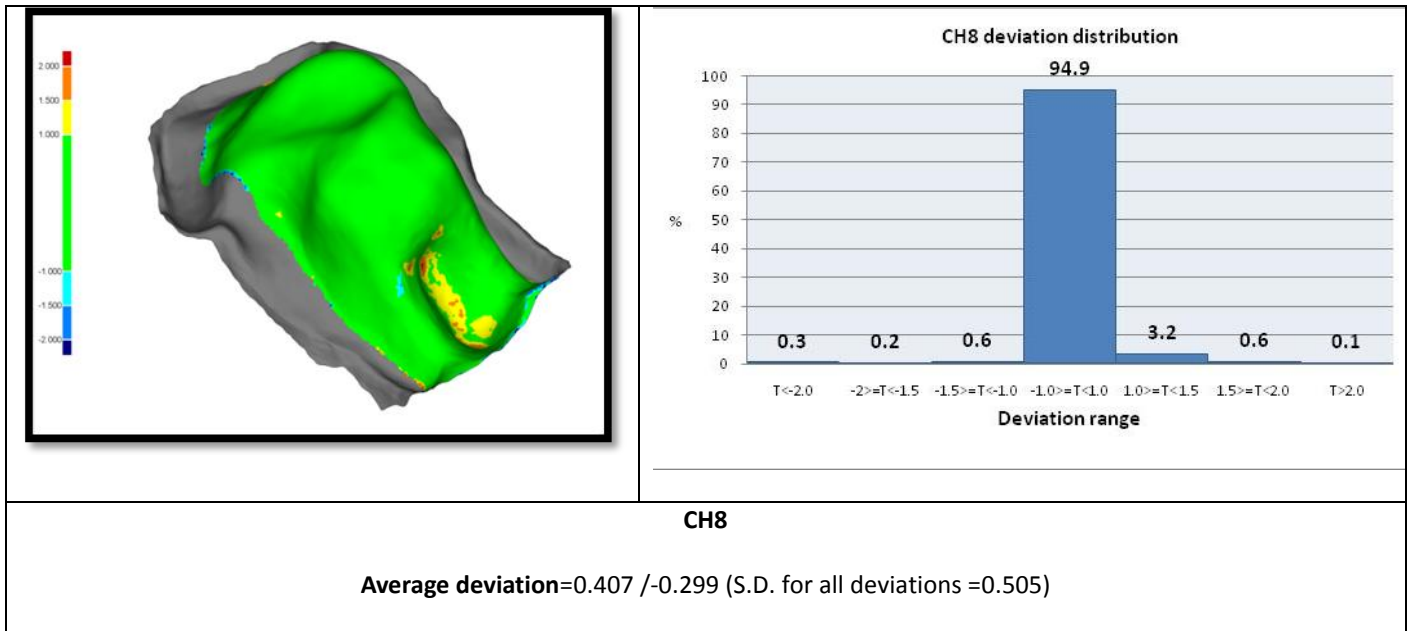


**Table 13. NW4 scan comparison (nominal tolerance  $T \pm 1.0\text{mm}$ )**

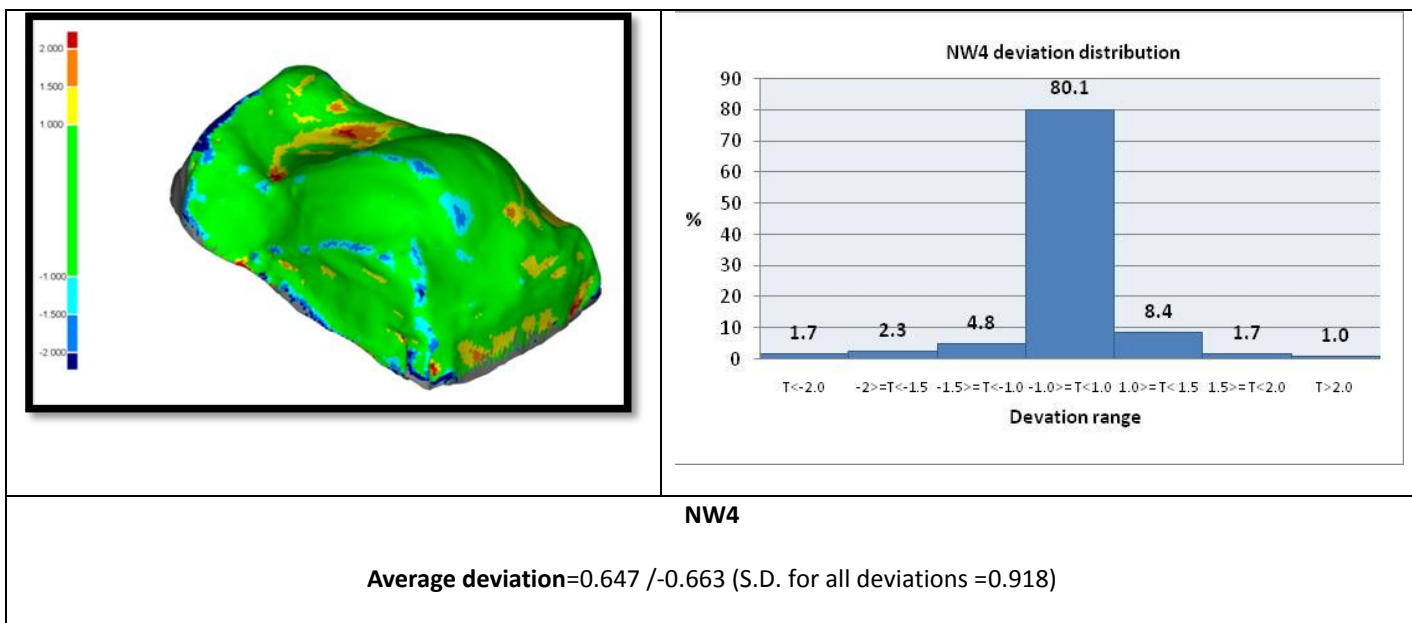


**Table 14. SWLM scan comparison (nominal tolerance  $\pm 1.0\text{mm}$ )**

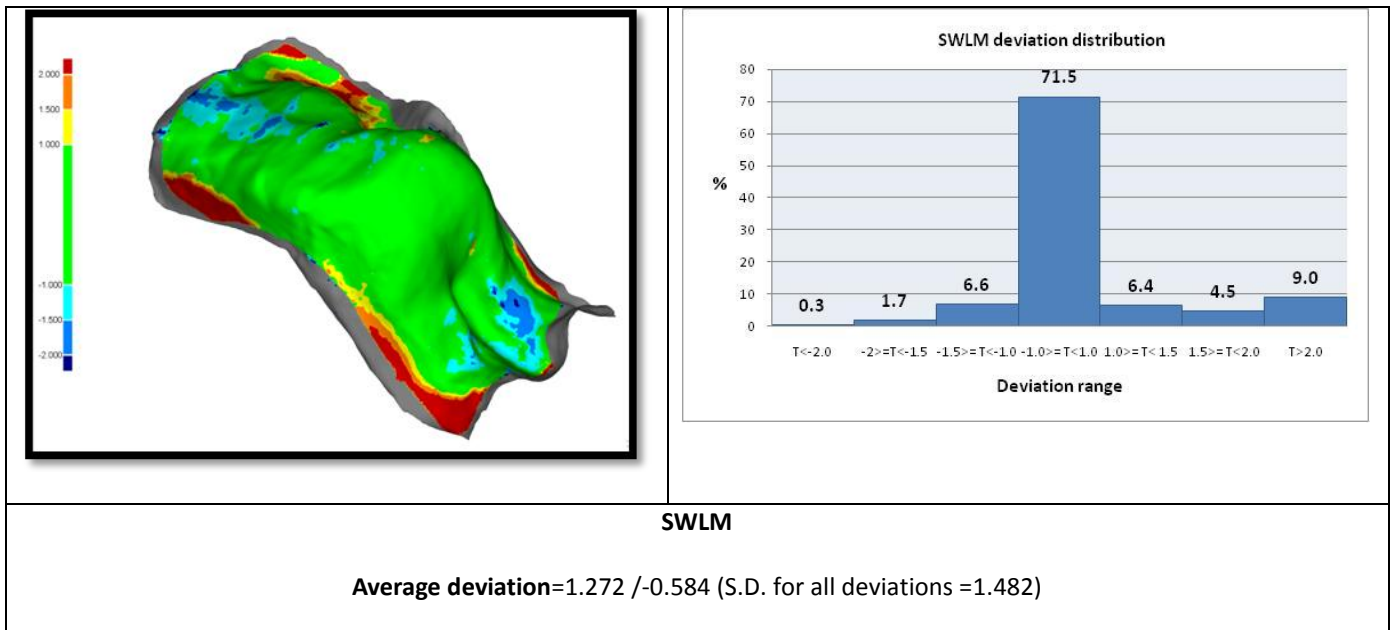


Table 12 to Table 14 reveal that the adjusted tolerances provide excellent agreement between the two scans, where 94.9%, 80.1% and 71.5% of comparison points are within  $\pm 1.0\text{mm}$ . SWLM (Table 14) still reveals localised large deviations at the corners of the shape (shown in red), which accounts for 9% of the comparison points. This anomaly is due to a damaged cast, which is discussed further in Section 7.1.

Clearly, these results validate the use of the Microscans for clinical work for the manufacturing of seating systems where it is estimated that previous working tolerances within special seating were within  $\pm 10\text{mm}$  (Shapcott 2008). The use of the Microscan for research purposes is dependent on the detail of analysis that is required. For the remit of this project, the Microscan is considered more than adequate to carry out shape analysis work. These conclusions rely on the assumption that the Faro scanner is the Gold standard, and it is noted that the Faro scanner has a specified accuracy of  $\pm 61\mu\text{m}$ .

## 6.2 Shape analysis

### 6.2.1 Bounding box sizes

The review of shape analysis techniques (Section 4) indicated ways to classify the shapes using global features such as area or volume. Information was recorded during the

processing of the raw data using Rhinoceros 3D 4.0 (Robert McNeel & Associates, Seattle, WA) of the size of the bounding boxes for each shape. These results are shown in Table 15 to Table 17. Bounding box sizes are calculated by using the minimum and maximum point in each direction (x, y, z), using the standard axes system explained in Section 5.4.2, Figure 29. These results can influence manufacturing techniques, which are discussed in Section 7.2.1.

**Table 15. Bounding box sizes for Bases**

Shape ID	X Dimension (mm)	Y Dimension (mm)	Z Dimension (mm)
NW1 base	466.0	171.8	304.5
NW4 BASE	506.6	257.6	391.0
NW5 BASE	421.2	237.5	368.9
NW6 base	438.5	195.3	372.0
NW7 base	517.4	238.3	369.6
NW8base	295.8	181.6	321.1
NW10 BASE	490.0	230.5	331.6
CH1base	440.3	220.3	374.9
CH2base	465.1	203.0	385.6
CH8base	392.1	234.7	316.3
CH9 base	450.2	175.6	541.0
SWJM Base	508.2	132.7	445.6
SWDF base	513.4	229.2	468.0
SWLM base	522.2	321.1	453.2
SWJD base	403.5	309.8	472.8
SWAR base	536.8	222.3	430.6
SWARY base	510.1	201.5	395.8
SWDH base	486.8	191.9	461.0
SWGJ base	507.2	214.1	418.3
SWTHD BASE	559.5	210.8	608.6
<b>AVERAGE</b>	<b>471.5</b>	<b>219.0</b>	<b>411.5</b>

**Table 16. Bounding box sizes for Backs**

Shape ID	X Dimension (mm)	Y Dimension (mm)	Z Dimension (mm)
NW1 back	376.0	343.3	385.8
NW2 BACK	413.6	263.2	463.9
NW3 BACK	429.2	170.2	405.2
NW6 back	338.6	378.0	403.7
NW 7 back	426.5	448.5	444.3
NW8 back	385.6	188.9	336.7
NW9 BACK	455.8	272.1	490.5
CH1back	382.7	253.6	378.1
CH2back	355.4	252.0	382.7
CH8back	408.1	307.4	346.8
CH9 back	233.5	307.4	522.4

<b>SWDF back</b>	370.8	315.7	432.4
<b>SWLM back</b>	484.2	184.8	448.0
<b>SWJD back</b>	335.7	228.3	449.6
<b>SWAR back</b>	386.4	442.5	446.3
<b>SWARY back</b>	428.0	312.8	413.2
<b>SWDH back</b>	360.1	293.9	461.6
<b>SWGJ back</b>	326.0	374.4	439.4
<b>SWKH BACK</b>	563.1	231.5	419.4
<b>SWMRBACK</b>	456.8	171.0	399.2
<b>AVERAGE</b>	<b>395.8</b>	<b>287.0</b>	<b>423.5</b>

Table 17. Summary of bounding box sizes for bases and backs

	Minimum size (mm)		Maximum size (mm)	
	Base	Back	Base	Back
<b>X Dimension</b>	295.8	233.5	559.5	563.1
<b>Y Dimension</b>	132.7	170.2	321.1	448.5
<b>Z Dimension</b>	304.5	336.7	608.6	522.4

## 6.2.2 Column representation and Histograms

As described in Section 5.4.4, the java program provided an output which created a .csv file with the average column height assigned to the correct grid reference as shown in Figure 36 to Figure 38. Using Excel's conditional formatting of cells, shape images are coloured according to the height of the column (where darker the orange; the higher the column). The grid cells that did not contain any points are labeled NaN (Not a number). The program also provided a summary of the column heights by grouping the heights into different class intervals.

Three different resolutions were tested using 10mm x 10mm; 20mm x 20mm and 50mm x 50mm grid sizes. The results for the shape CH1base (illustrated in Figure 35) are displayed in Figure 36 to Figure 38 for CH1base. The 10x10 grid provides 1428 total number of columns; the 20x20mm grid size provides 373 number of columns and the 50 x 50 grid results in 67 total number of columns. For this reason, it was decided that the 20x20 grid size was the optimum resolution to use for the shape analysis and for demonstration purposes (Section 6.2.2). The class interval of the histograms was defined as 10mm, which corresponds to the objectives (Section 2) where the research question for the project is: Can customised

support systems be represented by geometric shapes that are within  $\pm 10\text{mm}$  from the actual shape?

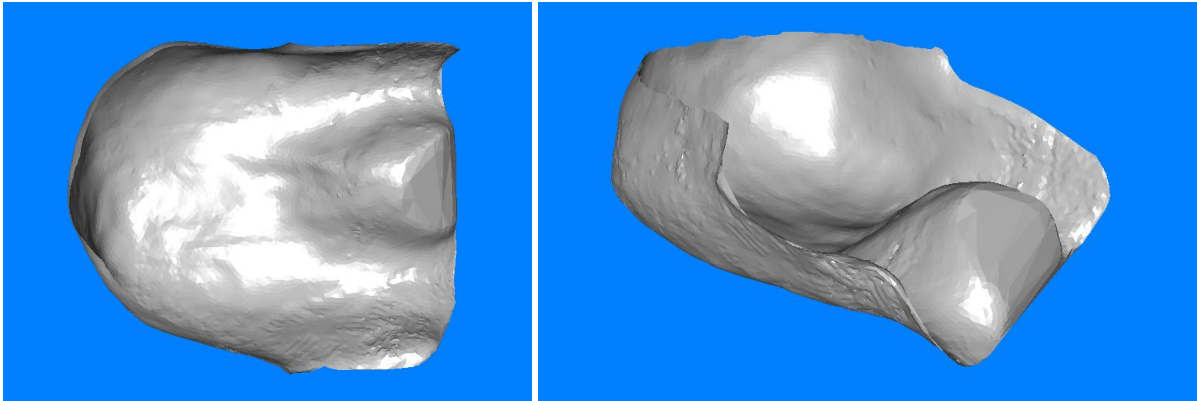


**Figure 35. Shape CH1 base processed scan images**

The histograms for all shapes (20 bases and 20 backs) were used as shape descriptors to enable further shape analysis. A selection can be found in the Appendices, Sections 11.4. The histograms produced from the Shape Frequency Tables provide information of the discretized shape volume which reduces the variables for analysis to take place. Section 6.3 describes the use of statistics to analyse these shape descriptors to allow quantitative shape comparisons to be made and to advance the understanding of these customized shapes.



NaN	159	136.6	129.2	125	120.1	117.3	118.4	116.6	115.7	107.6	NaN	NaN											
NaN	NaN	NaN	NaN	NaN	NaN	114.4	119.2	127.6	133.7	146.8	149.7	121.1	105	103.1	99.48	100.2	104.8	108.1	107.4	93.21	NaN	NaN	
NaN	NaN	NaN	103.9	115.5	120.5	125.8	133.8	138.4	125.9	87.62	69.35	70.48	70.67	69.68	68.32	68.33	74.28	75.47	73.69	61.59	42.5	NaN	
NaN	NaN	106.6	118.7	122.8	132.8	130.4	101.8	48.74	45.14	45.19	44.28	44.21	45.13	44.37	43.53	43.26	45.94	45.75	42.08	34.49	27.57	NaN	
NaN	97.04	117.1	129.2	121.5	71.87	44.41	40.97	36.73	34.49	33.43	32.59	32.8	32.61	32.89	32.48	33.6	33.55	32.67	29.35	21.62	12.47	NaN	
NaN	115	132.8	115	47.26	42.63	37.92	34.65	30.36	28.61	27.28	26.44	26.6	26.48	27.59	30.47	32.39	32.46	30.03	26.42	18.73	6.926	NaN	
107.9	119.4	112.1	46.59	41.47	37.6	33.22	29.32	26.57	25.66	24.94	24.45	25.88	28.13	32.14	34.6	37.85	39.2	37.93	34.16	25.49	10.47	0.049	
123.8	122.5	66.34	44.02	38.97	36.41	33.13	29.57	27.34	26.26	25.36	25.24	28.09	34.15	43.01	47.48	52.38	56.31	59.72	57	47.37	24.51	NaN	
132.8	72.17	45.51	42.37	38.91	36.53	34.1	30.74	28	26.42	26.05	28.61	35.29	46.91	58.88	65.18	73.45	80.21	83.96	83.23	64.48	36.8	NaN	
132	58.24	44.59	41.38	39.15	36.46	33.63	30.45	26.64	23.36	23.82	28.26	40.72	54.25	68.63	82.86	92.34	100.3	105	NaN	NaN	NaN	NaN	
130.1	61.01	47.41	40.96	38	34.99	30.8	27.73	24.36	22.56	24.5	28.84	38.94	56.29	75.66	90.74	102.2	110.6	115.6	NaN	NaN	NaN	NaN	
132.5	64.62	49.01	40.6	35.25	30.14	26.55	24.4	22.61	24.03	26.45	32.45	43.61	60.29	78.85	94.58	107.6	113.7	116.8	NaN	NaN	NaN	NaN	
136.1	69.02	52.62	41.42	33.18	27.16	23.71	23.04	23.88	25.83	29.24	35.01	44.84	56.62	66.99	82.27	97.23	106.3	110.2	109.2	NaN	NaN	NaN	
141.1	87.49	57.84	44.55	34.42	28.16	24.37	22.71	22.49	22.85	25.26	29.41	33.56	40.1	49.44	60.51	73.46	84.6	92.11	96.02	92.6	65.11	NaN	
138.2	124.5	66.55	49.94	39.34	31.4	26.61	24.56	22.7	21.81	23.28	26.78	30.2	34.19	39.38	44.83	49.46	56.43	60.4	64.24	61.32	46.84	NaN	
131.7	140.8	82.27	61.42	46.8	37.53	30.74	28.08	26.51	24.78	26.07	28.18	30.71	33.83	37.38	39.27	39.55	38.83	37.99	36.06	30.97	NaN	NaN	
NaN	142.7	137.5	85.41	61.41	47.02	38.94	35.77	33.72	32.66	32.76	35.09	35.81	39.3	41.96	45	42.97	38.88	36.04	32.55	25.65	NaN	NaN	
NaN	NaN	145.1	140.8	102.2	71.04	60.98	54.38	51.19	47.03	47.34	52.79	58.9	64.02	65.07	63.27	60.65	56.93	52.72	48.25	41.19	NaN	NaN	
NaN	NaN	NaN	152.7	150.2	139.9	133.8	127.8	126.8	122.2	125.2	129.5	125.9	123.5	121.7	115.5	109.2	105.8	98.7	90.8	83.4	75.15	NaN	

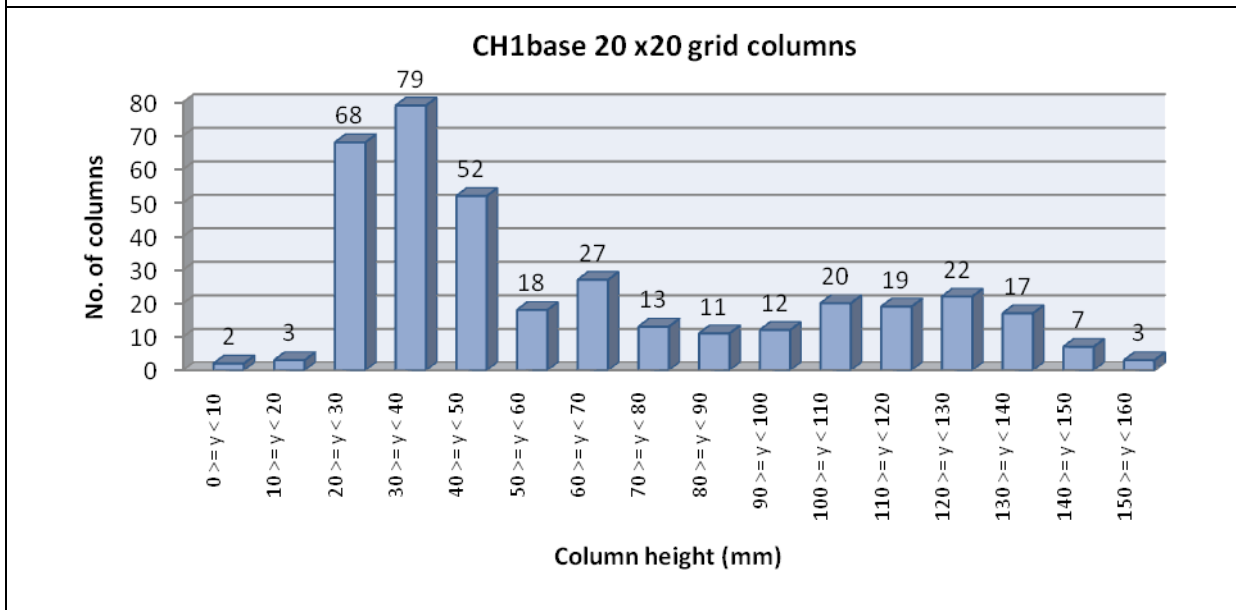


Figure 37. CH1base 20x20 grid results

NaN	NaN	NaN	129.66	148.57	119.72	112.48	115.63	103.88
NaN	118.41	126.05	121.1	94.292	68.49	67.498	72.754	52.562
117.8	113.38	45.853	32.458	29.135	29.652	32.891	30.876	14.856
118.16	42.475	33.989	27.169	26.738	41.676	58.025	60.745	33.269
113.57	40.505	32.304	24.653	29.006	61.076	95.802	109.91	NaN
118.75	40.912	25.579	23.564	31.93	54.259	82.854	98.771	83.039
131.26	58.89	32.397	25.729	27.871	35.492	44.403	50.112	48.316
143.82	131.83	111.29	105.76	108.5	98.995	92.621	77.343	65.089

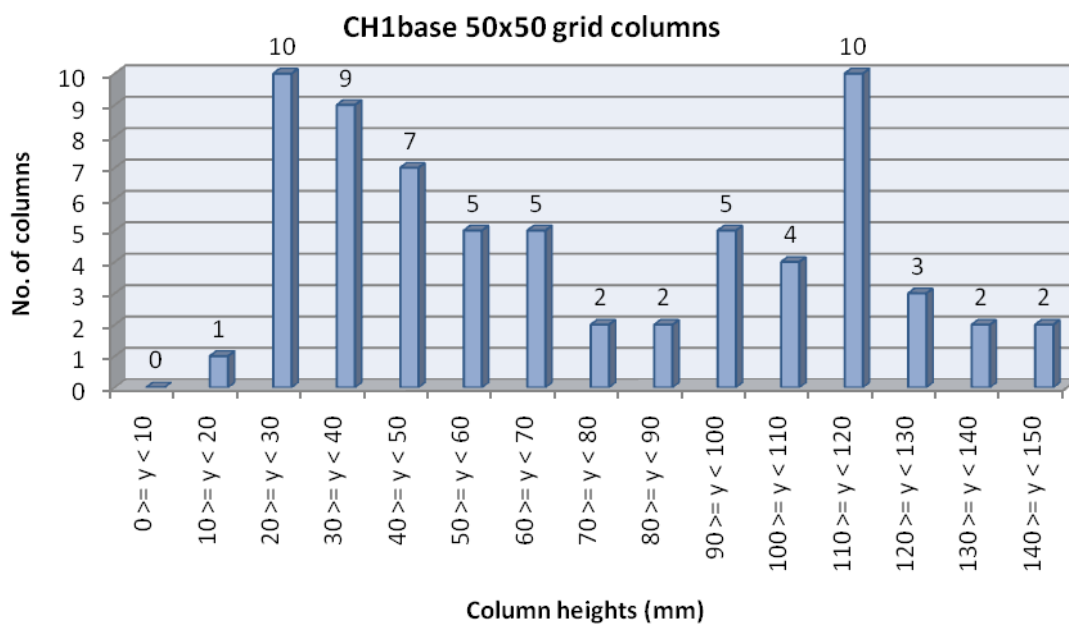


Figure 38. CH1base 50x50 grid results

### 6.2.3 Proposed manufacturing concept

The geometric column rod representation of the customised shapes provides an alternative manufacturing method to the current costly techniques (described in Section 1.3). This study has developed a process where results from the acquisition and analysis can be used to provide an insight into a potential low-cost manufacturing technique of these customised seating systems. The outputs from the shape acquisition and analysis for each shape are:

- Total grid size
- Total number of columns
- Heights of columns
- Heights of columns rounded to nearest 10mm
- Number of columns within a defined height range (frequency tables)

All of these results provide valuable information which can specify the shape of the seating system. The sample of 20 bases and 20 backs which were used in this project can be analysed to reveal the proportion of shapes which may be represented in this way. From a clinical service delivery perspective, the number of components (columns) required would be useful information. Figure 39 summarises the proportion of bases and backs which can be manufactured using the proposed geometric representations (where column heights are rounded to the nearest 10mm). These results may be used to select the optimum number of column heights to have in stock to achieve the fabrication of a certain proportion of seating systems. For example, if 25 different heights were chosen then the data suggests that 90% of Bases and 45% of Backs can be manufactured in this way. However, if 30 different heights were kept in stock then the data suggests that 90% of Bases and 75% of Backs may be manufacturing using column representations of the shapes.

These results do not provide an indication into the quantity of columns required, this is available from the frequency tables. To predict stock levels, these frequency tables should be analysed. Figure 40 analyses these quantities for the 20 base shapes by plotting the mean number of columns that are required for each column height. This information may be useful to estimate stock levels, however as the graph indicates the range of column heights can be very large, particularly at the lower spectrum of the column heights.

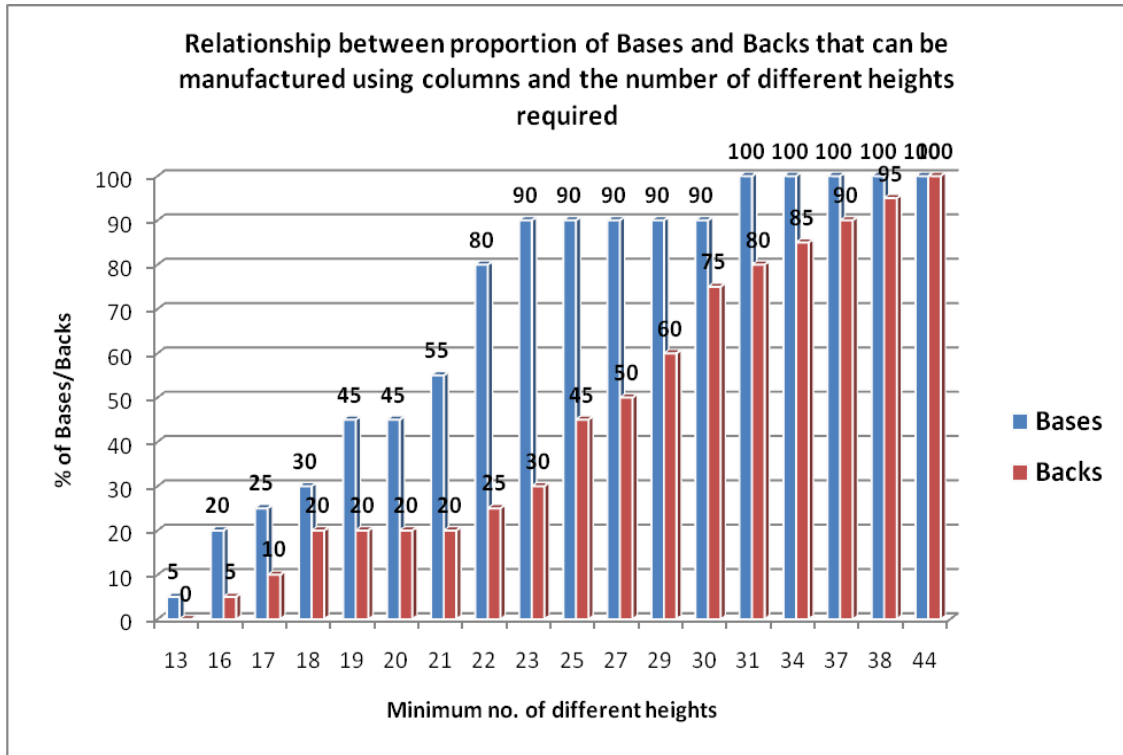


Figure 39. Graph showing the proportion of bases and backs which can be represented using 20 x 20 mm geometric columns

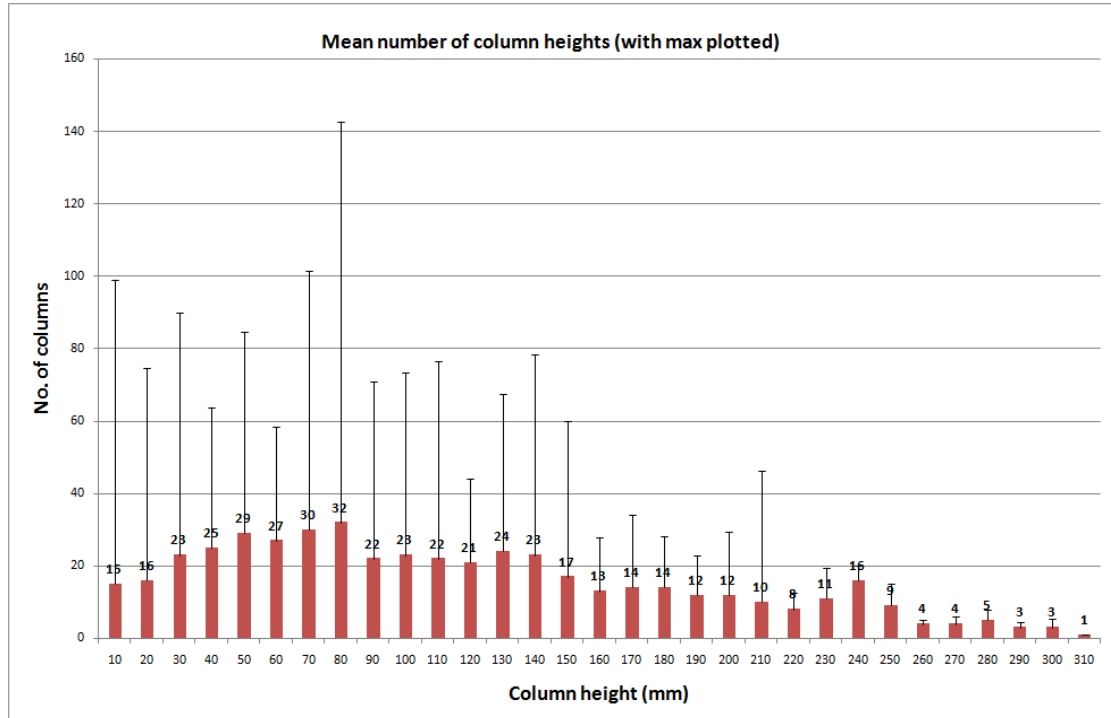
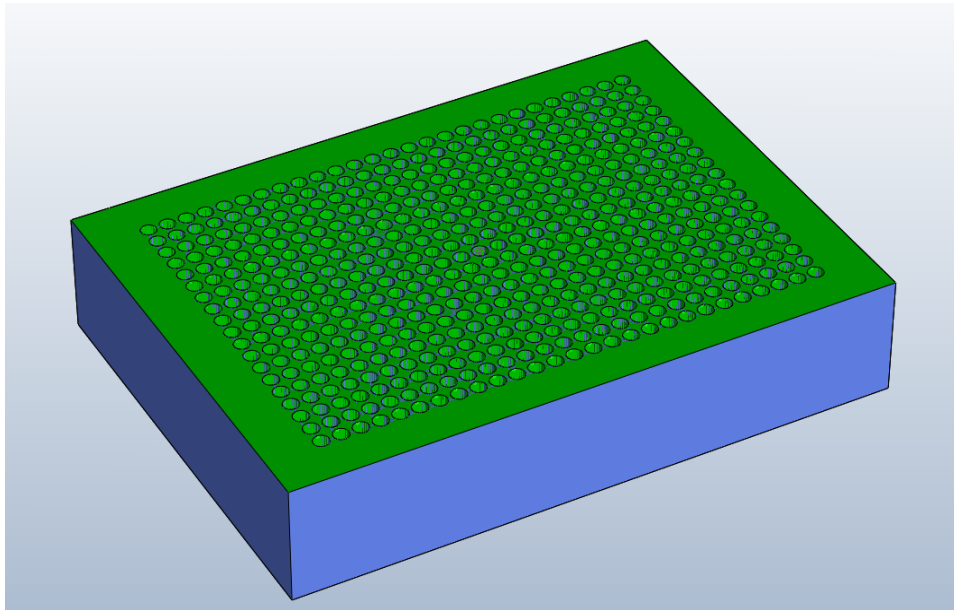


Figure 40. Graph showing the mean number of columns required for each height for the sample of 20 bases analysed. The maximum number for each column height is plotted.



version 4.0 (Robert McNeel & Associates, Seattle, WA) and exporting this to Maya Expert (version 7, Picasoft) to be cut into foam by the CNC machine.



**Figure 41. CAD image of grid block designed for dowel rods**

The task of constructing the shape was a useful exercise as it provided an insight into how this alternative manufacturing process could be implemented. The dowel rods were grouped into the different sizes (Figure 42 shows the initial set-up). Using the print-out of the grid layout, the dowel rods were inserted into the foam block into the correct grid reference, starting with the smaller heights. Figure 43 illustrates the final representation of a child's system using dowel rods and Figure 44 illustrates the use of a cover which would act as a smoothing mechanism. A larger (adult size) shape was also represented using the same method, as shown in Figure 45. Section 7.3 suggests possible methods to implement this potential manufacturing technique, where the dowel rods would be replaced with foam rods.

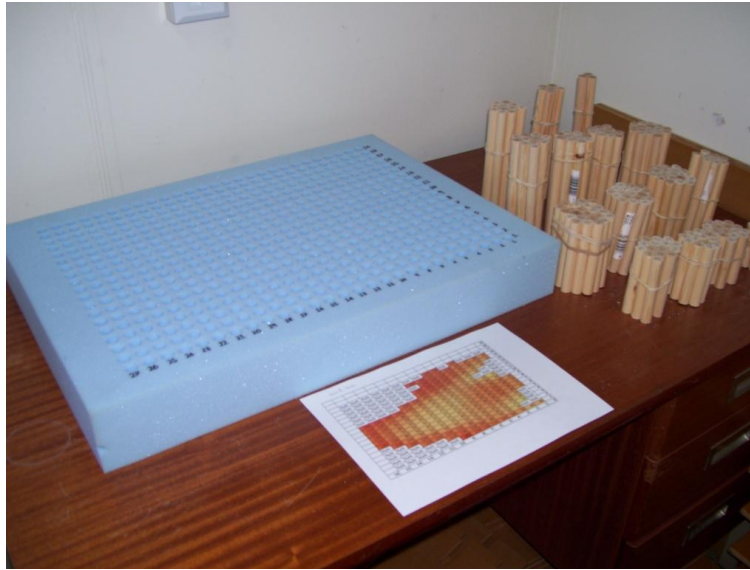


Figure 42. Initial set-up of column rod arrangement

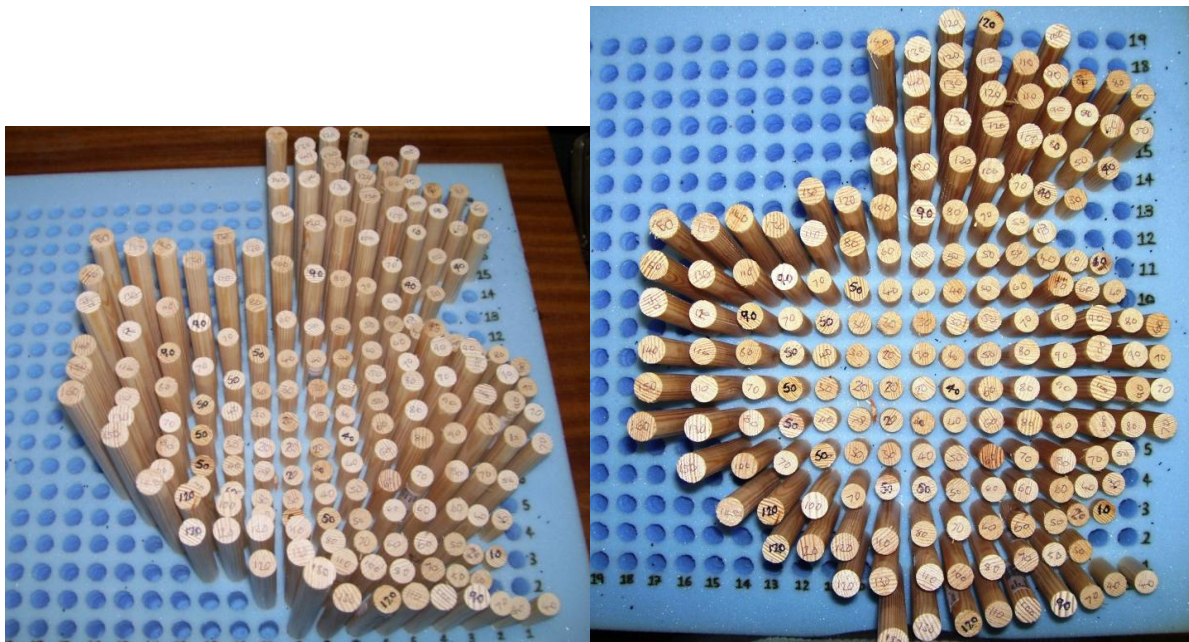


Figure 43. Representation using dowel rods for NW8base shape (child)



Figure 44. Material added to dowel rods to illustrate potential of using coverings to smooth the contours of the shape.

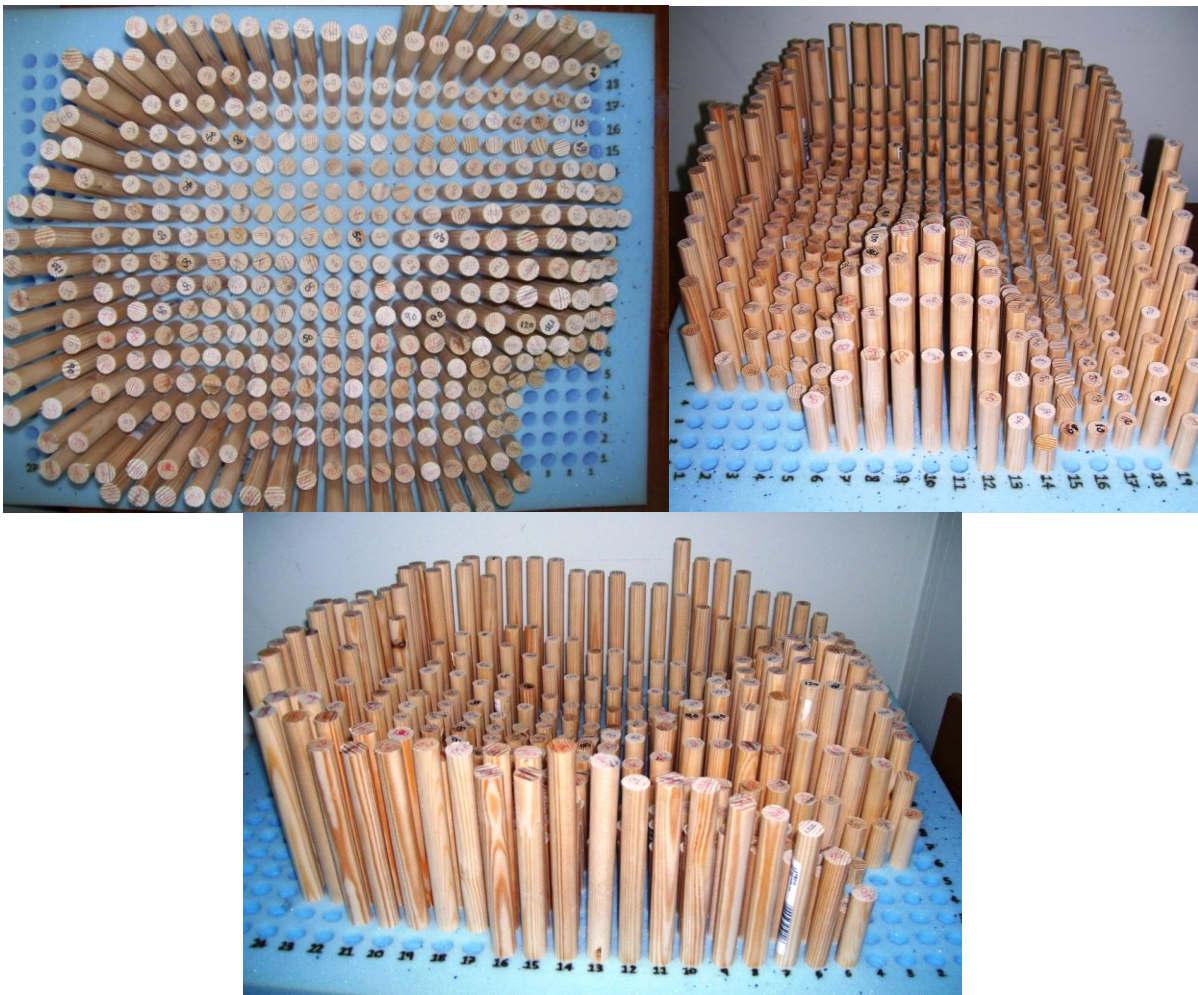
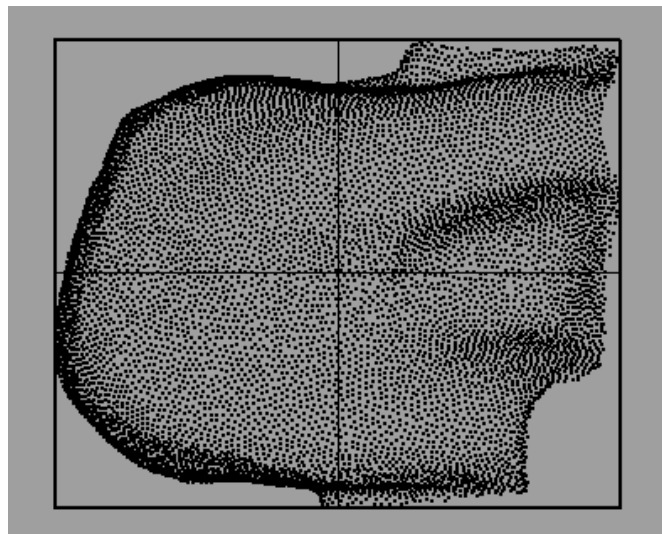


Figure 45. Dowel representation for CH2base shape (adult)

### 6.2.4 Standard Deviation and Coefficient of Variation

The java program developed for the analysis of shape data (described in Section 5.4.4) provided standard deviation and coefficient of variation values for each grid cell.

The need for this is to identify steep variations in the shape's contours within a defined grid cell. Figure 46 illustrates that certain areas of a shape contains a greater variation in height, where the points appear stacked on top of each other, this occurs in high contoured areas at the edges and around the pommel. Therefore, the mean value of the points within these grid cells may not be the best representation for column heights. Figure 47a shows the averaged column heights for CH2base for 20mmx20mm grid cell size. The standard deviation of the y values of the points will provide an indication into the range of heights. A high standard deviation value will result if there is a steep contour. Figure 47b displays the results for the S.D values for shape CH2base for a 20x20mm grid size.



**Figure 46.** CH2base scan data to illustrate that some areas contain a greater variation in heights of the points

The standard deviation reveals some 'hot spots' (the greatest S.D for CH2base is 62.27), as shown in Figure 47b. This reveals that these areas contain large variations in height.

In addition to the S.D, the coefficient of variation (CoV) for each cell was calculated. Figure 47c shows the coefficient of variation results. These areas mostly correlate with the S.D's hot spots, however because of CoV is a normalised measure it does highlight additional areas where the range of heights is greater in relation to the mean (e.g. in the bottom right-

hand corner of the shape a 62.57% CoV is calculated for one cell). The results for different grid resolution are illustrated in Figure 48 and Figure 49.

These results have the potential to increase the accuracy of the geometric representations of the shapes, because highly contoured areas can be highlighted using this method and therefore a finer resolution may be employed for these localised areas. These concepts are described further in the Discussion (Section 7).





NaN	NaN	147.41	144.22	154.19	161.23	122.73	95.182	80.467	46.253
137.38	137.88	115.32	86	94.863	81.276	63.76	33.769	27.637	16.533
140.73	90.926	45.691	23.536	15.403	17.311	22.695	39.152	45.334	30.996
137.72	61.814	31.493	22.48	27.582	44.917	76.762	105.84	103.74	66.276
130.09	63.577	41.409	39.021	52.96	78.748	107.59	130.44	108.26	72.794
130.09	55.191	43.194	47.845	57.931	68.195	76.469	78.726	67.075	72.999
139.33	102.19	54.378	49.406	49.654	48.467	43.974	25.122	13.206	NaN
141.04	134	131.61	126.02	119.71	101.44	85.753	53.431	NaN	NaN

a)

Standard Deviation of Y									
NaN	NaN	15.881	19.654	13.68	6.8401	24.703	21.536	18.56	14.418
13.594	34.897	42.412	42.141	46.11	40.483	35.275	10.661	10.636	5.3173
30.79	42.62	11.254	8.0295	3.1569	1.9673	6.8217	16.898	22.789	14.605
35.54	11.117	7.1327	5.2802	9.854	16.647	23.206	20.725	16.672	8.7508
37.029	7.6193	6.0648	5.2667	6.7865	9.7646	7.6164	5.5136	19.321	3.9965
38.459	6.8391	1.4613	3.4992	3.3133	8.1921	16.583	25.526	27.472	7.29
31.586	50.683	15.793	2.5044	1.9733	2.5585	3.4172	11.422	3.4033	NaN
0	27.778	39.773	43.266	43.209	32.728	26.004	23.588	NaN	NaN

b)

Coefficient of Variation									
NaN	NaN	10.773	13.627	8.872	4.2424	20.128	22.626	23.065	31.172
9.8952	25.31	36.776	49.001	48.607	49.81	55.324	31.57	38.484	32.162
21.88	46.873	24.631	34.116	20.495	11.364	30.058	43.161	50.27	47.121
25.806	17.984	22.649	23.489	35.727	37.061	30.231	19.581	16.071	13.204
28.464	11.984	14.646	13.497	12.814	12.4	7.0793	4.2268	17.847	5.4902
29.563	12.392	3.3832	7.3136	5.7194	12.013	21.685	32.423	40.957	9.9864
22.671	49.597	29.044	5.0691	3.9742	5.2787	7.7709	45.465	25.772	NaN
0	20.729	30.221	34.334	36.095	32.264	30.325	44.147	NaN	NaN

c)

Figure 49. CH2base 50x50mm grid size a) Mean column heights (Y) b) Standard deviation c) Coefficient of variation

### 6.2.5 Tolerance between represented shape and scan data

It was hypothesised that more than half of the seats will be reproducible using a set of generic geometric shapes, which are within a  $\pm 10\text{mm}$  tolerance from the true shape. The standard deviation provides an indication as to how well this tolerance is achieved. In addition, the java program was adapted to provide an output of the magnitude of deviation from the mean for each raw point.

By examining the shapes (NW8base and CH2base) modelled using dowel rods (Section 6.2.2); the  $\pm 10\text{mm}$  tolerance was tested using the java program. The outputs from the java program provided the magnitude of the difference between each raw point height (y coordinate) and the represented mean height (the column height rounded to the nearest 10). Table 19 summarises these comparisons.

**Table 19. Difference between represented shape and scan data for NW8base and CH2base.**

	NW8base (Child)		CH2base (Adult)	
	20mmx20mm grid cell size	10mmx10mm grid cell size	20mmx20mm grid cell size	10mmx10mm grid cell size
Number of raw points	3709		9800	
Number of points exceed $\pm 10\text{mm}$	1321 (35.6%)	693 (18.7%)	4035 (41.2%)	3072 (31.3%)

The results in Table 19 confirm that a smaller grid cell size (i.e. a finer resolution) provides a better representation of the true shape where fewer points exceed the tolerance of  $\pm 10\text{mm}$ . These results are discussed further in Section 7.2.2 .

### 6.3 Generic shapes investigation

As described in Section 4.3.3, Li et. al used cluster analysis to detect natural groupings amongst the shape data, where four clusters were identified (Li et al. 2000). This approach was explored briefly below to determine if a similar methodology would be applicable to this sample to identify generic shapes. Only the base shapes were investigated because of the results in Section 6.2.2 which indicates that the range of back shapes was more diverse.

### 6.3.1 Smoothed histograms

With no prior knowledge of the possible groupings of these shapes, exploratory data analysis (EDA) was used. EDA often uses graphical techniques to explore and provide insight into the data. A method was required which allowed some form of pattern-recognition to take place to aid the identification of similarities and differences between the shapes. The histograms produced (Figure 36 to Figure 38 in Section 6.2.2 and Appendices, Section 11.4) provided some insight, however when 5 or more histograms were plotted on the same graph, the ability to detect patterns was limited.

In order to compare and contrast the frequency tables resulting from the different bases, the Gaussian kernel was used to 'smooth' the histograms so that they could be superimposed onto one graph, as shown in Figure 50 to Figure 52. This is calculated simply by weighting each class interval mid-point in the histogram with a Gaussian (or Normal distribution density) kernel, centred on that mid-point, and with a standard deviation parameter chosen (experimentally) to equal the class-width (which equals 10). If the smoothing parameter is set to be small compared to the class-width of the frequency table, then the result is peaks matching the heights of each frequency. By setting the smoothing parameter to be smaller than the class width, the resultant curve reveals many spikes and lots of gaps. The resultant smoothed curve has a total area under the curve which equals 1; this changes the values of the y axes accordingly. It was considered that the absolute frequencies were not relevant for the purposes of exploratory data analysis where similarities in the graphs' features were being examined.

More specifically, the density at a point  $x$  is given by Equation 1.

$$f(x) = \sum_{i=1}^n \frac{f_i e^{-(x-x_i)^2/2\sigma^2}}{f\sigma\sqrt{2\pi}} ; \text{(Eq. 1)}$$

where  $f_i$  is the frequency of the class-interval with mid-point at  $x_i$ ,  $f$  is the total frequency, and  $n$  is the number of class intervals.

The algorithm described above was applied to each Shape Frequency Table using the Gaussian distribution as the probability density function. A purpose built application was used utilizing APL language (Sykes 2008).

These smoothed histograms were used to detect whether features from the shapes can be related to features on the graph. The graphs illustrated in Figure 50 to Figure 52 were generated to test suggested grouping of distributions. Table 20 describes these suggestions, where the features of the graphs (e.g. Bimodal or trimodal) were associated with features of the shapes.

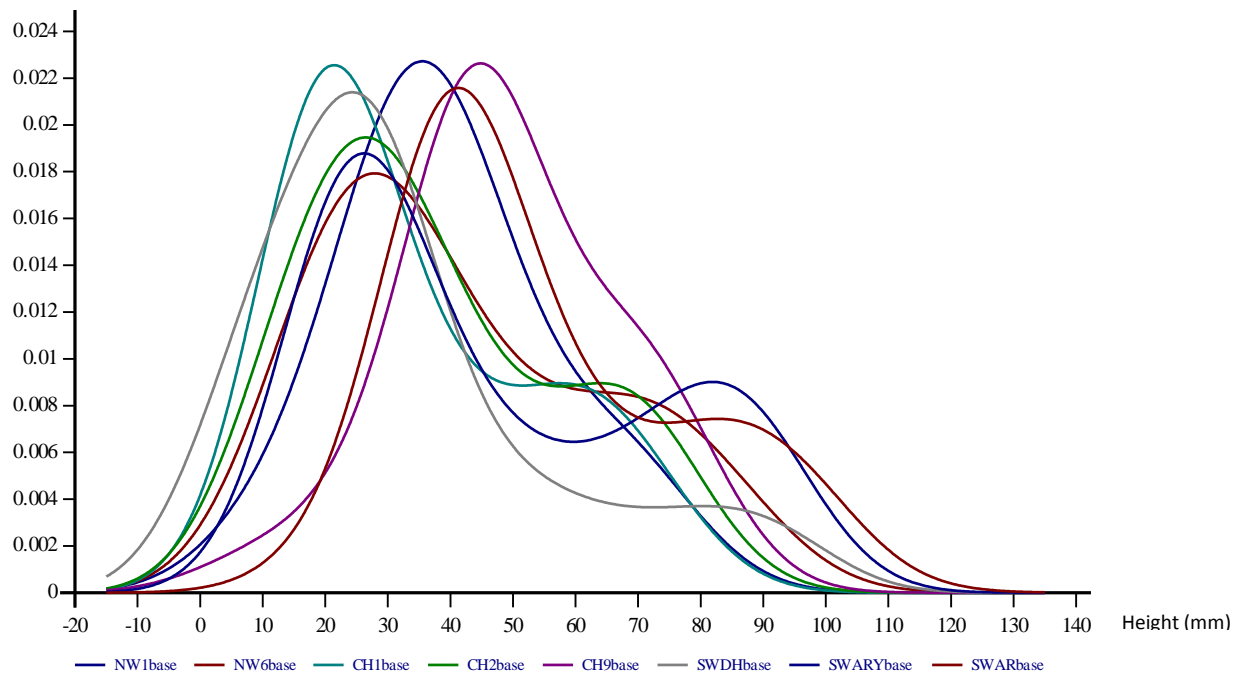


**Figure 50. Smoothed histograms for Bases (Group A)**

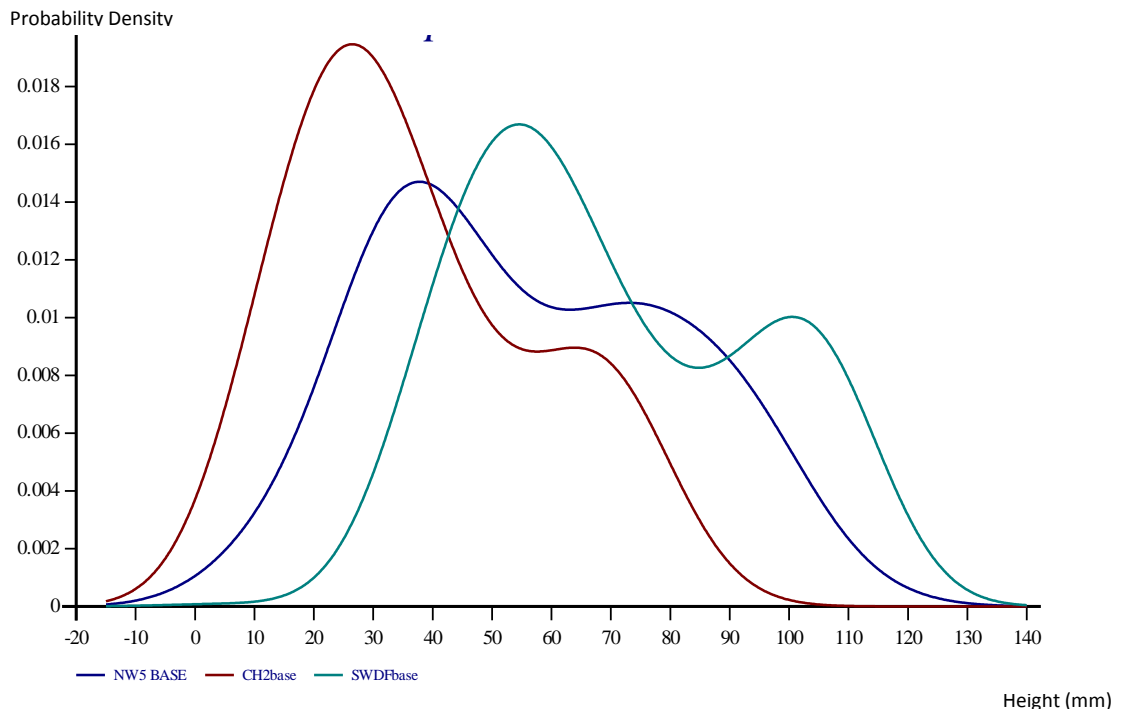


Figure 51. Smoothed histograms for Bases (Group B)

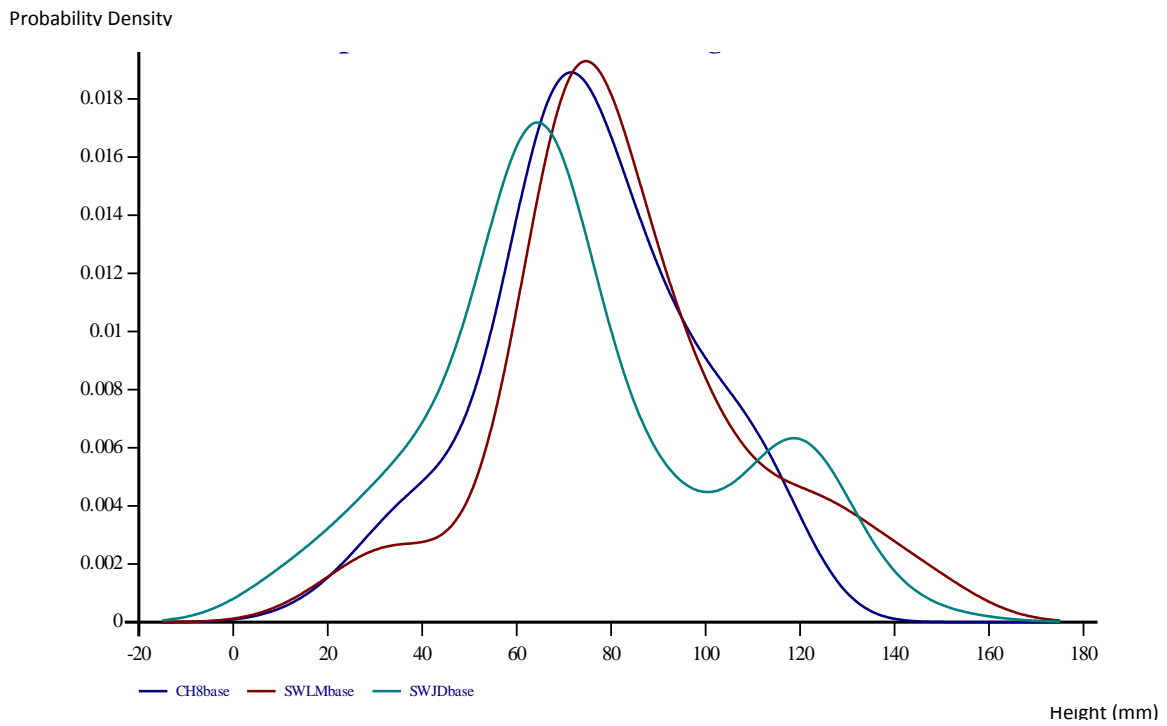


Figure 52. Smoothed histograms for Bases (Group C)

**Table 20. Description of potential groupings from visual analysis of smoothing histograms.**

Group	Graph features	Shape ID	Description
A	Bimodal (skewed)	NW1base	Pommel
		NW6base	Pommel
		CH1base	Pommel
		CH2base	Pommel
		CH9base	Pommel
		SWGJbase	Pommel cut-out
		SWDHbase	Pommel cut out
		SWARYbase	No pommel
		SWARbase	No pommel
B	Bimodal (with more equal modal frequencies)	NW5base	No pommel wide sides
		CH2base	No pommel wide sides
		SWDFbase	Pommel and leg channels
C	Unimodal	CH8base	Pommel and leg channels
		SWLM	Pommel and leg channels
		SWJD	Long leg channels-due to slope of thighs.

This approach of pattern-recognition was very subjective but the smoothed histograms did reveal similarities and differences between the shapes, however it was decided to investigate whether the frequency table shapes could be subject to a cluster analysis, thereby revealing groups of frequency tables with similarities, which may (or may not) correspond to identifiable characteristics in the original shape surfaces.

### 6.3.2 Cluster analysis and Chi-squared test

Cluster analysis is used to determine the intrinsic structure of clustered data when no information other than the observed values is available (Fraley & Raftery 1998). Cluster analysis aims to partition the data into meaningful subgroups. Hierarchical cluster analysis attempts to identify relatively homogeneous groups of cases (or variables) based on

selected characteristics, using an algorithm that starts with each case (or variable) in a separate cluster and combines clusters until only one is left.

This approach to cluster analysis is most suitable when clusters of a small number (less than a few hundred) are expected. Hierarchical cluster analysis begins by separating each object into a cluster by itself. At each stage of the analysis, the criterion by which objects are separated is relaxed in order to link the two most similar clusters until all of the objects are joined in a complete classification tree. The basic criterion for any clustering is distance. Objects that are near each other should belong to the same cluster, and objects that are far from each other should belong to different clusters. The objects in this case are the Shape Frequency Tables. A usual measure used for cluster analysis is the Euclidean distance (square root of the sum of the squared differences between values for the items) which would have been suitable if the surfaces were used directly for analysis. However this is not applicable in this investigation because the frequency tables are compared. Instead, the chi-square measure can be chosen as a statistical test of significance of the discrepancy between the observed and the expected results. This tool tests the hypothesis that the two sets of frequencies are compatible with the same probability distribution which provides an appropriate measure of distance. In other words, by comparing two frequency tables, i.e. the proportions in each row of a column are the same for each column. These calculation steps are explained in the Appendices, Section 11.5.

A dendrogram (Figure 53) was constructed which grouped the Shape Frequency Tables according to distances dictated by the chi-square values Table 24 in Appendices, Section 11.5.

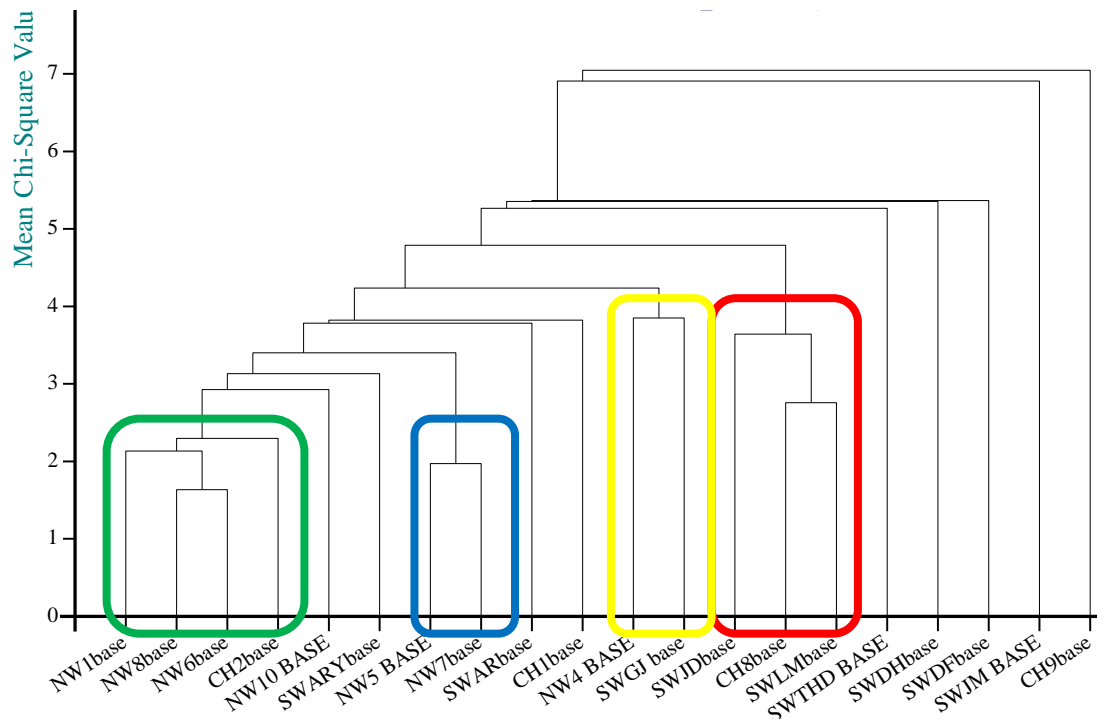


**Figure 53. Dendrogram which reveals 4 potential clusters**

As Figure 53 illustrates, the first dichotomy divided the 20 shapes into two clusters of 1 and 19 shapes. This large cluster of 19 shapes is hierarchically subdivided into 4 shapes (that appear as outliers) and 15 shapes which appear to belong to one cluster at linkage distance 4.788. At linkage distance 4.788, a possible two-cluster solution presents:

- C1 (red)= SWLMbase, CH8base and SWJDbase
- C2 (yellow)= SWGJbase and NW4base

Two further clusters can also be considered at linkage distance 2.293:

- C3 (blue)= NW5base and NW7base
- C4 (green)=NW1base, NW8base, NW6base and CH2base

Further work is clearly required to confirm these results (Section 9). However, this approach has demonstrated a possible statistical method which may aid the classification and identification of generic shapes.

---

## 7 DISCUSSION

---

In the specialist field of wheelchair seating there is insufficient knowledge or scientific evaluation of customised postural support shapes. The predominant methodology for capturing shape information employs vacuum consolidation followed by the manufacture of a plaster cast. As a result, shape information is rarely digitally recorded which has hindered the scientific evaluation of the shape of individuals with disabilities. The purpose of this project was to utilise scanning technologies (a low-cost and high-cost scanner) to capture the 3D information of customised support systems to enable the development of shape recording, processing and analysis techniques. This study has provided the following results and outcomes:

- Shape acquisition technology comparisons and recommendations
- Data acquisition equipment validation
- Shape analysis processes have been developed, to provide:
  - Bounding box sizes
  - Generic geometric shape representations
  - Shape frequency tables used as shape descriptors to enable statistical comparisons
  - Statistical measures to set criteria for grid cell size (or resolution)
  - Overall increased understanding of the shapes
- Potential manufacturing techniques explored by the definition and utilisation of generic shapes

The implications from these results are discussed in the following sections.

### 7.1 Shape acquisition comparisons and Microscan validation

Several shape acquisition methods were explored in the project to ascertain the current state of the technology available, some of which are currently used (and commercially

available) in the special seating field (such as the Otto Bock Shape System and Invacare's Pin Dot Machine). The use of electronic shape capture is well established in the prosthetics and orthotics fields (Ohio Willow Wood 2007), where several commercial shape measurement and design products exist. Very few of these techniques allow measurements to be taken of the weight bearing seated area and most of them cannot be adapted to a wheelchair. The measuring resolutions of human shape capture using these techniques ranged from 3.9 to 50mm in the reviewed methods. The resolution of the scanners employed in this project is far greater than that reported in the literature and existing tolerances used within special seating is estimated to be approximately  $\pm 10\text{mm}$ . However, there is a lack of scientific knowledge of the optimum tolerances of special seating systems for different individuals with different disabilities and functional needs.

The shape acquisition methods reviewed in the literature have only been designed to capture base cushion shapes, and not backrests (with the exceptions of (Yamazaki 1992) and PinDot). It therefore appears that there is a lack of research into backrest shapes. This project analyses the shapes of both bases and backs.

The shape acquisition literature reviewed described consistent measuring apparatus which is clearly essential for research purposes where comparisons are required. The shapes used in this project have been sourced from three special seating centres to achieve a representative sample of the variety of shapes. This also ensures that the results are not specific to one special seating centre. The disadvantage of this approach is that each centre employs different shape capturing methods; possibly introducing variations which cannot be controlled. Another area of inconsistency is that some of the casts used for the project had the pommel area removed. The pommel is usually cut out to allow for a drop-down pommel which may be removed to ease transfers and toileting. The results show that there is no clear distinction from the results between bases which have pommels and those that do not. However, for non-pommel casts the Shape Frequency Tables (SFT) would be missing a small proportion of columns, which may have implications on the exploratory data analysis reported in Section 6.3, where comparisons are made between the SFTs. This inconsistency was beyond the control of the author, however for future work an additional exclusion criteria may be specified for the sample of casts. The exclusion of these non-pommel casts

may provide clearer comparisons to allow generic shapes to be identified. The shape acquisition techniques reported in the literature (for example (Li et al. 2000)) do not consider the effect of posture at the time of measurement on the shape pattern. One particular study (Li et al. 2000) attempted to reduce these affects by ensuring a neutral position was adopted during each data collection process. These variations were not controlled in this project because customised shapes for seating systems typically accommodate asymmetrical body postures where bone structure deformities are usually present.

The results from the 3D comparisons between the Faro scanner (high-cost, gold standard) and Microscan (low cost) revealed very good agreement. The best deviation results were calculated for the Chailey (CH) casts, where 76.9% (CH1) and 78.6% (CH8) of comparison points were within a  $\pm 0.5\text{mm}$  tolerance. The tolerances were adjusted to  $\pm 1.0\text{mm}$  and 94.9% (CH8) of points compared were within  $\pm 1.0\text{mm}$ . The coloured-3D graphical results show that areas that exceed these tolerances appear to be at the edges and within deep recesses of the shapes. Scanning in tight concave areas can be difficult because of the angle of the reflections back to the scanner's camera. For this reason, these areas may be more prone to noise and errors.

The 3D comparisons results also provide an interesting insight into the different manufacturing techniques used by the three special seating centres to manufacture the plaster impression of a client. For example, both Swansea casts (SWJD and SWLM) that were compared indicates that an overall distortion of the shape appears to have occurred rather than in localised areas. In particular, SWLM appears to have experienced its greatest distortion at the edges. Swansea casts are manufactured using Plaster of Paris to create a shell impression of the vacuum consolidated bead bag. This shell-type cast is more prone to damage as they can become flexible. In comparison, the other cast types from North Wales and Chailey are solid. This is a likely reason for the relatively poorer results for the SWJD and SWLM comparison, where the Microscan was performed a few months after the Faro scan. It was concluded that the period between time of the Faro scan and Microscan and the manner of storage allowed distortion or damage to the shape.

A consequence of these results is that the Digital Seating Service at Swansea REU have now eliminated this plastering technique by using the Microscan to scan the bead bag impression of the client within a short time of the shape being captured. The results from this project further support the use of scanning technologies for the recording of shape data for clinical work as detailed information can be retained in digital file for possible future work such as reproductions and alterations. In addition, reproductions using the digital method have a significant cost reduction when compared to previous liquid foam techniques.

Despite these discrepancies, it was considered that the results for the comparable casts validated the use of the lower cost laser scanner for both research purposes and clinical work utilising CAD/CAM techniques (Digital Seating Service). This validation was made on the basis that the data are superior to that available from most shape collection devices used clinically and from clinical experience it is considerably greater to previous/existing tolerances used within the special seating field. In addition, the comparison of time of scans reveals that a Faro scan can take up to double the time compared to Microscan. This is an important factor when considering service delivery aspects for the CAD/CAM production of seating systems.

These results provide useful information to manufacturers of special seating systems where more affordable scanning technologies (such as the Microscan, which costs approximately £15,000) should be considered as a viable option to advance the clinical services within the field.

## **7.2 Shape analysis processes**

The literature review of shape analysis techniques revealed that many shape analysis techniques have been formulated to aid the retrieval process within database systems. It is apparent that the primary challenge in building a shape analysis and retrieval system is to develop a computational representation of shape (or shape descriptors) to allow similarity queries to be performed.

### **7.2.1 Bounding box sizes**

Simple global descriptors that can only discriminate shapes with large differences, such as area were investigated in this project by obtaining the sizes of each shape's bounding box. These basic results can provide important information which may aid the manufacturing of these customised moulded systems. It is common for these customised systems to be mounted into an ABS (plastic) box which are individually made to suit the dimensions of the customised system. The range of sizes from the results obtained may be used to design pre-prepared standardised mounting systems. For example, a set of three sizes may be designed to be adjustable to accommodate the sizes specified in this project. This would have important implications by reducing time and costs and may also aid issues surrounding the crash-testing of these components which is currently not possible because of their unique dimensional properties. The bounding box dimensions are dependent on the rotational position of the raw scan data of the shape that was set in Rhino 3D. A consistent approach was used and specified in Section 5.4.2. However, to achieve a more accurate position of these shapes in 3D space, procedures will have to be in place at the time of scanning where the orientation of the scan data in 3D space is defined. The current orientation protocols used by Digital Seating Service may be adapted for further shape acquisition for research.

The bounding box sizes provide the dimension of the minimum size of the mounting ABS box; however a thickness of 25.4 mm (1 inch) is typically specified as the minimum amount of foam underneath the lowest part of the client. This is thought to be important in order to eliminate pressure high spots. This extra thickness can be accounted for by adding the known constant to the X and Y dimensions to determine definitive bounding box sizes.

### **7.2.2 Geometric shape representations**

At the high-end of the spectrum of shape analysis, a shape can be decomposed into its parts automatically through algorithms that decompose its surface or approximate its volume with a set of simple primitives. This concept was explored further by representing the shapes as column rods. This concept was considered applicable to the project as it provides a method of analysing the shapes, however it is not analysing the surface directly but instead a 'shape function' is derived, defined as a 'Shape Frequency Table'. In addition, this

shape representation approach provides a representation of the volume that would equate to the final manufactured seating system.

This project has developed a shape analysis process to derive these shape frequency tables. The analysis process utilises java programming language to execute the calculation steps to provide an output of the column heights (and the frequency of the heights) for a defined column size. The program can also provide a grid layout indicating the location of each column height. The Shape Frequency Tables were used to produce Histograms to act as shape descriptors, which were used as part of exploratory data analysis to allow comparisons to be made, and the use of cluster analysis was investigated (as described in Section 6.3).

### **7.2.3 Use of statistical measures as grid cell size dictator**

Additional statistical measures were investigated to improve the shape representation approach, by highlighting areas where non representative column heights are located. This typically occurs in steep areas of the shape where the range of heights for the raw points was large. To address this, the standard deviation and coefficient of variation was used to highlight these areas. This approach can be likened to Jackowski et. al's method which uses a subdivision algorithm that positions large triangles in flat areas and small triangles in detailed areas in a shape to achieve a high compression rate by approximating digital 3D (of spherical topology) shape by a rational Gaussian (RaG) surface (Jackowski et al. 2003).

The standard deviation results can also reveal other potential problem areas where undercutting or recesses occur. This is where there is a large concave curvature on the sides of the shape. Figure 54 shows an example of this phenomenon where the grid cell averages the points from the lower flat portions of the shape and the high sides. This provides a high standard deviation (S.D) and coefficient of variation (CoV) values, as shown in Figure 56 and Figure 57 respectively by the darker orange cells located on the inside of the sides. Figure 54 confirms these results as the average heights for a 20mmx20mm are higher on the interior side of the shape at the steep edges.

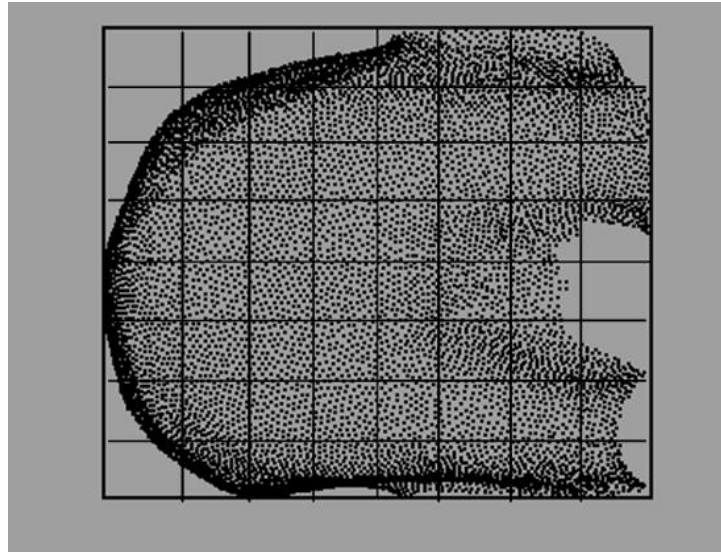


Figure 54. CH1 base highlighting potential misrepresentative areas on curved sides

NaN	159	136.6	129.2	125	120.1	117.3	118.4	116.6	115.7	107.6	NaN	NaN											
NaN	NaN	NaN	NaN	NaN	NaN	114.4	119.2	127.6	133.7	146.8	149.7	121.1	105	103.1	99.48	100.2	104.8	108.1	107.4	93.21	NaN	NaN	
NaN	NaN	NaN	103.9	115.5	120.5	125.8	133.8	138.4	125.9	87.62	69.35	70.48	70.67	69.68	68.32	68.33	74.28	75.47	73.69	61.59	42.5	NaN	
NaN	NaN	106.6	118.7	122.8	132.8	130.4	101.8	48.74	45.14	45.19	44.28	44.21	45.13	44.37	43.53	43.26	45.94	45.75	42.08	34.49	27.57	NaN	
NaN	97.04	117.1	129.2	121.5	71.87	44.41	40.97	36.73	34.49	33.43	32.59	32.8	32.61	32.89	32.48	33.6	33.55	32.67	29.35	21.62	12.47	NaN	
NaN	115	132.8	115	47.26	42.63	37.92	34.65	30.36	28.61	27.28	26.44	26.6	26.48	27.59	30.47	32.39	32.46	30.03	26.42	18.73	6.926	NaN	
107.9	119.4	112.1	46.59	41.47	37.6	33.22	29.32	26.57	25.66	24.94	24.45	25.88	28.13	32.14	34.6	37.85	39.2	37.93	34.16	25.49	10.47	0.049	
123.8	122.5	66.34	44.02	38.97	36.41	33.13	29.57	27.34	26.26	25.36	25.24	28.09	34.15	43.01	47.48	52.38	56.31	59.72	57	47.37	24.51	NaN	
132.8	72.17	45.51	42.37	38.91	36.53	34.1	30.74	28	26.42	26.05	28.61	35.29	46.91	58.88	65.18	73.45	80.21	83.96	83.23	64.48	36.8	NaN	
132	58.24	44.59	41.38	39.15	36.46	33.63	30.45	26.64	23.36	23.82	28.26	40.72	54.25	68.63	82.86	92.34	100.3	105	NaN	NaN	NaN	NaN	
130.1	61.01	47.41	40.96	38	34.99	30.8	27.73	24.36	22.56	24.5	28.84	38.94	56.29	75.66	90.74	102.2	110.6	115.6	NaN	NaN	NaN	NaN	
132.5	64.62	49.01	40.6	35.25	30.14	26.55	24.4	22.61	24.03	26.45	32.45	43.61	60.29	78.85	94.58	107.6	113.7	116.8	NaN	NaN	NaN	NaN	
136.1	69.02	52.62	41.42	33.18	27.16	23.71	23.04	23.88	25.83	29.24	35.01	44.84	56.62	66.99	82.27	97.23	106.3	110.2	109.2	NaN	NaN	NaN	
141.1	87.49	57.84	44.55	34.42	28.16	24.37	22.71	22.49	22.85	25.26	29.41	33.56	40.1	49.44	60.51	73.46	84.6	92.11	96.02	92.6	65.11	NaN	
138.2	124.5	66.55	49.94	39.34	31.4	26.61	24.56	22.7	21.81	23.28	26.78	30.2	34.19	39.38	44.83	49.46	56.43	60.4	64.24	61.32	46.84	NaN	
131.7	140.8	82.27	61.42	46.8	37.53	30.74	28.08	26.51	24.78	26.07	28.18	30.71	33.83	37.38	39.27	39.55	38.83	37.99	36.06	30.97	NaN	NaN	
NaN	142.7	137.5	85.41	61.41	47.02	38.94	35.77	33.72	32.66	32.76	35.09	35.81	39.3	41.96	45	42.97	38.88	36.04	32.55	25.65	NaN	NaN	
NaN	NaN	145.1	140.8	102.2	71.04	60.98	54.38	51.19	47.03	47.34	52.79	58.9	64.02	65.07	63.27	60.65	56.93	52.72	48.25	41.19	NaN	NaN	
NaN	NaN	NaN	152.7	150.2	139.9	133.8	127.8	126.8	122.2	125.2	129.5	125.9	123.5	121.7	115.5	109.2	105.8	98.7	90.8	83.4	75.15	NaN	

Figure 55. Average column heights for CH1base showing higher column heights on the interior side of the shape at the top-left side

NaN	18.08	6.92	4.037	2.942	2.399	1.828	0.996	1.11	1.349	0	NaN	NaN											
NaN	NaN	NaN	NaN	NaN	NaN	7.111	13.44	20.71	28.75	34.13	38.17	35.41	10.48	9.73	9.448	8.709	9.744	7.403	6.512	10.1	NaN	NaN	
NaN	NaN	NaN	0	16.44	25.9	34.48	45.64	54.54	63.11	47.06	11.34	10.29	9.874	9.897	9.225	10.03	10.71	12.55	14.59	12.26	5.416	NaN	
NaN	NaN	12.61	25.4	42.72	57.25	67.57	69.81	5.063	4.281	4.942	3.953	4.166	5.188	5.037	4.534	5.523	5.339	4.261	4.821	5.258	5.736	NaN	
NaN	6.122	29.96	54.09	66.99	53.01	2.873	2.224	2.608	2.107	2.368	2.687	2.797	2.941	2.728	1.521	1.569	2.142	3.437	3.314	4.117	4.609	NaN	
NaN	28.15	53.83	69	2.254	1.906	1.768	1.746	1.842	1.217	1.306	0.997	0.659	0.704	0.975	0.926	0.565	0.794	1.735	1.975	2.752	4.023	NaN	
12.91	39.12	67.9	2.298	1.6	1.593	1.505	1.144	1.153	0.649	0.34	0.322	0.646	1.07	2.839	2.872	2.993	2.958	4.073	4.626	6.042	5.142	0	
27.43	58.85	47.22	1.528	1.137	0.971	1.135	0.99	0.606	0.507	0.655	0.92	2.009	3.248	4.032	4.56	5.686	6.862	7.911	8.052	11.06	12.03	NaN	
36.2	38.53	2.051	1.241	0.969	0.771	0.975	1.069	0.677	0.352	0.479	1.682	3.88	4.581	5.174	6.945	6.736	7.177	5.759	0	3.476	10.57	NaN	
35.88	6.513	1.51	0.728	0.799	1.014	1.02	0.942	1.378	0.847	0.51	2.667	3.944	4.258	4.515	4.953	5.139	5.316	3.525	NaN	NaN	NaN	NaN	
36.23	5.513	2.767	1.206	1.155	1.262	1.494	1.34	1.504	0.533	0.979	1.706	4.144	5.782	5.01	4.981	3.313	2.87	1.812	NaN	NaN	NaN	NaN	
33.87	6.168	3.502	1.497	1.559	1.708	2.013	1.318	0.702	1.483	1.766	3.464	5.236	6.98	4.897	5.19	2.253	1.496	0.527	NaN	NaN	NaN	NaN	
33.81	5.632	4.296	2.598	2.026	1.349	0.694	0.155	0.698	1.022	1.365	2.275	4.912	6.069	6.851	7.358	6.269	4.599	3.543	0	NaN	NaN	NaN	
28.42	29.88	4.76	3.724	2.415	1.369	1.011	0.165	0.435	0.862	1.515	1.999	2.739	3.9	5.184	6.77	9.035	8.782	7.349	7.507	6.236	11.71	NaN	
20.18	42.25	6.146	4.508	2.815	2.303	1.736	1.167	1.005	0.747	0.848	0.855	1.441	1.436	2.165	3.122	5.035	8.253	10.5	11.97	13.52	9.773	NaN	
8.672	30.06	8.832	6.888	3.995	2.906	2.005	1.486	1.318	1.57	1.44	0.846	1.329	1.294	1.041	0.968	1.135	2.889	2.678	3.824	4.426	NaN	NaN	
NaN	16.32	32.9	22.05	6.999	4.899	4.072	3.436	3.432	3.052	2.86	3.269	3.14	2.945	2.802	2.862	2.763	2.772	2.808	3.078	4.15	NaN	NaN	
NaN	NaN	17.34	30.35	30.94	11.19	9.162	7.313	6.622	5.273	5.753	7.71	10.2	10.72	10.62	7.839	7.74	8.648	7.782	6.317	9.201	NaN	NaN	
NaN	NaN	NaN	10.69	22.77	29.94	33.66	35.93	37.65	38.99	39.12	37.96	29.16	22.57	20.55	21.95	22.17	19.53	18.94	17.89	17.83	13.49	NaN	

Figure 56. Standard Deviation results for CH1base highlights the higher S.D values on the interior side of the shape at the top-left side

NaN	11.37	5.064	3.125	2.353	1.997	1.558	0.842	0.952	1.166	0	NaN	NaN											
NaN	NaN	NaN	NaN	NaN	NaN	6.216	11.28	16.23	21.49	23.25	25.51	29.25	9.979	9.437	9.497	8.688	9.3	6.848	6.066	10.84	NaN	NaN	
NaN	NaN	NaN	0	14.24	21.49	27.42	34.11	39.41	50.14	53.71	16.35	14.6	13.97	14.2	13.5	14.67	14.42	16.63	19.8	19.91	12.74	NaN	
NaN	NaN	11.83	21.4	34.78	43.1	51.82	68.55	10.39	9.483	10.94	8.926	9.422	11.5	11.35	10.42	12.77	11.62	9.315	11.46	15.24	20.8	NaN	
NaN	6.308	25.59	41.88	55.14	73.75	6.468	5.429	7.101	6.11	7.085	8.245	8.528	9.02	8.293	4.684	4.671	6.384	10.52	11.29	19.05	36.96	NaN	
NaN	24.47	40.53	60.01	4.769	4.471	4.662	5.039	6.067	4.254	4.787	3.772	2.476	2.661	3.533	3.039	1.744	2.445	5.778	7.478	14.69	58.08	NaN	
11.97	32.77	60.59	4.932	3.857	4.238	4.529	3.901	4.34	2.528	1.362	1.315	2.497	3.803	8.834	8.301	7.906	7.545	10.74	13.55	23.71	49.1	0	
22.17	48.04	71.18	3.472	2.917	2.667	3.425	3.349	2.218	1.931	2.584	3.644	7.151	9.51	9.374	9.603	10.85	12.18	13.25	14.13	23.35	49.06	NaN	
27.25	53.39	4.506	2.93	2.491	2.11	2.86	3.478	2.419	1.332	1.839	5.879	11	9.766	8.786	10.66	9.172	8.947	6.86	0	5.39	28.72	NaN	
27.18	11.18	3.386	1.759	2.04	2.781	3.032	3.092	5.173	3.627	2.141	9.439	9.684	7.85	6.578	5.977	5.565	5.301	3.358	NaN	NaN	NaN	NaN	
27.84	9.037	5.836	2.943	3.039	3.605	4.853	4.833	6.174	2.364	3.998	5.917	10.64	10.27	6.622	5.489	3.24	2.594	1.566	NaN	NaN	NaN	NaN	
25.57	9.545	7.146	3.688	4.423	5.667	7.582	5.403	3.104	6.171	6.677	10.67	12.01	11.58	6.211	5.488	2.095	1.316	0.451	NaN	NaN	NaN	NaN	
24.84	8.161	8.165	6.273	6.107	4.968	2.927	0.674	2.923	3.958	4.667	6.499	10.95	10.72	10.23	8.944	6.447	4.328	3.214	0	NaN	NaN	NaN	
20.14	34.16	8.229	8.359	7.018	4.862	4.146	0.727	1.936	3.775	6	6.795	8.162	9.726	10.49	11.19	12.3	10.38	7.978	7.818	6.735	17.98	NaN	
14.6	33.92	9.236	9.026	7.156	7.337	6.522	4.752	4.425	3.426	3.64	3.192	4.771	4.201	5.497	6.963	10.18	14.62	17.38	18.63	22.05	20.86	NaN	
6.587	21.35	10.74	11.21	8.536	7.745	6.522	5.293	4.971	6.335	5.525	3.002	4.327	3.824	2.785	2.464	2.869	7.441	7.048	10.61	14.29	NaN	NaN	
NaN	11.44	23.93	25.81	11.4	10.42	10.46	9.607	10.18	9.345	8.729	9.317	8.77	7.495	6.679	6.359	6.429	7.131	7.792	9.458	16.18	NaN	NaN	
NaN	NaN	11.96	21.56	30.28	15.76	15.02	13.45	12.94	11.21	12.15	14.61	17.32	16.75	16.33	12.39	12.76	15.19	14.76	13.09	22.34	NaN	NaN	
NaN	NaN	NaN	7.001	15.16	21.39	25.15	28.11	29.69	31.89	31.25	29.32	23.16	18.28	16.88	19.01	20.3	18.46	19.19	19.7	21.38	17.95	NaN	

Figure 57. Coefficient of variation for CH1base highlights the higher CoV values on the interior side of the shape at the top-left side

The coefficient of variation was investigated as an alternative statistical output which would act as a dimensionless measure, which could prove more useful than the standard deviation to allow comparisons between shapes. The standard deviation values are dependent on the size of the shape. The usefulness of the coefficient of variation is inconclusive because when the mean value for each column is near zero, the coefficient of variation is sensitive to small changes in the mean, provided high CoV values revealing false hot spots, as shown in Figure 58.



### 7.3 Manufacturing approach

Applying the shape analysis process developed in this project could provide a potential low-cost method to fabricate these customised systems. The proportion of bases and backs which can be manufactured using the proposed geometric representations (where column heights are rounded to the nearest 10mm) was investigated as part of the analysis. As demonstrated in Section 6.2.2, Figure 39, the results may be used to select the optimum number of column heights to have in stock to achieve the fabrication of a certain proportion of seating systems. For example, if 25 different heights were chosen then the data suggests that 90% of Bases and 45% of Backs can be manufactured in this way. However, if 30 different heights were kept in stock then the data suggests that 90% of Bases and 75% of Backs may be manufactured using column representations of the shapes. The advantage of this is that scanning and analytical techniques may enable special seating providers to reduce the need for expensive CNC manufacturing techniques.

These results also clearly indicate that the range of back shapes is more diverse because a consistently smaller proportion of backs can be fabricated when compared to the bases. This confirms the clinical knowledge that the range of upper body skeletal deformities can be more diverse and require more support than pelvic shapes, where back postural systems are often supporting the client against the effect of gravity and side contours (also known as lateral supports) are often deeper to compensate for this. For this reason, it was decided to concentrate on the analysis of bases to investigate the feasibility of manufacturing these customised systems using geometric shapes.

In order to demonstrate this potential low-cost manufacturing technique for customised seating systems, a model was manufactured using dowel rods to represent foam rods. This demonstration was performed for two shapes (Figure 43 to Figure 45 in Section 6.2.2), which provided an appreciation into the best technique to use when inserting the correct heights according to the grid layout into the foam grid. It took approximately 10 seconds to retrieve the correct column height and insert into the correct grid reference. The number of columns range from 184 to 631 which equates to 30 minutes to 1 hour 45 minutes fabrication time. This could have significant implications to a clinical service where the

number of client appointment visits could be reduced. In addition, this time would increase with experience.

The data was analysed to predict stock levels by plotting the mean number of columns that are required for each column height for the 20 base shapes, as shown in Figure 40 in Section 6.2.2. This information may be useful to estimate stock levels, however as the graph indicates the range of column heights can be very large as illustrated by the maximum plots on the graph, particularly at the lower spectrum of the column heights.

It was hypothesised that more than half of the seats will be reproducible using a set of generic geometric shapes, which are within a  $\pm 10\text{mm}$  tolerance from the true shape. The standard deviation provides an indication as to how well this tolerance is achieved. However in addition this tolerance was tested (Table 19, Section 6.2.5) for the two shapes which were modelled (NW8base and CH2base). The results show that 64.4% of the raw points were within  $\pm 10\text{mm}$  tolerance of the represented shape for NW8base and 58.8% of raw points were within  $\pm 10\text{mm}$  tolerance for CH2base's represented shape, both using a 20mm x20mm grid cell size. It was predicted that a smaller shape would provide a greater number of deviations from the tolerance because of the finer contours. However this was not the case when compared with the larger shape (CH2base). This area would require further investigation to confirm these assumptions. The results did confirm that a smaller grid cell size provided a better representation to the scan data, where for NW8base the number of points within the  $\pm 10\text{mm}$  tolerance increased from 64.4% (20mmx20mm) to 81.3% (10mmx10mm).

The areas which exceed  $\pm 10\text{mm}$  tolerance correlated with the areas identified by high standard deviation values, which were localised to edges. It should also be considered that flexible foam columns would respond differently to the rigid dowel rods used in the demonstration. In reality in a foam system the areas that exceed  $\pm 10\text{mm}$  would deform when loaded and therefore the effect of deviations is likely to be reduced. It is common practise in current customised systems to overlay the shape with a single 12 to 25mm layer of foam to form a smoother continuous surface.

This potential manufacturing technique explored by the definition and utilisation of generic geometric shapes could be implemented for a defined proportion of customised shapes. The results show (from the sample used in this project) that 80% of Bases and 25% of Backs can be manufactured using 22 (10mm to 220mm) different sized columns.

The shape analysis process devised in this project produces Shape Frequency Tables or histograms which act as shape descriptors. As described in Section 4.2 (Literature Review), histograms provide a shape classification or descriptor to enable analysis or to act as a database retrieval mechanism. To advance this proposed low-cost manufacturing technique, it is envisaged that a scanned 3D shape may be entered onto 'the database' where the output would reveal whether the shape can or cannot be manufactured using geometric shapes by matching the Shape Histograms with other Shape Histograms within the database. If the shape can be manufactured using geometric shapes, a similar program used in this project could be used to provide an instruction sheet to construct the shape which defines the height and location of the columns. The database would have to be generated using a large collection of shapes from around the UK.

The preliminary work using cluster analysis to classify the sample of shapes in this project was inconclusive. The cluster analysis attempted to group the Shape Frequency Tables which represented the distribution of the geometric representation of the shapes. Research reported in the literature used cluster analysis to classify body-seat interface shapes using defined shape parameters (Li et al. 2000). In addition, the subjects used for this particular study were 30 elderly people (Li et al. 2000), whereas the 25 samples used in this project are customised seating systems typically used to accommodate skeletal deformities which would indicate that the degree of variation would be far greater.

---

## 8 CONCLUSION

---

This project has developed shape acquisition and analysis processes to scientifically advance the knowledge of individuals' shapes with complex disabilities. The processes have employed 3D laser scanning technologies where results confirmed the use of the lower cost laser scanner for both research purposes and clinical work utilising CAD/CAM techniques (Digital Seating Service).

Shape analysis processes were devised by representing the shape volume as standardised geometric shapes (column rods). Preliminary work employed cluster analysis to investigate the classification of the shapes. A potential low-cost manufacturing technique was explored using these geometric shape representations, which provided valuable results relating to the proportion of bases and backs which may be fabricated using this technique. These results suggest that small-scale manufacturers of customised seating systems, such as small NHS Special Seating Units, may be able to fabricate their customised seating systems using the proposed geometric representations for a certain proportion of the shapes which would be a low-cost technique. For the remaining proportion of shapes, external CNC technologies could be sourced which could be geographically central to several Special Seating Units.

To increase the accuracy of the geometric representations, statistical measures were investigated, where standard deviation values for each grid cell highlighted areas where the geometric representations exceeded the  $\pm 10\text{mm}$  tolerance.

The project is a pilot, the purpose of which was to develop protocols for acquisition and analysis of 3D information on seating systems. It is envisaged that these promising results will form the foundation of a larger study in the future with larger sample sizes.

---

## 9 FUTURE WORK

---

The work reported in this project has provided promising results from the processes developed. It is therefore hoped that further work will utilise and improve on these methodologies. A larger sample size should be used to confirm the results reported in this project. In addition, the following areas are proposed for further work:

- Low-cost scanner investigation
  - It would be useful to investigate other low cost scanners or shape acquisition methods on the market to determine their suitability for research purposes and clinical work.
- The  $\pm 10\text{mm}$  tolerance should be investigated further to ascertain how well the represented shapes match the scan data.
  - From clinical experience, it is known that different patient populations have different tolerance needs for special seating. It would therefore be interesting to begin to able to define this with the use of 3D scanning technology
- Test different resolutions of geometric shape representation (i.e. grid cell size)
  - The optimum resolution could be determined by using standard deviation measures. The use of the standard deviation may be able to dictate the best grid cell size (e.g. 5mm x 5mm, 10mm x 10mm etc.) by defining certain criteria or thresholds to achieve a closer representation to the true shape. This is particularly applicable for the highly-contoured steep edges as reported in this project.
  - The use of pressure mapping equipment could be used to investigate the optimum resolution to use for the geometric shape representations. A patient-involved study could be designed which tested these shape representations where pressure mapping would reveal interface pressures

between the patient and shape which could be used to validate the geometric representation concept.

- Investigate other geometric shape representations
  - The top of each column may be angled to represent the steep edges of a shape. This could be determined by the use of regression techniques which can provide the best plane fit at each column. It may be that an angled wedge is added to the top of a proportion of the columns.
- Feasibility of proposed low-cost fabrication technique
  - Further work is required to determine the most efficient method of constructing the shapes from geometric shapes to improve the time of fabrication
  - It was suggested in the Discussion (Section 7.3) that scanned 3D shape may be entered onto a database where the output would reveal whether the shape can or cannot be manufactured using geometric shapes. To create this database, a large shape sample would have to be scanned and processed to collect a large range of shape histograms.
- Investigate if a relationship exists between different shape patterns and the individual's diagnosis, age, gender etc.
- Investigate the shapes of off-the-shelf cushions by scanning a selection of seating products and analysing them in a similar way as demonstrated in this study. This may reveal similarities to a defined proportion of shapes, which would imply that standard shapes (less labour-intensive) may be used instead of customised systems.
- The work and results reported in this project will influence the routine clinical work at Swansea REU which employs the technologies reported. As part of the Digital Seating Service, all scan data is retained which can be used to increase the sample size of future work.

- This shape data can be used to collect outcome measures which are important for clinical work. For example, the rate of postural deformity can begin to be measured in some way using the processes defined in this project.
- It is anticipated that the use of Geomagic Qualify (Geomagic Inc., CA) may become routine to validate some of the CAD/CAM techniques used in the Digital Seating Service
- The ability to identify generic shapes using shape analysis techniques such as cluster analysis is an area which requires further work.
  - A larger sample size would be required to confirm if generic shapes exist amongst custom seating systems. In addition, the above work may be repeated for different resolution to establish if generic shapes are apparent using Shape Frequency Tables defined at a different grid cell size.
  - Principal component analysis is a potential technique which should be explored to reduce the 3D shape information into important variables which would act as an alternative approach to shape representation.

---

## 10 REFERENCES

---

- Ankerst, M. et al., 1999. 3D shape histograms for similarity search and classification in spatial databases. *In Advances in Spatial Databases, 6th International Symposium, SSD'99, Hong Kong*, 207--226.
- Azouz, Z.B. et al., 2006. Characterizing human shape variation using 3D anthropometric data. *The Visual Computer*, 22(5), 302-314.
- Bennett, G., Dealey, C. & Posnett, J., 2004. The cost of pressure ulcers in the UK. *Age Ageing*, 33(3), 230-235.
- Brienza D. et al., 1996. A system for the analysis of seat support surfaces using surface shape control and simultaneous measurement of applied pressures. *Rehabilitation Engineering, IEEE Transactions on*, 4(2), 103-113.
- Brienza D. et al., 1993. Design of a computer-controlled seating surface for research applications. *Rehabilitation Engineering, IEEE Transactions on*, 1(1), 63-66.
- Buck, S., 1996. "Neglect...or respect for our elders? Seating for the institutionalized elderly". *Proceedings of the International Seating Symposium*, 96, 211-214.
- Chen, D. et al., 2003. On Visual Similarity Based 3D Model Retrieval. *Computer Graphics Forum*, 22(3), 223-232.
- Creaform, 2008. ERGOscan 3D Laser Scanner. Available at: <http://www.creaform3d.com/en/handyscan3d/products/ergoscan.aspx> [Accessed December 15, 2008].
- Creaform, 2007. Meeting the automotive industry's high standards. How to get accurate data for analysis from a car interior. Automotive Case Study. Available at: <http://www.creaform3d.com/en/pdf/carseat.pdf> [Accessed December 13, 2008].
- Cyberware, 1999. Whole Body Colour 3D Scanner Model WB4. Available at: <http://www.cyberware.com/products/scanners/wb4.html> [Accessed January 5, 2009].
- Dengsheng & Guojun, 2004. Review of shape representation and description techniques. *Pattern Recognition*, 37(1), 1-19.
- Di3D, 2008. Dimensional Imaging - World Leading 3D & 4D Surface Imaging. Available at: <http://www.di3d.com/> [Accessed December 30, 2008].

- Fraley, C. & Raftery, A.E., 1998. How many clusters? Which clustering method? Answers via model-based cluster analysis. *The Computer Journal*, 41, 578--588.
- Funkhouser, T. et al., 2005. Shape-based retrieval and analysis of 3d models. *Communications of the ACM*, 48(6), 58-64.
- Jackowski, M., Satter, M. & Goshtasby, A., 2003. Approximating Digital 3D Shapes by Rational Gaussian Surfaces. *IEEE Transactions on Visualization and Computer Graphics*, 9(1), 56-69.
- Kadaba, M.P. et al., 1984. Ultrasound mapping of the buttock-cushion interface contour. *Archives of Physical Medicine and Rehabilitation*, 65(8), 467-9.
- Lee, J. & Lou, L., 2003. Using texture and shape features to retrieve sets of similar medical images. *Biomedical Engineering-Applications, basis, communications*, 15(5), 193-199.
- Li, Y. et al., 2000. Determination of generic body-seat interface shapes by cluster analysis. *Rehabilitation Engineering, IEEE Transactions on*, 8(4), 481-489.
- Li, Y., Aissaoui, R. & Dansereau, J., 1998. A mathematical model for comparison of contoured seating shapes. *Proceedings of the 21st annual RESNA conference*, June, 146-148.
- Li, Y. et al., 2004. Development and evaluation of a new body-seat interface shape measurement system. *Biomedical Engineering, IEEE Transactions on*, 51(11), 2040-2050.
- Lu, G. & Sajjanhar, A., 1999. Region-based shape representation and similarity measure suitable for content-based image retrieval. *Multimedia Systems*, 7(2), 165-174.
- Manufacturing Engineering, 2008. CNC Carving Shapes Medical Devices. Available at: [http://findarticles.com/p/articles/mi\\_qa3618/is\\_200802/ai\\_n24394324](http://findarticles.com/p/articles/mi_qa3618/is_200802/ai_n24394324) [Accessed December 13, 2008].
- Mori, G., Belongie, S. & Malik, J., 2001. Shape contexts enable efficient retrieval of similar shapes. *Computer Vision and Pattern Recognition*, 1, 723--730.
- Na, S. et al., 2005. Evaluation of driver's discomfort and postural change using dynamic body pressure distribution. *International Journal of Industrial Ergonomics*, 35(12), 1085-1096.

- Nakaya, H. & Okiyama, H., 1993. A Development of Statistical Human Back Contour Model for Backrest Comfort Evaluation. *SAE International, Technical Report 930114*, 77-87.
- Ohio Willow Wood, 2007. Shape Capture White Paper. Available at: <http://www.owwco.com/omega/pdf/shape%20capture%20white%20paper.pdf> [Accessed December 15, 2008].
- Papageorgiou, I., Baxter, M.J. & Cau, M.A., 2001. Model-based Cluster Analysis of Artefact Compositional Data. *Archaeometry*, 43, 571-588.
- Paquet, E., 2004. Exploring Anthropometric Data Through Cluster Analysis. *Digital Human Modelling for Design and Engineering, National Research Council Canada*. Available at: [http://iit-iti.nrc-cnrc.gc.ca/publications/nrc-46564\\_e.html](http://iit-iti.nrc-cnrc.gc.ca/publications/nrc-46564_e.html) [Accessed January 5, 2009].
- Perkash, I. et al., 1984. Development and evaluation of a universal contoured cushion. *Paraplegia*, 22(6), 358-65.
- PMG, 2008. Posture & Mobility Group Research page. Available at: <http://www.pmguk.co.uk/Research/Information/> [Accessed October 14, 2008].
- Polhemus, 2007. Polhemus: PATRIOT Digitizer. Available at: [http://www.polhemus.com/?page=Motion%20Tracking\\_PATRIOT%20Digitizer](http://www.polhemus.com/?page=Motion%20Tracking_PATRIOT%20Digitizer) [Accessed December 13, 2008].
- Pontikos, D., 2004. Model-Based Clustering of World Craniometric Variation. Available at: <http://dienekes.50webs.com/arp/articles/anthropologica/clustering.html> [Accessed June 21, 2008].
- Pope, P., 2007. *Severe and Complex Neurological Disability, Management of the Physical Condition*, Butterworth-Heinemann, Elsevier Ltd.
- Robinette, K., Daanen, H. & Paquet, E., 1999. The CAESAR project: a 3-D surface anthropometry survey. *Proceedings. Second International Conference on 3-D Digital Imaging and Modelling*, 380-386.
- Shapcott, N., 2008. Special Seating Estimated Tolerance, from 30+years clinical experience (personal communication).
- Sykes, A., 2008. Adapted from OOSTats- an object-orientated approach to Statistical calculations. Presented at *Dyalog Users Conference 2008*, [http://www.dyalog.com/dyalog\\_08.htm](http://www.dyalog.com/dyalog_08.htm):Acadvent Ltd .

- Verver, M. et al., 2005. Aspects of seat modelling for seating comfort analysis. *Applied Ergonomics*, 36(1), 33-42.
- Wahab, D. et al., 2008. Designing for comfort and reliability in an intelligent car seat. Available at: [http://findarticles.com/p/articles/mi\\_7109/is\\_ai\\_n28551379](http://findarticles.com/p/articles/mi_7109/is_ai_n28551379) [Accessed January 5, 2009].
- Wall, J. & Colley, T., 2003. Preventing pressure ulcers among wheelchair users: preliminary comments on the development of a self-administered risk assessment tool. *Journal of Tissue Viability*, 13(2), 48-60.
- Watson, N. & Woods, B., 2005. The Origins and Early Developments of Special/Adaptive Wheelchair Seating. *Social History of Medicine*, 18(3), 459-474.
- Yamazaki, N., 1992. Analysis of sitting comfortability of driver's seat by contact shape. *Ergonomics*, 35(5-6), 677-92.
- Zacharkow, D., 1988. *Posture : Sitting, Standing, Chair Design and Exercise* , Springfield, IL: Charles C. Thomas. **IN** Li, Y et al., 2000. Determination of generic body-seat interface shapes by cluster analysis. *Rehabilitation Engineering, IEEE Transactions on*, 8(4), 481-489.

---

## 11 APPENDICES

---

### 11.1 Photographs of samples (Plaster casts)

#### CHAILEY CASTS



CH1



CH1



CH9

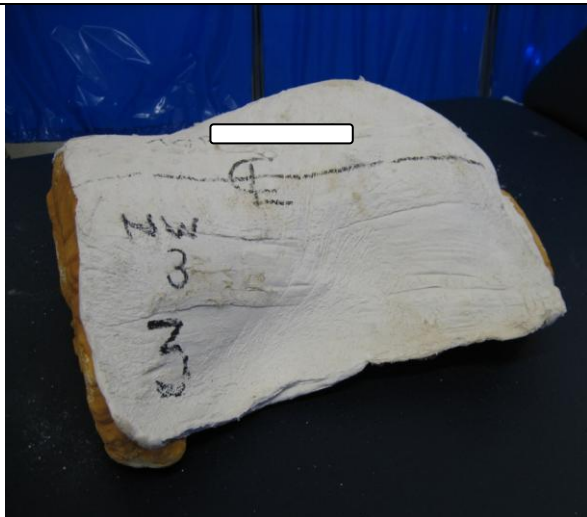
**NORTH WALES**



NW1



NW2



NW3



NW4

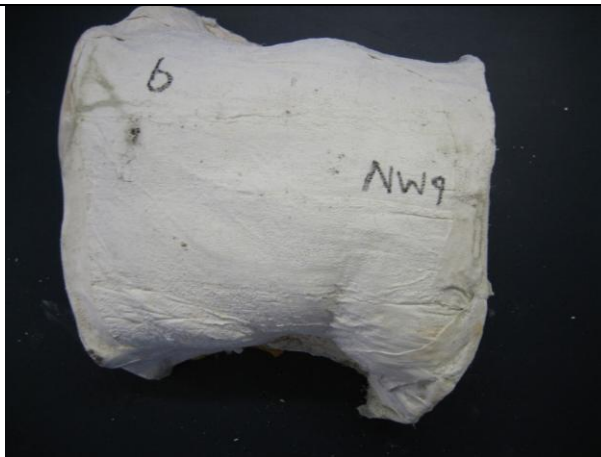
**NORTH WALES 2**



NW7



NW8



NW9



NW10

### SWANSEA CASTS



SWARY



SWAR



SWDH



SWJD



SWLM

## 11.2 Scanner comparison reports

Extracts from Geomagic Qualify, version 9 (Geomagic Inc., CA)'s 3D comparison reports testing critical tolerances  $\pm 1.0\text{mm}$  and  $\pm 2.0\text{mm}$ .

- Faro scan= reference scan
- Microscan= test scan

## 11.3 Java program code

```
package com.lorna.analysis;

import java.io.*;
import java.math.BigDecimal;
import java.util.Iterator;
import java.util.Vector;

// Referenced classes of package com.lorna.analysis:
//      Analysis

public class CSVExport {

    public CSVExport() {}

    public static void main(String args[])
    {
        if ( args.length != 2 )
        {
            System.err.print("Wrong number of Parameters");
            System.exit(-1);
        }
        File dir = new File("./");
        // The list of files can also be retrieved as File objects
        File[] files = dir.listFiles();
        FilenameFilter filter = new FilenameFilter()
        {
            public boolean accept(File dir, String name)
            {
                return name.endsWith(".txt");
            }
        };
        files = dir.listFiles(filter);

        System.out.println( "Found " + files.length + " file(s) to be processed");
        for(int i = 0; i < files.length; i++)
        {
            System.out.print("Processing " + files[i].getName() + " .....");
            Analysis analysis = new Analysis(files[i].getName(), args[0]);
            try
            {
                String s = files[i].getName().replace(".txt", args[0] + "_" + args[1] + ".csv");
                BufferedWriter bufferedwriter = new BufferedWriter(new FileWriter(s));
```

```
//size of grid
//System.out.println( "Size of grid:" + analysis.getMaxGridX() + "x" + analysis.getMaxGridZ());
bufferedwriter.write( "Size of grid:," + (analysis.getMaxGridX() + 1) + "x" + (analysis.getMaxGridZ() + 1) );
bufferedwriter.newLine();

//display the number of points
bufferedwriter.write("Number of Points:," + analysis.getNumberOfPoints());
bufferedwriter.newLine();
bufferedwriter.newLine();

bufferedwriter.write("Average Value of Y");
bufferedwriter.newLine();
Vector vector = new Vector();
for(int j = analysis.getMaxGridZ(); j >= 0; j--)
{
    for(int j1 = 0; j1 < analysis.getMaxGridX() + 1; j1++)
    {
        Double mean = analysis.getMeanY(j1, j);
        //System.out.println(mean);
        vector.add(mean);
        bufferedwriter.write(mean.toString());
        if(j1 != analysis.getMaxGridX())
            bufferedwriter.write(",");
        else
            bufferedwriter.newLine();
    }
}

bufferedwriter.newLine();
bufferedwriter.write("Average Value of Y (Nearest 10)");
bufferedwriter.newLine();
int numberOfColumn = 0;
for(int j = analysis.getMaxGridZ(); j >= 0; j--)
{
    for(int j1 = 0; j1 < analysis.getMaxGridX() + 1; j1++)
    {
        //System.out.println(mean);
        try
        {
            {
                BigDecimal Bvalues = new BigDecimal( analysis.getMeanY(j1, j) / 10);
                Bvalues = Bvalues.setScale(0, BigDecimal.ROUND_HALF_UP);
                bufferedwriter.write( (Bvalues.multiply(new BigDecimal(10)).toString()) );
                numberOfColumn++;
            }
        }
        catch (java.lang.NumberFormatException e)
```

```
    {}

    if(j1 != analysis.getMaxGridX())
        bufferedwriter.write(",");
    else
        bufferedwriter.newLine();
    }
}

bufferedwriter.newLine();
bufferedwriter.write("Standard Deviation of Y");
bufferedwriter.newLine();
for(int k = analysis.getMaxGridZ(); k >= 0; k--) {
    for(int k1 = 0; k1 < analysis.getMaxGridX() + 1; k1++) {
        Double double3 = Double.valueOf(analysis.getSDY(k1, k));
        bufferedwriter.write((new StringBuilder()).append("").append(double3).toString());
        if(k1 != analysis.getMaxGridX())
            bufferedwriter.write(",");
        else
            bufferedwriter.newLine();
    }
}

bufferedwriter.newLine();
bufferedwriter.write("Coefficient of Variation");
bufferedwriter.newLine();
for(int l = analysis.getMaxGridZ(); l >= 0; l--) {
    for(int l1 = 0; l1 < analysis.getMaxGridX() + 1; l1++) {
        Double double4 = Double.valueOf((analysis.getSDY(l1, l) / analysis.getMeanY(l1, l)) * 100D);
        bufferedwriter.write((new StringBuilder()).append("").append(double4).toString());
        if(l1 != analysis.getMaxGridX())
            bufferedwriter.write(",");
        else
            bufferedwriter.newLine();
    }
}

int range = Integer.parseInt(args[1]);

bufferedwriter.newLine();
if(args.length == 2) {
    bufferedwriter.write("Ranges");
    bufferedwriter.newLine();
    Double maxY = analysis.getMaxY();
    int maximumRange = (int)((maxY - maxY % range) / range + 1);
```

```
for(int j2 = 0; j2 < maximumRange; j2++) {
    bufferedwriter.write( (j2 * range) + " >= y < " + (j2 * range + range) );
    int count = 0;
    Iterator iterator = vector.iterator();
    while ( iterator.hasNext() )
    {
        Double values = (Double)iterator.next();
        if(values < (j2 * range + range) && values >= (j2 * range))
            count++;
    }
    bufferedwriter.write((new StringBuilder()).append(",").append(count).toString());
    bufferedwriter.newLine();
}
}
bufferedwriter.newLine();

//Round all grid cells to nearest 10
bufferedwriter.write("Nearest 10");
bufferedwriter.newLine();

BigDecimal maxY = new BigDecimal( analysis.getMaxy() / 10);
maxY = maxY.setScale(0, BigDecimal.ROUND_HALF_UP);
//System.out.println(maxY.intValue());
for(int i1 = 0; i1 <= maxY.intValue(); i1++) {
    int left = i1 * 10;
    //bufferedwriter.write( left );
    //System.out.print( left );
    int count = 0;
    Iterator iterator = vector.iterator();
    while ( iterator.hasNext() )
    {
        //System.out.println("df");
        Double values = (Double)iterator.next();
        try
        {
            BigDecimal Bvalues = new BigDecimal( values / 10);
            Bvalues = Bvalues.setScale(0, BigDecimal.ROUND_HALF_UP);

            if( (Bvalues.intValue() *10) == (i1 *10) )
            {
                //System.out.println(Bvalues.intValue() * 10 + " == " + (i1 * 10) );
                count++;
            }
        }
    }
}
catch (java.lang.NumberFormatException e){}
```

```

    }
    bufferedwriter.write( i1*10 + ",," + count );
    //System.out.println( " " + count );
    bufferedwriter.newLine();
}

bufferedwriter.newLine();
bufferedwriter.write( "Number of Columns:," + numberOfColumn);
bufferedwriter.newLine();
bufferedwriter.newLine();
bufferedwriter.write( "Deviation from Mean (nearest 10)");
bufferedwriter.newLine();
bufferedwriter.write( "GRID,mean,No of Y,greater than 10,dev1,dev2,etc");
bufferedwriter.newLine();
for(int z = analysis.getMaxGridZ(); z >= 0; z--) {
    for(int x = 0; x < analysis.getMaxGridX() + 1; x++) {
        Double mean = Double.valueOf(analysis.getMeanY(x, z));
        try
        {
            BigDecimal Bmean = new BigDecimal( mean / 10);
            Bmean = Bmean.setScale(0, BigDecimal.ROUND_HALF_UP);
            mean = Bmean.doubleValue()* 10;
        }
        catch (NumberFormatException nfe){

        }

        bufferedwriter.write(x + " " + z + "," + mean);
        Vector<Double> ys = analysis.getYPoints(x, z);
        bufferedwriter.write(", " + ys.size());
        Iterator<Double> iterator = ys.iterator();
        String output = "";
        int greaterThan10 = 0;
        while (iterator.hasNext())
        {
            double y = iterator.next();
            double diffFromMean = y - mean;
            if ( Math.abs(diffFromMean) > 10 )
            {
                greaterThan10++;
            }
            output = output + "," + Math.abs(diffFromMean);
            //bufferedwriter.write(", " + Math.abs(diffFromMean));
        }
        bufferedwriter.write(", " + greaterThan10 + output);
        bufferedwriter.newLine();
    }
}

```

```
    }  
    bufferedwriter.close();  
    System.out.println(" done");  
    }  
    catch(IOException ioexception) {  
        ioexception.printStackTrace();  
    }  
    }  
}
```

```
package com.lorna.analysis;  
  
import java.io.*;  
import java.util.Iterator;  
import java.util.Vector;  
  
// Referenced classes of package com.lorna.analysis:  
//     Point  
  
public class Analysis {  
  
    public double getMeanY(int i, int j) {  
        Double mean = 0.0;  
        int number = 0;  
        Iterator<Point> iterator = storage.iterator();  
        while (iterator.hasNext())  
        {  
            Point point = (Point)iterator.next();  
            if(point.getGridx() == i && point.getGridz() == j) {  
                number++;  
                mean = mean + point.getY()  
                ;  
            }  
        }  
        return mean / number;  
    }  
  
    public double getSDY(int x, int z)  
    {  
        double mean = getMeanY(x, z);  
        Vector<Double> vector = new Vector<Double>();  
  
        Iterator<Point> iterator = storage.iterator();  
  
        while (iterator.hasNext())
```

```
{
    Point point = (Point)iterator.next();
    if(point.getGridx() == x && point.getGridz() == z) {
        double sq = (point.getY() - mean) * (point.getY() - mean);
        vector.add(sq);
    }
}

Double total = 0.0;
for(Iterator<Double> sqIterator = vector.iterator(); sqIterator.hasNext();)
{
    total += ((Double)sqIterator.next()).doubleValue();
}

Double sqmean = total / vector.size();
Double sd = Math.sqrt(sqmean);
return sd;
}

public int getMaxGridX() {
    return maxGridX;
}

public void setMaxGridX(int i) {
    maxGridX = i;
}

public int getMaxGridZ() {
    return maxGridZ;
}

public void setMaxGridZ(int i) {
    maxGridZ = i;
}

public Analysis(String fileName, String interval) {
    this.maxGridX = 0;
    this.maxGridZ = 0;
    this.storage = new Vector<Point>();
    this.fileName = fileName;
    this.interval = Integer.parseInt( interval );
    this.processData();
}

public int getAverageColumnHeight(int i, int j) {
    int k = 0;
    Iterator<Point> iterator = null;
    iterator = storage.iterator();
    do {
```

```

        if(!iterator.hasNext())
            break;
        Point point = (Point)iterator.next();
        Double double1 = Double.valueOf(point.getY());
        if(double1.doubleValue() < (double)(i * j + j) && double1.doubleValue() >=
(double)(i * j))
            k++;
    } while(true);
    return k;
}

public double getMaxy() {
    return maxy;
}

public void processData() {
    Iterator<Point> iterator = null;
    try {
        BufferedReader bufferedreader = new BufferedReader(new FileReader(fileName));
        String line;
        while((line = bufferedreader.readLine()) != null) {
            String points[] = line.split(" ");
            storage.addElement(new Point(
                Double.valueOf(points[0].replace("'", "").trim()).doubleValue(),
                Double.valueOf(points[1].replace("'", "").trim()).doubleValue(),
                Double.valueOf(points[2].replace("'", "").trim()).doubleValue()));
        }
        bufferedreader.close();
    }
    catch(NullPointerException nullpointerexception) {
        nullpointerexception.printStackTrace();
    }
    catch(FileNotFoundException filenotfoundexception) {
        filenotfoundexception.printStackTrace();
    }
    catch(IOException ioexception) {
        ioexception.printStackTrace();
    }
    iterator = storage.iterator();
    minx = ((Point)storage.firstElement()).getX();
    miny = ((Point)storage.firstElement()).getY();
    maxy = ((Point)storage.firstElement()).getY();
    minz = ((Point)storage.firstElement()).getZ();

    // Calculate minimums
    while ( iterator.hasNext())
    {
        Point point = (Point)iterator.next();
        if(point.getX() < minx)

```

```

        minx = point.getX();
        if(point.getY() < miny)
            miny = point.getY();
        if(point.getZ() < minz)
            minz = point.getZ();
    }

    // normalise points
    iterator = storage.iterator();
    while ( iterator.hasNext())
    {
        Point point = (Point)iterator.next();
        point.setX(point.getX() - minx);
        point.setY(point.getY() - miny);
        point.setZ(point.getZ() - minz);
        if(point.getY() > maxy)
            maxy = point.getY();
    }

    // plot where y should be on the grid and calculate the size of the GRID
    int j;
    Point point;
    iterator = storage.iterator();
    while ( iterator.hasNext() )
    {
        point = (Point)iterator.next();
        int i = (int)(point.getX() - point.getX() % (double)interval) / interval;
        //System.out.println( point.getX() + " - " + point.getX() % interval + " / " + interval);
        if(i > maxGridX)
            maxGridX = i;
        point.setGridx(i);
        j = (int)(point.getZ() - point.getZ() % (double)interval) / interval;
        if(j > maxGridZ)
            maxGridZ = j;
        point.setGridz(j);
    }
}

public Vector<Double> getYPoints(int x, int z)
{
    Vector<Double> ys = new Vector<Double>();
    Iterator<Point> iterator = null;
    iterator = storage.iterator();
    Point point;
        while (iterator.hasNext())
        {
            point = (Point)iterator.next();

            if (point.getGridx() == x && point.getGridz() == z)

```

```
        {
            ys.add(point.getY());
        }
    }
    return ys;
}

public int getNumberofPoints()
{
    return storage.size();
}

private static final long serialVersionUID = 1L;
private int interval;
private double minx;
private double miny;
private double maxy;
private double minz;
private int maxGridX;
private int maxGridZ;
private String fileName;
private Vector<Point> storage;
}
```

```
package com.lorna.analysis;

public class Point {

    public int getGridx() {
        return this.gridx;
    }

    public void setGridx(int gridx) {
        this.gridx = gridx;
    }

    public int getGridz() {
        return this.gridz;
    }

    public void setGridz(int gridz) {
        this.gridz = gridz;
    }

    Point(double x, double y, double z) {
        this.x = x;
        this.y = y;
    }
}
```

```
        this.z = z;
    }

    public double getX() {
        return this.x;
    }

    public void setX(double x) {
        this.x = x;
    }

    public double getY() {
        return this.y;
    }

    public void setY(double y) {
        this.y = y;
    }

    public double getZ() {
        return this.z;
    }

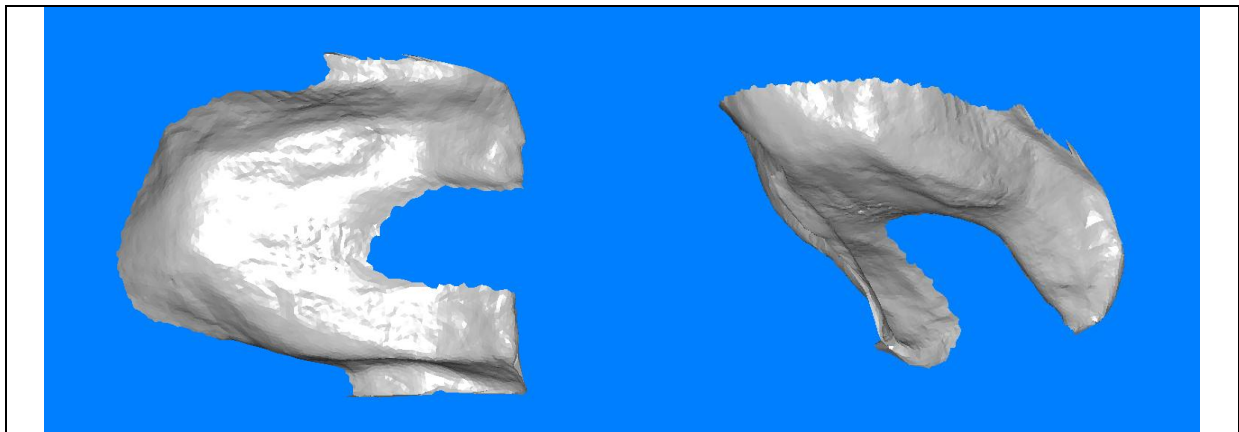
    public void setZ(double z) {
        this.z = z;
    }

    private double x;
    private double y;
    private double z;
    private int gridx;
    private int gridz;
}
```

## 11.4 Results: Grid Layout and Histograms

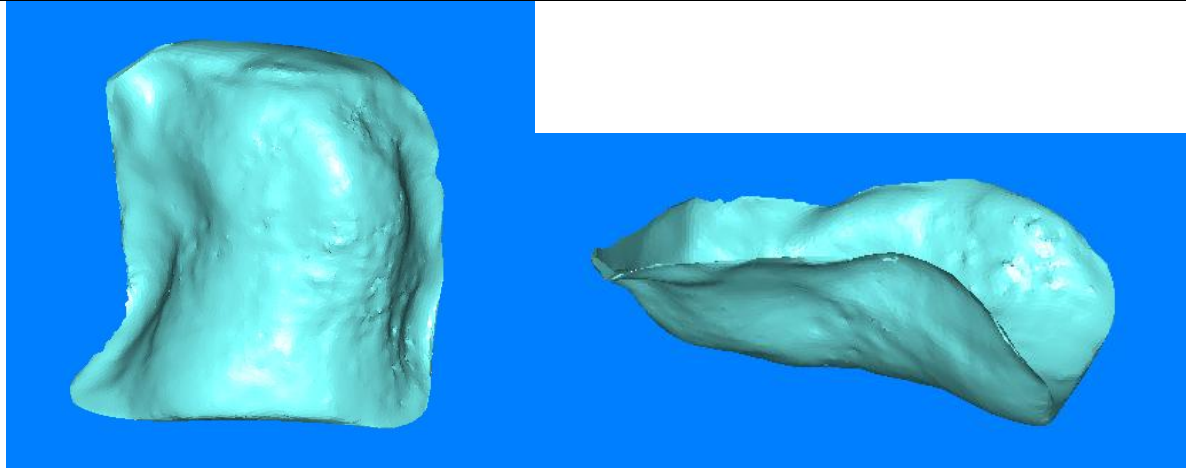
The grid layout and histograms (from the Shape Frequency Tables) as dictated by the geometric representations (20x20mm column size) are inserted below for a selection of shapes.

### SWGJ base

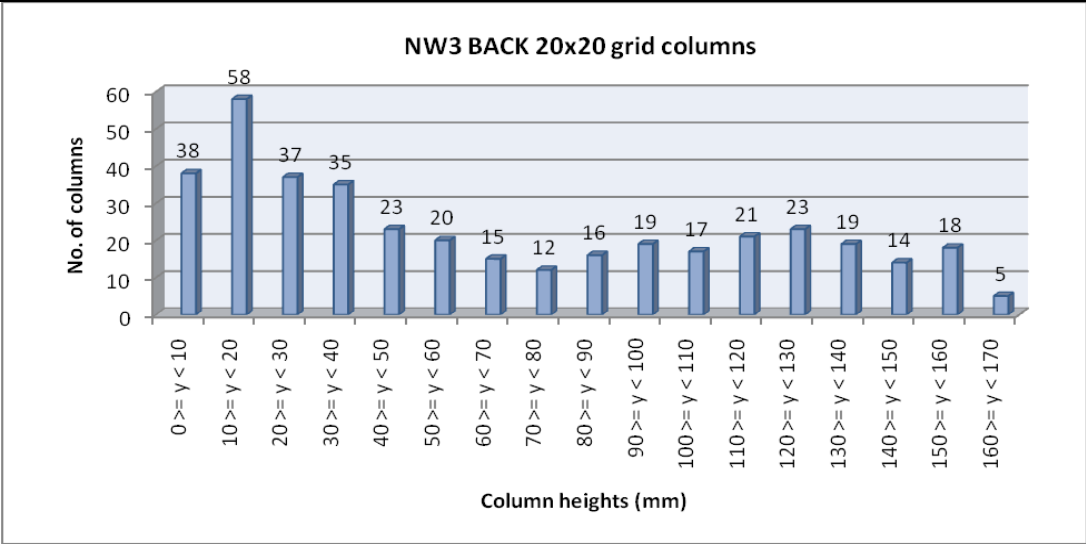








NaN	113	101	NaN																					
NaN	131	117	94.3	NaN																				
NaN	NaN	127	135	143	144	146	NaN	143	130	107	84.1	NaN												
NaN	123	124	128	134	136	136	142	148	151	151	152	155	157	159	159	153	137	110	86.4	73.7	69.9			
128	124	124	121	120	121	125	133	139	141	144	148	153	158	160	155	131	104	73.6	62.7	56.8	58.1			
126	121	123	118	112	112	114	119	126	129	133	139	145	148	134	113	86.3	61.6	44	37.8	38	45.8			
119	112	114	106	96.3	93.9	95.5	104	111	115	116	115	112	104	89.4	66	48.7	34.9	26.3	21.4	23.4	NaN			
113	98.6	96.9	87.2	77.9	73.7	73	81	88.2	96	94.3	88.5	76.4	65	56.3	44.7	33.2	21.7	14.2	10.6	13.7	NaN			
106	86.2	75.1	66.4	59.3	55	53.7	56.3	60.7	66.5	64.9	61	53.3	45.3	39.2	31.2	22.2	13	7.44	4.68	7.39	NaN			
101	77.4	57.8	48.9	44.5	42.6	41.3	40.1	40	40.5	42.2	43.1	36.3	33	28.8	22.6	15.3	8.3	4.18	2.75	4.47	NaN			
96.3	66	47.7	39.1	36.4	35.2	34.3	31.2	28.3	29.7	32.6	30.6	26.5	24.4	21.2	17.1	11	6.37	3.39	3	4.21	NaN			
86.3	56.4	41.1	34.4	32.2	30.2	26.5	22.7	21.8	25.2	25	24	20.7	17.5	15.1	12.7	7.78	5.9	3.48	3.38	6.19	NaN			
83.6	52.9	37.3	30.6	26.9	23.9	20.5	18.5	18.4	19.9	19.5	18.3	15.4	13.4	12.2	10.5	7.27	5.91	5.07	4	5.29	NaN			
92.1	51.1	33.9	25.7	20.3	17.9	15.2	14.7	14.8	15.6	15.9	15.4	13.1	13.7	13.5	13	10.8	8.13	6.67	5.99	6.92	NaN			
98.2	56.1	36.2	23.1	16.2	11.7	8.88	7.62	8.33	10.1	12.1	13.1	12.3	15.4	17	19.9	18.4	14.4	11.3	10.3	11.2	NaN			
109	71.3	44.8	26.9	15.2	8.62	4.91	3.59	4.46	5.5	7.63	12.8	14.3	17.4	22	25.9	26.3	23.4	20.1	16.7	18.5	NaN			
NaN	96.6	64.2	46.6	22.2	11.6	6.21	4.72	5.36	7.44	10.2	16.8	20.1	22.6	29.1	37.4	41.5	39.1	35.9	32.2	30.3	36.5			
NaN	116	87.3	73.1	50.7	31.5	18.2	15.3	14.3	18.2	21.6	23.4	33.3	38	45.1	53.6	60.8	59.8	57	52.3	46.7	46.6			
NaN	129	122	108	83.4	67.7	55.4	35.5	34.2	35.8	40.5	47.3	57.9	72.9	81.5	98.8	108	108	97.9	80.8	72.5	61.3			
NaN	NaN	138	132	118	108	101	93.5	91.6	94	99.4	110	118	127	134	151	155	148	134	115	96.5	80.3			
NaN	NaN	NaN	138	137	129	128	134	144	151	154	157	158	163	166	165	162	154	142	125	107	NaN			



**SWDH back**



## 11.5 Chi-squared test calculations

The calculations steps performed to obtain the chi-square test results (used for cluster analysis are outlined below:

1. Calculate expected frequencies under the assumption of homogeneity (= row total times column total divided by grand total for each cell)

E.g.  $(8 \times 317) / 690 = 3.675$

E.g.  $(8 \times 373) / 690 = 4.325$

(Highlighted in Table 21)

**Table 21. Chi-square test calculations 1**

	F1 (NW1base)	F2 (CH1base)	Row Total	Expected Frequencies	
0 >= y < 10	6	2	8	3.675	4.325
10 >= y < 20	7	3	10	4.594	5.406
20 >= y < 30	10	68	78	35.835	42.165
30 >= y < 40	13	79	92	42.267	49.733
40 >= y < 50	25	52	77	35.375	41.625
50 >= y < 60	54	18	72	33.078	38.922
60 >= y < 70	44	27	71	32.619	38.381
70 >= y < 80	45	13	58	26.646	31.354
80 >= y < 90	33	11	44	20.214	23.786
90 >= y < 100	17	12	29	13.323	15.677
100 >= y < 110	14	20	34	15.620	18.380
110 >= y < 120	6	19	25	11.486	13.514
120 >= y < 130	18	22	40	18.377	21.623
130 >= y < 140	13	17	30	13.783	16.217
140 >= y < 150	10	7	17	7.810	9.190

150 >= y < 160	1	3	4	1.838	2.162
160 >= y < 170	1	0	1	0.459	0.541
Column Total	317	373	690	3.675	4.325

2. a) Calculate  $(\text{observed}-\text{expected})^2/\text{expected}$  for each cell (as highlighted in Table 21, refer to Table 21)

E.g.  $(6-3.675)^2/3.675 = 1.470$

E.g.  $(2-4.325)^2/4.325 = 1.250$

3. Sum of these values which equals the chi-square value (Table 22)  
 4. Calculate the Degrees of freedom =  $(\text{no. of rows}-1) * (\text{no. of columns}-1)$

The degrees of freedom is used to describe the number of values that are free to vary or are independent.

**Table 22. Chi-square test calculations 2**

<b>(Observed-expected)<sup>2</sup>/Expected</b>	
1.470	1.250
1.260	1.071
18.625	15.829
20.265	17.223
3.043	2.586
13.233	11.246
3.971	3.375
12.642	10.744
8.087	6.873
1.015	0.862
0.168	0.143
2.620	2.227

0.008	0.007
0.044	0.038
0.614	0.522
0.382	0.325
0.636	0.541
1.470	1.250
<b>Chi-square value (i.e. total)</b>	
<b>=162.94</b>	
<b>Degrees of Freedom= 16</b>	

5. Calculate the p-value using chi-square distribution tables. Conventionally if  $p < 0.05$ , the hypothesis of homogeneity is rejected which means that there is a less than 5% probability that any deviation from the expected results is due to chance only. The p-value for a one-tailed chi-square test is the probability that a value chosen at random from a particular chi-square distribution would be greater than or equal to the value of an observed value (the chi-square value) from the same distribution.
6. All values were  $p < 0.05$ , therefore for a more meaningful measure for the purposes of performing cluster analysis- Chi-square value/Degrees of Freedom was used as a measure of similarity between each frequency
7. Each frequency was tested with each other which resulted in matrix of distance values (Table 23). The above calculations were carried out in Microsoft Excel, and APL programming language (Sykes 2008) was used to complete all of the tests
8. The dendrogram was constructed by starting with the smallest 'distance' between any two shapes. Then the smallest distance between either of these shapes is obtained by using the matrix. This is repeated until all shapes are used.  
These distances are listed in Table 24.

**Table 23. Matrix of distance values (Chi-square/degrees of freedom) for Bases**

	NW1 base	NW4 BASE	NW5 BASE	NW6base	NW7base	NW8 base	NW10 BASE	CH1base	CH2base	CH8base	CH9base	SWJM BASE	SWGJ base	SWDFbase	SWL Mbase	SWJDbase	SWARbase	SWARYbase	SWDHbase	SWTHD BASE
NW1base	0.00	8.83	5.08	3.93	5.71	2.13	4.08	10.18	4.73	13.86	8.75	7.12	13.87	16.08	15.91	8.97	7.89	8.74	9.27	11.58
NW4 BASE	8.83	0.00	4.24	5.72	4.56	4.48	5.02	10.61	9.11	6.69	10.69	13.14	3.85	8.10	10.62	4.79	9.44	9.90	10.66	7.80
NW5 BASE	5.08	4.24	0.00	4.22	1.97	3.40	4.50	11.73	7.86	5.99	8.42	14.10	6.11	8.86	8.27	5.53	4.11	5.84	10.49	9.35
NW6base	3.93	5.72	4.22	0.00	5.88	1.63	2.93	4.86	2.30	10.85	10.93	8.88	11.13	15.57	12.78	7.60	9.58	3.13	5.36	5.32
NW7base	5.71	4.56	1.97	5.88	0.00	4.30	5.34	12.11	9.82	6.14	8.86	13.21	6.80	6.78	9.71	5.79	3.78	8.72	12.63	11.65
NW8base	2.13	4.48	3.40	1.63	4.30	0.00	3.30	3.82	2.36	9.64	7.05	6.91	8.07	11.91	11.48	5.76	7.02	4.81	6.26	6.11
NW10 BASE	4.08	5.02	4.50	2.93	5.34	3.30	0.00	9.51	5.40	11.03	11.46	8.06	11.18	15.41	13.03	7.45	8.23	6.86	5.42	5.27
CH1base	10.18	10.61	11.73	4.86	12.11	3.82	9.51	0.00	5.79	15.76	21.20	13.97	16.25	21.03	17.75	10.44	17.30	7.67	10.16	8.99
CH2base	4.73	9.11	7.86	2.30	9.82	2.36	5.40	5.79	0.00	14.78	15.14	9.77	16.67	19.68	16.51	9.92	15.18	7.29	6.88	7.16
CH8base	13.86	6.69	5.99	10.85	6.14	9.64	11.03	15.76	14.78	0.00	14.18	26.32	7.96	6.79	2.76	3.64	11.59	12.45	17.54	14.10
CH9base	8.75	10.69	8.42	10.93	8.86	7.05	11.46	21.20	15.14	14.18	0.00	18.81	13.29	12.62	16.41	10.23	7.67	18.88	24.23	20.48
SWJM BASE	7.12	13.14	14.10	8.88	13.21	6.91	8.06	13.97	9.77	26.32	18.81	0.00	21.82	25.13	27.01	16.38	16.21	16.01	9.85	11.39
SWGJ base	13.87	3.85	6.11	11.13	6.80	8.07	11.18	16.25	16.67	7.96	13.29	21.82	0.00	5.37	11.04	5.48	9.59	15.00	19.21	16.76
SWDFbase	16.08	8.10	8.86	15.57	6.78	11.91	15.41	21.03	19.68	6.79	12.62	25.13	5.37	0.00	11.42	7.57	9.67	18.79	24.98	22.58
SWLMbase	15.91	10.62	8.27	12.78	9.71	11.48	13.03	17.75	16.51	2.76	16.41	27.01	11.04	11.42	0.00	5.70	14.35	13.85	18.85	16.58
SWJDbase	8.97	4.79	5.53	7.60	5.79	5.76	7.45	10.44	9.92	3.64	10.23	16.38	5.48	7.57	5.70	0.00	9.04	10.59	12.75	11.48
SWARbase	7.89	9.44	4.11	9.58	3.78	7.02	8.23	17.30	15.18	11.59	7.67	16.21	9.59	9.67	14.35	9.04	0.00	12.76	19.17	17.80
SWARYbase	8.74	9.90	5.84	3.13	8.72	4.81	6.86	7.67	7.29	12.45	18.88	16.01	15.00	18.79	13.85	10.59	12.76	0.00	7.97	10.45
SWDHbase	9.27	10.66	10.49	5.36	12.63	6.26	5.42	10.16	6.88	17.54	24.23	9.85	19.21	24.98	18.85	12.75	19.17	7.97	0.00	5.82
SWTHD BASE	11.58	7.80	9.35	5.32	11.65	6.11	5.27	8.99	7.16	14.10	20.48	11.39	16.76	22.58	16.58	11.48	17.80	10.45	5.82	0.00

**Table 24. Distance values used to construct Dendrogram (shown in Figure 53), colours corresponding to****Table 23**

Base 1	Base 2	Distance value
NW1base	NW8base	2.133344
NW8base	NW6base	1.63436
NW6base	CH2base	2.295893
CH2base	NW10 BASE	2.926943
NW10 BASE	SWARYbase	3.132594
SWARYbase	NW5 BASE	3.400825
NW5 BASE	NW7base	1.973282
NW7base	SWARbase	3.78491
SWARbase	CH1base	3.824392
CH1base	NW4 BASE	4.237316
NW4 BASE	SWGJ base	3.850129
SWGJ base	SWJDbase	4.788094
SWJDbase	CH8base	3.640929
CH8base	SWLMbase	2.757151
SWLMbase	SWTHD BASE	5.267984
SWTHD BASE	SWDHbase	5.355048
SWDHbase	SWDFbase	5.365844
SWDFbase	SWJM BASE	6.910893
SWJM BASE	CH9base	7.048352